

INFRASTRUTTURE VIARIE IN SOTTERRANEO

TUNNELS IN WEAK ROCK

Prof. Ing. Geol. Eugenio Castelli

ecastelli@units.it

Rock-Support Interaction analysis for tunnels in weak rock masses

Introduction

Tunnelling in weak rock presents some special challenges to the geotechnical engineer since misjudgements in the design of support systems can lead to very costly failures. In order to understand the issues involved in the process of designing support for this type of tunnel it is necessary to examine some simple basic concepts of how a rock mass surrounding a tunnel deforms and how the support systems act to control this deformation. This Rock-Support Interaction or Convergence-Confinement analysis is limited to circular tunnels in an in-situ stress field in which all three principal stresses are equal and where the rock mass exhibits elastic-perfectly plastic shear failure. It should not be used for the detailed design of tunnels in more complex rock masses and in-situ stress fields. More comprehensive analyses are available for these situations (Hoek et al, 2008).

Deformation around an advancing tunnel

Figure 1 shows the results of a three-dimensional finite element analysis of the deformation and failure of the rock mass surrounding a circular tunnel advancing through a weak rock mass subjected to equal stresses in all directions. The plot shows displacement vectors in the rock mass, the shape of the deformed tunnel profile and the shape of the plastic zone surrounding the tunnel. Figure 2 gives a graphical summary of the most important features of this analysis.

Elastic deformation of the rock mass starts about two diameters ahead of the advancing face and reaches its maximum value at about two diameters behind the face. At the face position about one third of the total radial closure of the tunnel has already occurred as the tunnel face deforms inwards as illustrated in Figures 1 and 2. Whether or not the deformations induce stability problems in the tunnel depends upon the ratio of rock mass strength to the in situ stress level, as will be demonstrated in the following pages.

Note that it is assumed that the deformation process described occurs immediately upon excavation of the face. This is a reasonable approximation for most tunnels in rock. The effects of time dependent deformations upon the performance of the tunnel and the design of the support system will not be discussed in this chapter.

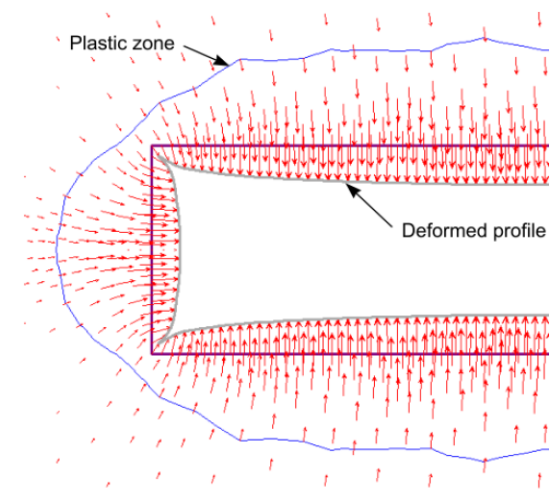


Figure 1: Vertical section through an axis-symmetric three-dimensional finite element model of the failure and deformation of the rock mass surrounding the face of an advancing circular tunnel. The plot shows displacement vectors as well as the shape of the deformed tunnel profile.

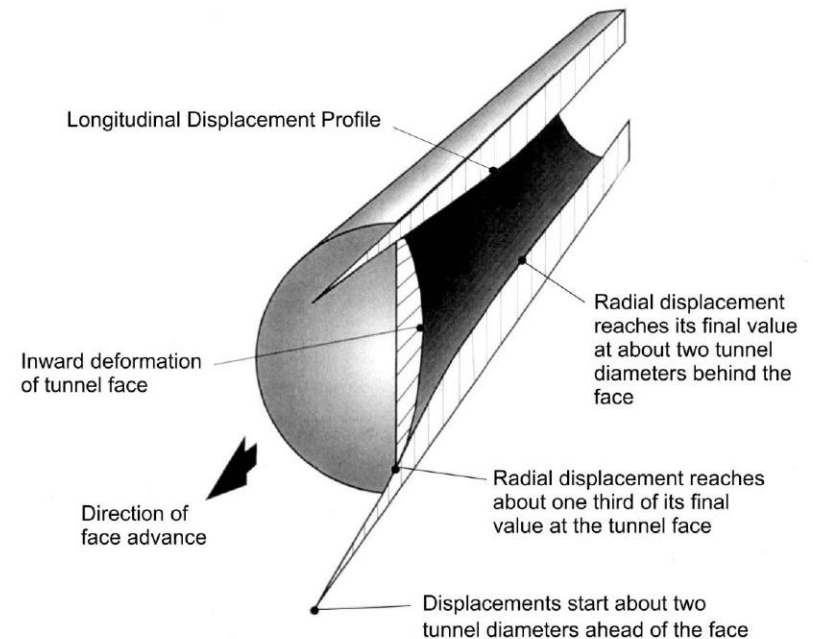


Figure 2: Pattern of elastic deformation in the rock mass surrounding an advancing tunnel.

Tunnel deformation analysis

In order to explore the concepts of rock support interaction in a form which can readily be understood, a very simple analytical model based on the Mohr-Coulomb failure criterion will be utilised. This model involves a circular tunnel subjected to a hydrostatic stress field in which the horizontal and vertical stresses are equal.

In this analysis it is assumed that the surrounding homogeneous weak rock mass behaves as an elastic-perfectly plastic material in which failure involving slip along closely spaced intersecting discontinuities is assumed to occur with zero plastic volume change (Duncan Fama, 1993).

Definition of failure criterion

It is assumed that the onset of plastic failure, for different values of the effective confining stress σ_3' , is defined by the Mohr-Coulomb criterion and expressed as:

$$\sigma_1' = \sigma_{cm} + k\sigma_3' \quad (1)$$

The uniaxial compressive strength of the rock mass σ_{cm} is defined by:

$$\sigma_{cm} = \frac{2c' \cos \phi'}{(1 - \sin \phi')} \quad (2)$$

and the slope k of the σ_1' versus σ_3' plot as:

$$k = \frac{(1 + \sin \phi')}{(1 - \sin \phi')} \quad (3)$$

where σ_1' is the axial stress at which failure occurs
 σ_3' is the confining stress
 c' is the cohesive strength and
 ϕ' is the angle of friction of the rock mass

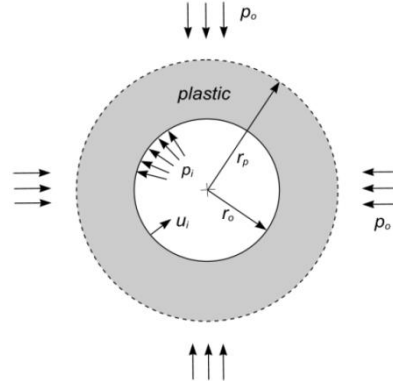


Figure 3: Plastic zone surrounding a circular tunnel.

Analysis of tunnel behaviour

Assume that a circular tunnel of radius r_o is subjected to hydrostatic stresses p_o and a uniform internal support pressure p_i as illustrated in Figure 3. Failure of the rock mass surrounding the tunnel occurs when the internal pressure p_i is less than a critical support pressure p_{cr} , which is defined by:

$$p_{cr} = \frac{2p_o - \sigma_{cm}}{1 + k} \quad (4)$$

If the internal support pressure p_i is greater than the critical support pressure p_{cr} , no failure occurs, the behaviour of the rock mass surrounding the tunnel is elastic and the inward radial elastic displacement u_{ie} of the tunnel wall is given by:

$$u_{ie} = \frac{r_o(1 + \nu)}{E_m}(p_o - p_i) \quad (5)$$

where E_m is the Young's modulus or deformation modulus and ν is the Poisson's ratio of the rock.

When the internal support pressure p_i is less than the critical support pressure p_{cr} , failure occurs and the radius r_p of the plastic zone around the tunnel is given by:

$$r_p = r_o \left[\frac{2(p_o(k-1) + \sigma_{cm})}{(1+k)((k-1)p_i + \sigma_{cm})} \right]^{\frac{1}{k-1}} \quad (6)$$

For plastic failure, the inward radial displacement u_{ip} of the walls of the tunnel is:

$$u_{ip} = \frac{r_o(1 + \nu)}{E} \left[2(1 - \nu)(p_o - p_{cr}) \left(\frac{r_p}{r_o} \right)^2 - (1 - 2\nu)(p_o - p_i) \right] \quad (7)$$

Input:	sigci = 10 MPa	mi = 10	GSI = 25
	mu = 0.30	ro = 3.0 m	po = 2.0 Mpa
	pi = 0.0 MPa	pi/po = 0.00	

Output:	mb = 0.69	s = 0.0000	a = 0.525
	k = 2.44	phi = 24.72 degrees	coh = 0.22 MPa
	sigcm = 0.69 MPa	E = 749.9 MPa	pcr = 0.96 MPa
	rp = 6.43 m	ui = 0.0306 m	ui= 30.5957 mm

sigcm/po = 0.3468	rp/ro = 2.14	ui/ro = 0.0102
-------------------	--------------	----------------

Calculation:

									Sums
sig3	1E-10	0.36	0.71	1.1	1.43	1.79	2.14	2.50	10.00
sig1	0.00	1.78	2.77	3.61	4.38	5.11	5.80	6.46	29.92
sig3sig1	0.00	0.64	1.98	3.87	6.26	9.12	12.43	16.16	50
sig3sq	0.00	0.13	0.51	1.15	2.04	3.19	4.59	6.25	18

Cell formulae:

```

mb = mi*EXP((GSI-100)/28)
s = IF(GSI>25,EXP((GSI-100)/9),0)
a = IF(GSI>25,0.5,0.65-GSI/200)
sig3 = Start at 1E-10 (to avoid zero errors) and increment in 7 steps of sigci/28 to 0.25*sigci
sig1 = sig3+sigci*(((mb*sig3)/sigci)+s)^a
k = (sumsig3sig1 - (sumsig3*sumsig1)/8)/(sumsig3sq-(sumsig3^2)/8)
phi = ASIN((k-1)/(k+1))*180/PI()
coh = (sigcm*(1-SIN(phi*PI()/180)))/(2*COS(phi*PI()/180))
sigcm = sumsig1/8 - k*sumsig3/8
E = IF(sigci>100,1000*10^((GSI-10)/40),SQRT(sigci/100)*1000*10^((GSI-10)/40))
pcr = (2*po-sigcm)/(k+1)
rp = IF(pi<pcr,ro*(2*(po*(k-1)+sigcm)/((1+k)*((k-1)*pi+sigcm)))^(1/(k-1)),ro)
ui = IF(rp>ro,ro*((1+mu)/E)*(2*(1-mu)*(po-pcr)*((rp/ro)^2)-(1-2*mu)*(po-pi)),ro*(1+mu)*(po-pi)/E)

```

Figure 4: Spreadsheet for the calculation of rock mass characteristics and the behaviour of rock mass surrounding a circular tunnel in a hydrostatic stress field.

A more elaborate analysis of the same problem, using the the Hoek-Brown fail criterion, has been published by Carranza-Torres and Fairhurst (1999) and Carranza Torres (2004). The details of these analyses are beyond the scope of this discussion the results have been incorporated into a program called RocSupport¹ and are used in following discussion.

Dimensionless plots of tunnel deformation

A useful means of studying general behavioural trends is to create dimensionless plots from the results of parametric studies. One such dimensionless plot is presented in Fig 5. This plot was constructed from the results of a Monte Carlo analysis in which the parameters for rock mass strength and tunnel deformation were varied at random in 2000 iterations. It is remarkable that, in spite of the very wide range of conditions included in these analyses, the results follow a very similar trend and that it is possible to fit curves which give a very good indication of the average trend.

¹ Available from www.rocscience.com

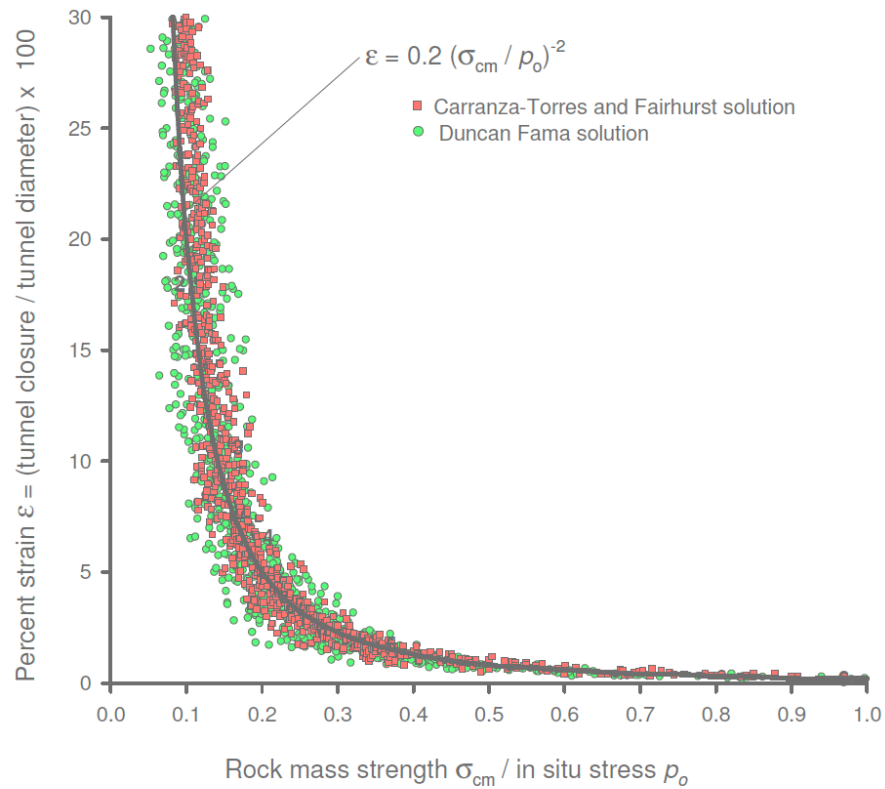


Figure 5: Tunnel deformation versus ratio of rock mass strength to in situ stress based on a Monte-Carlo analysis which included a wide range of input parameters².

Figure 5 is a plot of the ratio of tunnel wall displacement to tunnel radius against the ratio of rock mass strength to in situ stress. Once the rock mass strength falls below 20% of the in situ stress level, deformations increase substantially and, unless these deformations are controlled, collapse of the tunnel is likely to occur.

Based on field observations and measurements, Sakurai (1983) suggested that tunnel strain levels in excess of approximately 1% are associated with the onset of tunnel

² Using the program @RISK in conjunction with a Microsoft Excel spreadsheet for estimating rock mass strength and tunnel behaviour (equations 4 to 7). Uniform distributions were sampled for the following input parameters, the two figures in brackets define the minimum and maximum values used: Intact rock strength σ_{ci} (1,30 MPa), Hoek-Brown constant m_i (5,12), Geological Strength Index GSI (10,35), In situ stress (2, 20 MPa), Tunnel radius (2, 8 m).

instability and with difficulties in providing adequate support. Field observations by Chern et al (1998), plotted in Figure 6, confirm Sakurai's proposal.

Note that some tunnels which suffered strains as high as 5% did not exhibit stability problems. All the tunnels marked as having stability problems were successfully completed but the construction problems increased significantly with increasing strain levels. Hence, the 1% limit proposed by Sakurai is only an indication of increasing difficulty and it should not be assumed that sufficient support should be installed to limit the tunnel strain to 1%. In fact, in some cases, it is desirable to allow the tunnel to undergo strains of as much as 5% before activating the support.

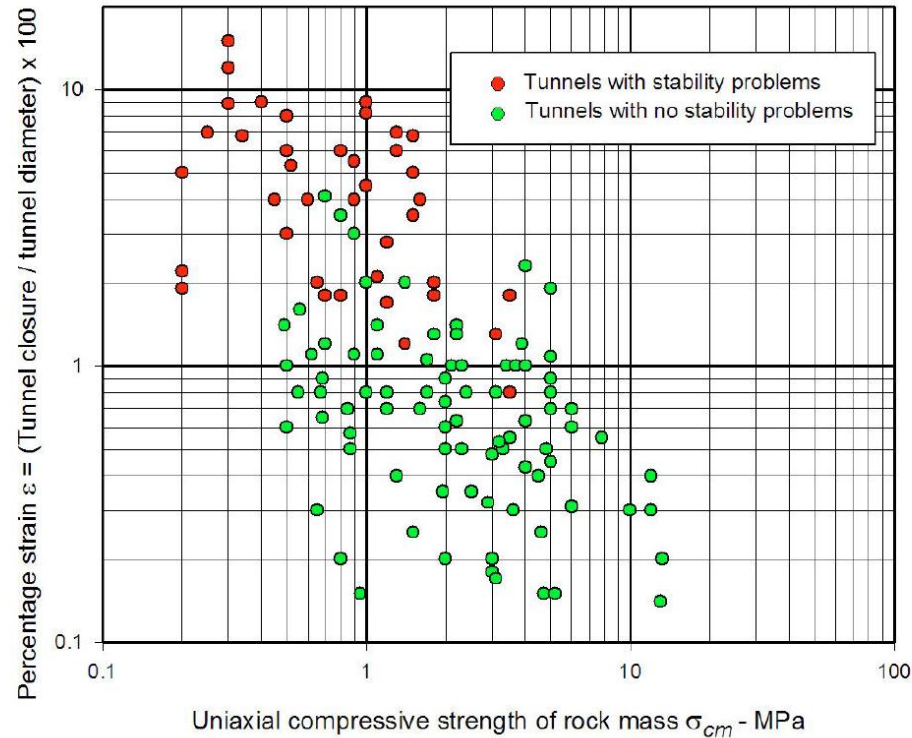


Figure 6: Field observations by Chern et al (1998) from the Second Freeway, Pinglin and New Tienlun headrace tunnels in Taiwan.

Figure 5 is for the condition of zero support pressure ($p_i = 0$). Similar analyses were run for a range of support pressures versus in situ stress ratios (p_i/p_o) and a statistical curve fitting process was used to determine the best fit curves for the generated data for each p_i/p_o value. The resulting curve for tunnel displacement for different support pressures is given in Figure 7.

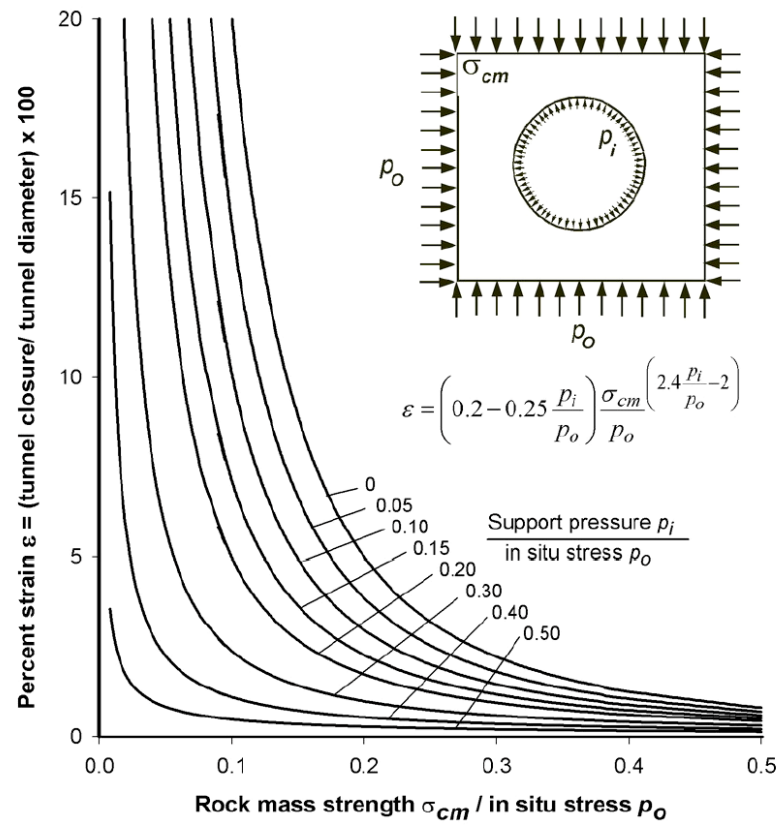


Figure 7: Ratio of tunnel deformation to tunnel radius versus the ratio of rock mass strength to in situ stress for different support pressures.

The series of curves shown in Figures 7 are defined by the equation:

$$\varepsilon\% = \frac{u_i}{r_o} \times 100 = \left(0.2 - 0.25 \frac{p_i}{p_o} \right) \frac{\sigma_{cm}}{p_o} \left(\frac{2.4 \frac{p_i}{p_o} - 2}{p_o} \right) \quad (8)$$

where r_p = Plastic zone radius

u_i = Tunnel sidewall deformation

r_o = Original tunnel radius in metres

p_i = Internal support pressure

p_o = In situ stress = depth below surface \times unit weight of rock mass

σ_{cm} = Rock mass strength = $2c' \cos \phi' / (1 - \sin \phi')$

A similar analysis was carried out to determine the size of the plastic zone surrounding the tunnel and this is defined by:

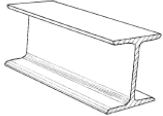
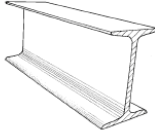
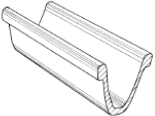
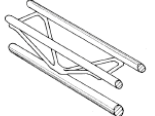
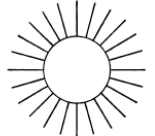
$$\frac{rp}{ro} = \left(1.25 - 0.625 \frac{p_i}{p_o} \right) \frac{\sigma_{cm}}{p_o} \left(\frac{p_i}{p_o} \right)^{-0.57} \quad (9)$$


Estimates of support capacity

Hoek and Brown (1980a) and Brady and Brown (1985) have published equations which can be used to calculate the capacity of mechanically anchored rockbolts, shotcrete or concrete linings or steel sets for a circular tunnel. No useful purpose would be served by reproducing these equations here but they have been used to estimate the values plotted in Figure 8 (from Hoek, 1998).

Figure 8 gives maximum support pressures (p_{sm}) and maximum elastic displacements (u_{sm}) for different support systems installed in circular tunnels of different diameters. Note that, in all cases, the support is assumed to act over the entire surface of the tunnel walls. In other words, the shotcrete and concrete linings are closed rings, the steel sets are complete circles, and the mechanically anchored rockbolts are installed in a regular pattern that completely surrounds the tunnel.

Because this model assumes perfect symmetry under hydrostatic loading of circular tunnels, no bending moments are induced in the support. In reality, there will always be some asymmetric loading, particularly for steel sets and shotcrete placed on rough rock surfaces. Hence, induced bending will result in support capacities that are lower than those given in Figure 8. Furthermore, the effect of not closing the support ring, as is frequently the case, leads to a drastic reduction in the capacity and stiffness of steel sets and concrete or shotcrete linings.

Support type	Flange width - mm	Section depth - mm	Weight - kg/m	Curve number	Maximum support pressure $p_{i\max}$ (MPa) for a tunnel of diameter D (metres) and a set spacing of s (metres)	
 Wide flange rib	305	305	97	1	$p_{i\max} = 19.9D^{-1.23}/s$	
	203	203	67	2	$p_{i\max} = 13.2D^{-1.3}/s$	
	150	150	32	3	$p_{i\max} = 7.0D^{-1.4}/s$	
	203	254	82	4	$p_{i\max} = 17.6D^{-1.29}/s$	
 I section rib	152	203	52	5	$p_{i\max} = 11.1D^{-1.33}/s$	
	171	138	38	6	$p_{i\max} = 15.5D^{-1.24}/s$	
 TH section rib	124	108	21	7	$p_{i\max} = 8.8D^{-1.27}/s$	
	220	190	19	8	$p_{i\max} = 8.6D^{-1.03}/s$	
 3 bar lattice girder	140	130	18	9	$p_{i\max} = 18.3D^{-1.02}/s$	
	220	280	29	10	$p_{i\max} = 0.354/s^2$	
 Rockbolts or cables spaced on a grid of $s \times s$ metres	140	200	26	11	$p_{i\max} = 0.267/s^2$	
	19	108	21	12	$p_{i\max} = 0.184/s^2$	
	17	108	21	13	$p_{i\max} = 0.10/s^2$	
	SS39 Split set	14	108	21	14	$p_{i\max} = 0.05/s^2$
	EXX Swellex	15	108	21	15	$p_{i\max} = 0.11/s^2$
	20mm rebar	16	108	21	16	$p_{i\max} = 0.17/s^2$
	22mm fibreglass	17	108	21	17	$p_{i\max} = 0.26/s^2$
	Plain cable	18	108	21	18	$p_{i\max} = 0.15/s^2$
	Birdcage cable	19	108	21	19	$p_{i\max} = 0.30/s^2$

Support type	Thickness - mm	Age - days	UCS - MPa	Curve number	Maximum support pressure $p_{i\max}$ (MPa) for a tunnel of diameter D (metres)
 Concrete or shotcrete lining	1m	28	35	20	$p_{i\max} = 57.8D^{-0.92}$
	300	28	35	21	$p_{i\max} = 19.1D^{-0.92}$
	150	28	35	22	$p_{i\max} = 10.6D^{-0.97}$
	100	28	35	23	$p_{i\max} = 7.3D^{-0.98}$
	50	28	35	24	$p_{i\max} = 3.8D^{-0.99}$
	50	3	11	25	$p_{i\max} = 1.1D^{-0.97}$
	50	0.5	6	26	$p_{i\max} = 0.6D^{-1.0}$

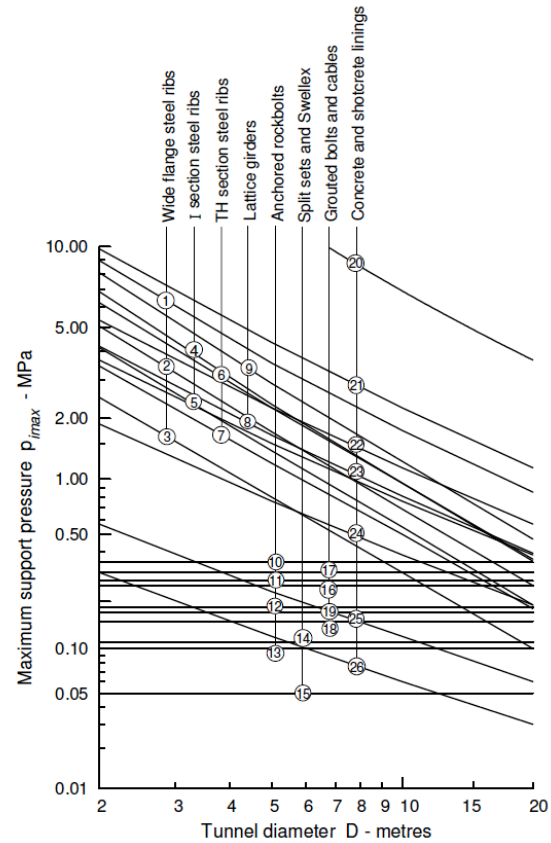


Figure 8: Approximate maximum capacities for different support systems installed in circular tunnels. Note that steel sets and rockbolts are all spaced at 1 m.

ANALISI DEL COMPORTAMENTO ALLO SCAVO (IN ASSENZA DI INTERVENTI)

Esaminiamo il comportamento allo scavo del fronte, in funzione delle caratteristiche geomeccaniche degli ammassi e considerate le coperture geostatiche più rappresentative presenti in progetto, in assenza di interventi.

La valutazione dell'evoluzione dello stato tensionale nel terreno a seguito della realizzazione di una galleria viene condotta attraverso l'analisi dei fenomeni deformativi del mezzo attraversato, che forniscono informazioni sul comportamento della cavità nei riguardi della stabilità a breve e a lungo termine.

Il comportamento del cavo e del fronte è infatti funzione, oltre che delle caratteristiche geometriche della cavità stessa e dei carichi litostatici cui è soggetta, delle caratteristiche di resistenza e di deformabilità del nucleo d'avanzamento, inteso come il prisma di terreno individuato a monte del fronte dallo stesso profilo di scavo per una profondità di circa un diametro. Infatti, se il nucleo non è costituito da materiale sufficientemente rigido e resistente, tale da mantenere in campo elastico il proprio comportamento tenso-deformativo, si sviluppano fenomeni deformativi e plasticizzazioni rilevanti in avanzamento sul fronte, cui conseguono il detensionamento e il decadimento delle caratteristiche geomeccaniche del terreno al contorno del cavo. Se, viceversa, il comportamento del nucleo d'avanzamento si mantiene in campo elastico, esso svolge un'azione di precontenimento del cavo, che si mantiene a sua volta in condizioni elastiche, conservando le caratteristiche di massima resistenza del materiale attraversato.

LE CONDIZIONI AL FRONTE

Lungo lo sviluppo della galleria si hanno le tre situazioni indicate in figura: N è quella di una zona a sufficiente distanza dal fronte, B è quella presente in corrispondenza del fronte di scavo e V è quella relativa alle condizioni iniziali di sollecitazione dell'ammasso roccioso, prima che si incominci a risentire dell'avvicinamento del fronte.

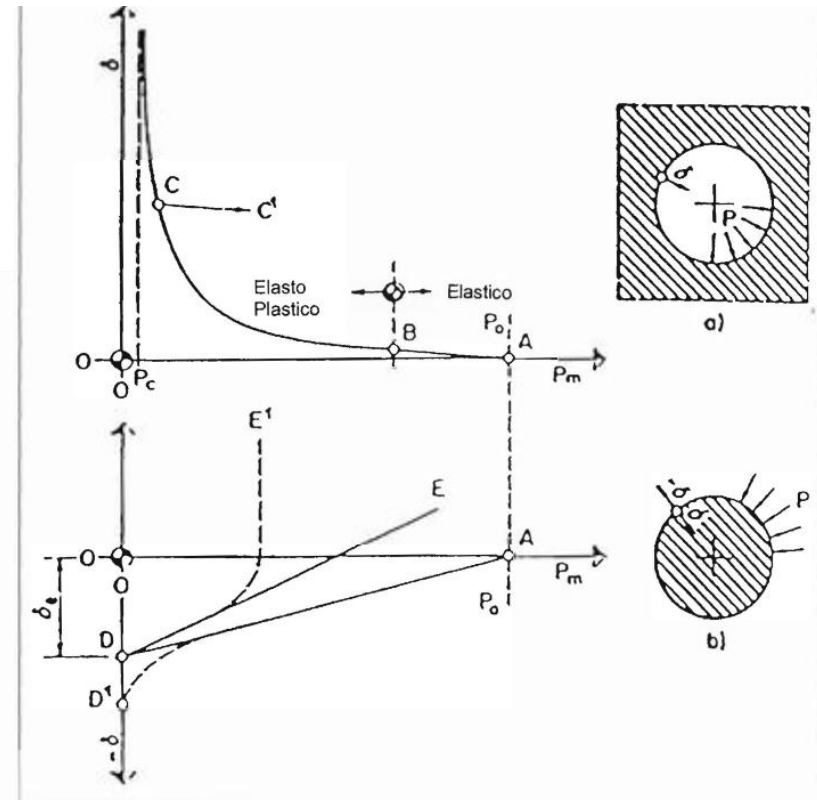
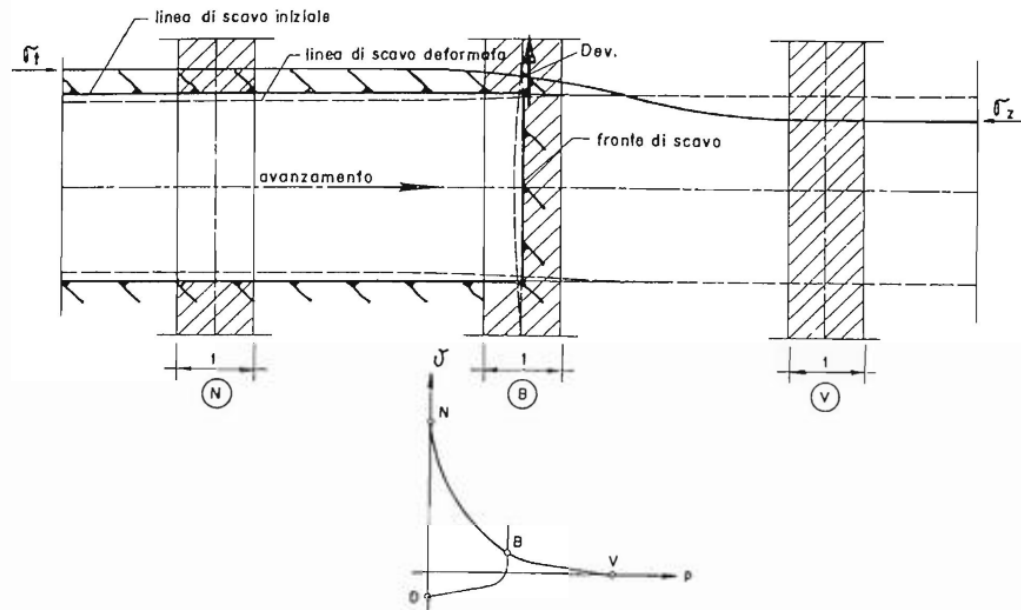


Figura 6.23. Curve caratteristiche del nucleo scavato in prossimità del fronte: a) per l'ammasso roccioso; b) per il nucleo di roccia asportato; nel caso di comportamento elastico ed elasto-plastico

Il comportamento del fronte di scavo, al quale è legato quello della cavità, può essere sostanzialmente ricondotto alle seguenti tre categorie:

Categoria A: Galleria a fronte stabile

Se il fronte di scavo è stabile, lo stato tensionale al contorno della cavità in prossimità del fronte si mantiene in campo prevalentemente elastico, ed i fenomeni deformativi osservabili sono di piccola entità e tendono ad esaurirsi rapidamente. In questo caso anche il comportamento del cavo sarà stabile, mantenendosi prevalentemente in campo elastico, e quindi non si rendono necessari interventi preventivi di consolidamento, se non localizzati e in misura molto ridotta. Il rivestimento definitivo costituirà allora il margine di sicurezza per la stabilità a lungo termine.

Categoria B: Galleria a fronte stabile a breve termine

Questa condizione si verifica quando lo stato tensionale indotto dall'apertura della cavità supera la resistenza meccanica del materiale al fronte, che non ha più un comportamento di tipo elastico, ma rientra nell'ambito di un comportamento di tipo elasto-plastico. I fenomeni deformativi connessi con la conseguente redistribuzione delle tensioni risultano più accentuati che nel caso precedente, e producono nell'ammasso al fronte una decompressione che porta al superamento della resistenza caratteristica del materiale. Questa decompressione può essere opportunamente controllata con adeguati interventi di preconsolidamento del fronte e/o di consolidamento al contorno del cavo. In tal modo si fornisce l'opportuno contenimento all'ammasso, che manterrà un comportamento stabile. Nel caso non si prevedano opportuni interventi, lo stato tenso-deformativo potrà evolvere verso situazioni di instabilità del cavo durante le fasi realizzative. Anche in questo caso, il rivestimento definitivo costituirà il margine di sicurezza per il comportamento a lungo termine.

Categoria C: Galleria a fronte instabile

L'instabilità progressiva del fronte di scavo è attribuibile ad un accentuarsi dei fenomeni deformativi in campo plastico, che risultano immediati e più rilevanti, manifestandosi prima ancora che avvenga lo scavo, oltre il fronte stesso. Tali deformazioni producono una decompressione significativa dell'ammasso al fronte, e portano ad un progressivo e rapido decadimento delle caratteristiche geomeccaniche del materiale. Questo tipo di decompressione più accentuata deve essere contenuta prima dell'arrivo del fronte di scavo, e richiede pertanto interventi di preconsolidamento sistematici in avanzamento, che consentano di creare artificialmente l'effetto arco capace di far evolvere la situazione verso configurazioni di equilibrio stabile.

Per la determinazione delle categorie di comportamento, occorre prendere in esame le seguenti caratteristiche:

- le caratteristiche di resistenza e deformabilità dell'ammasso connesse con le varie strutture geologiche che interessano le gallerie;
- i carichi litostatici corrispondenti alle coperture in gioco;
- la forma e le dimensioni della sezione di scavo;
- lo schema di avanzamento.

Tipologie di intervento in fase costruttiva

Sono stati definiti tre tipi di comportamento d'ammasso allo scavo che prevedono l'impiego di opportuni interventi scelti in base alle caratteristiche geotecniche/geomeccaniche dei terreni interessati dagli scavi, determinando così la scelta delle sezioni tipo più adatte.

CASO A) fronte stabile:

I fenomeni deformativi avvengono in campo elastico; il materiale ha comportamento di tipo lapideo per cui si possono ipotizzare locali fenomeni di instabilità al contorno riconducibili per lo più al distacco gravitativo di blocchi o volumi rocciosi, individuati dall'intreccio di superfici di discontinuità preesistenti nell'ammasso oppure create dai fenomeni di distensione prodotti dalle modalità di scavo. Il probabile comportamento allo scavo tipo A, "a fronte stabile", consente di prevedere, quali interventi di prima fase, interventi di solo contenimento del cavo, quale la realizzazione di uno strato di spritz-beton a seguito della messa in opera di bulloni radiali o centine, in funzione del grado di discontinuità dell'ammasso. I carichi gravanti sulla struttura in questi contesti geomeccanici sono prevalentemente di tipo gravitativo, funzione della frequenza dei giunti e delle fratture ed in particolare modo della resistenza al taglio delle superfici di discontinuità. Il rilascio di tali solidi di carico, in categorie di comportamento tipo A, non avviene generalmente all'apertura del cavo, bensì in un secondo tempo quale conseguenza del richiamo di umidità al contorno dello scavo, della circolazione d'acqua nelle fratture, dall'alterazione della roccia a contatto con gli agenti atmosferici, nonché dalle sollecitazioni dinamiche conseguenti alle vibrazioni prodotte durante le operazioni di scavo con esplosivo. E' pertanto opportuno stabilizzare i suddetti cunei mediante la messa in opera di bulloni metallici radiali di tipo passivo, ad ancoraggio puntuale in presenza di modesti gradi di separazione d'ammasso, o ad ancoraggio continuo per gradi di separazione maggiori, e realizzare un guscio di spritz-beton a protezione della superficie di scavo ed a contenimento del cavo.

CASO B) fronte stabile a breve termine:

Si possono ipotizzare fenomeni di instabilità più o meno diffusi al contorno del cavo, dovuti alla plasticizzazione dell'ammasso roccioso e conseguenti fenomeni deformativi (convergenze radiali) di ordine centimetrico. Tali deformazioni, se non regimate mediante opportuni e tempestivi interventi di preconsolidamento e/o di consolidamento, possono innescare decompressioni progressivamente crescenti all'interno dell'ammasso roccioso, sviluppando di conseguenza carichi maggiori sia nel breve termine che nel lungo termine.

Come interventi di preconsolidamento si possono utilizzare: chiodi in vetroresina al fronte per aumentare le caratteristiche di resistenza del nucleo; drenaggi al contorno in caso di presenza d'acqua per lo scarico delle pressioni interstiziali.

Gli interventi di consolidamento lungo la cavità consistono principalmente in: priverestimento costituito da spritz-beton; centine metalliche. Questi interventi di preconsolidamento e consolidamento concorreranno a formare diverse sezioni tipo (descritte in seguito) che si differenziano tra di loro in funzione delle formazioni geologiche incontrate.

CASO C) fronte instabile:

I fenomeni deformativi, in assenza di interventi, sono di entità maggiore rispetto al caso precedente, fino ad arrivare alla rottura e al collasso del cavo, legato all'instabilità del fronte di scavo. Perché si possa realizzare l'avanzamento in galleria, senza innescare fenomeni deformativi incontrollabili, è indispensabile operare "preconsolidamenti" lanciati oltre il fronte di scavo, che garantiscano sia la tenuta del fronte stesso che quella della fascia di terreno perimetrale al cavo. Questi preconsolidamenti possono essere di diversa natura, in funzione delle differenti caratteristiche geologiche delle formazioni attraversate lungo il tracciato:

- jet-grouting sub-orizzontale o micropali;
- anello consolidato da iniezioni cementizie;
- chiodi in vetroresina al fronte;
- drenaggi.

Sono inoltre necessari interventi di consolidamento al contorno del cavo in modo da fornire il necessario contenimento nel breve termine. Questi interventi possono essere il rivestimento di 1^a fase con spritz-beton e centine metalliche. In previsione di un comportamento tipo C, al fine di effettuare un controllo dello stato deformativo al fronte, appare consigliabile l'esecuzione di un preconsolidamento sistematico del fronte mediante elementi strutturali o tubi in vetroresina ad aderenza migliorata, tali da irrigidire il nucleo di scavo e ridurre i valori di estrusione del fronte e conseguentemente di preconvergenza del cavo. Tale operazione consentirebbe di mantenere le proprietà del materiale prossime alle condizioni di picco, o al limite di ridurre il decadimento. Le deformazioni al fronte si traducono infatti in decompressione al contorno del cavo con decremento della resistenza d'ammasso e incremento delle spinte sui priverestimenti.

Andrà inoltre prevista la realizzazione dei priverestimenti a seguito di ogni singolo sfondo di avanzamento, mediante posa in opera di centine metalliche ed un congruo strato di spritz-beton.

Sempre per la categoria di comportamento C occorre inoltre prevedere la possibilità di stabilizzare, a breve distanza dal fronte, il piede della centina, mediante il getto di arco rovescio e murette a distanze anche inferiori ai 2 diametri dal fronte di scavo.

ANALISI DELLE CATEGORIE DI COMPORTAMENTO

Nella fase di diagnosi, sulla base degli elementi raccolti nella fase conoscitiva, vengono sviluppate le previsioni sul comportamento deformativo del cavo in assenza di interventi, al fine di giungere all'individuazione di tratte a comportamento omogeneo, suddivise nelle tre categorie di comportamento precedentemente descritte.

Gli strumenti numerici che possono essere adottati per la determinazione del comportamento dell'ammasso allo scavo sono vari, tra questi troviamo:

- 1) Metodo delle Linee Caratteristiche;
- 2) Analisi di stabilità al fronte mediante il "Metodo di Tamez";
- 3) Analisi con il "Metodo di Broms e Bennemark".

L'analisi di stabilità al fronte mediante "Metodo di Tamez" risulta utile laddove valori bassi di copertura geostatica sconsiglino l'applicazione del "Metodo delle Linee Caratteristiche"; infatti, venendo a mancare l'ipotesi di base, ovvero che la pressione al contorno del cavo sia di tipo idrostatica, i risultati forniti dal "Metodo delle Linee Caratteristiche" sarebbero poco rappresentativi del reale comportamento dell'ammasso; in questi casi, un'indicazione della stabilità del fronte di scavo a basse coperture può, invece, essere fornita dal Metodo di Tamez che valuta l'equilibrio limite del prisma di terreno potenzialmente instabile in prossimità del fronte; tuttavia questo strumento non fornisce indicazioni sul comportamento deformativo dell'ammasso in prossimità del fronte e quindi non può essere impiegato quale unico strumento per la definizione degli interventi di stabilizzazione da prevedere in avanzamento. Le analisi di stabilità del fronte mediante la metodologia di Broms e Bennemark, permette di stimare le condizioni di stabilità in condizioni non drenate, con riferimento al breve termine.

Metodo delle Linee Caratteristiche

Le linee caratteristiche consistono nel simulare lo scavo di una galleria nell'ipotesi di simmetria assiale e di stato di deformazione piana.

Per linee caratteristiche di una cavità si intendono delle curve che legano le pressioni di contenimento, esercitate in senso radiale sul bordo della galleria dalle opere di stabilizzazione e di rivestimento, agli spostamenti radiali al suo contorno (convergenze).

Lo scavo è rappresentato come una graduale riduzione di una pressione fittizia "p" applicata alle pareti della galleria, tramite cui si simula il progressivo deconfinamento del terreno prodotto dall'avvicinarsi del fronte di scavo alla sezione di calcolo e al successivo avanzamento del fronte stesso, cui corrisponde una convergenza radiale "u" crescente in funzione delle caratteristiche dell'ammasso.

Esse possono quindi essere utilizzate, oltre che per valutare il comportamento dell'ammasso allo scavo, anche per determinare lo stato di sollecitazione sui diversi interventi costituenti la galleria, mediante la sovrapposizione degli effetti delle curve caratteristiche della cavità e dei singoli interventi che la costituiscono. Per ogni galleria è possibile costruire due curve caratteristiche principali:

- la linea caratteristica del fronte, valida presso il fronte di scavo, detta curva caratteristica del fronte, che tiene conto dell'effetto tridimensionale delle tensioni vicino ad esso e che permette di risalire, mediante considerazioni sulla resistenza del nucleo, all'entità della convergenza già subita dalla galleria nella sezione in corrispondenza al fronte di scavo;
- la linea caratteristica del cavo, valida per qualsiasi sezione sufficientemente lontana dal fronte, detta curva caratteristica della cavità, per la quale lo stato di tensione può considerarsi piano. In generale, ove la curva caratteristica non intersechi in un valore finito l'asse delle deformazioni radiali, la galleria risulta instabile senza adeguati interventi di stabilizzazione.

Se la galleria è scavata in assenza di sostegni, il valore finale della pressione di confinamento è pari a 0; in caso contrario allo stato finale è presente una pressione di confinamento > 0 che rappresenta la pressione di equilibrio del cavo ottenuta dall'intersezione della curva caratteristica della cavità e dei rivestimenti impiegati come spiegato nel seguito in dettaglio.

Sulla base delle elaborazioni effettuate, è quindi possibile esprimere delle considerazioni sul comportamento dell'ammasso allo scavo, con particolare riguardo alla prevedibile entità dei fenomeni deformativi del fronte e del cavo e all'estensione dell'eventuale fascia di materiale al contorno della cavità in cui il livello tensionale supera il limite elastico.

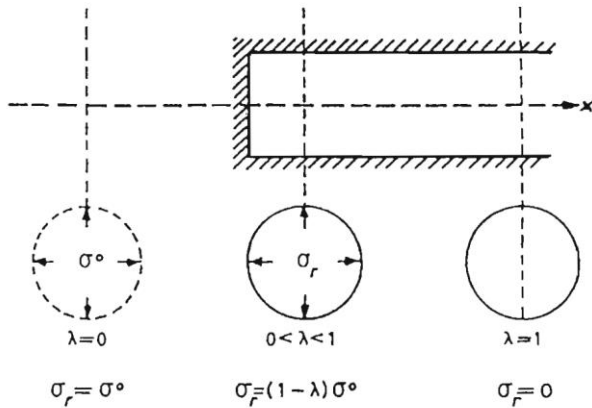
Valutando lo spostamento al fronte "u_f" è possibile pertanto individuare a priori il comportamento della galleria, distinguendo tra fronte stabile (A), stabile a breve termine (B) ed instabile (C).

In generale il Metodo delle Linee Caratteristiche è valido nei casi in cui si ritenga lecito ipotizzare che l'andamento delle sollecitazioni indotte dallo scavo, sotto l'azione delle spinte di montagna, sia di tipo idrostatico; ciò si verifica generalmente per coperture almeno $H > 3D$ (D = diametro di scavo della galleria); valori di copertura inferiori conducono a un risultato poco rappresentativo dell'effettivo comportamento dell'ammasso roccioso.

Lo scavo della galleria causa una variazione delle condizioni d'equilibrio preesistenti. All'avanzare del fronte si ha una progressiva chiusura, o convergenza, immediatamente dietro il fronte.

L'analisi delle convergenze, per il tratto più prossimo al fronte di scavo, è un problema tridimensionale che può essere analizzato con modelli numerici.

È stato mostrato che è possibile, considerando altre incertezze, affrontare il problema come un problema equivalente di deformazione piana. In un problema di deformazione piana, la tensione radiale σ_r è applicata al contorno della galleria e diminuisce da un valore iniziale σ^0 fino a zero, nel caso non vi sia alcun sostegno.



Il sostegno temporaneo fornito dal fronte della galleria, all'avanzamento tende a ridursi progressivamente. La tensione radiale σ_r simula l'effetto del fronte e tale supporto temporaneo fittizio è dato dalla seguente espressione:

$$\sigma_r = (1 - \lambda) \cdot \sigma^0$$

dove il parametro λ , definito tasso di deconfinamento, varia da 0 a 1.

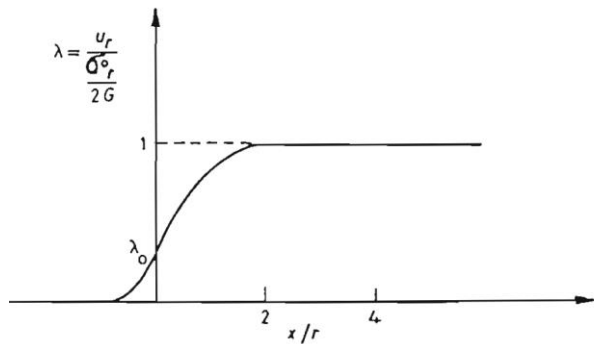
Nel caso elastico si ha che

$$\lambda = \frac{u_r(x)}{u_r^\infty}$$

dove

$u_r(x)$ è la componente radiale dello spostamento ad una distanza x dal fronte di scavo

u_r^∞ è la componente radiale dello spostamento a distanza infinita dal fronte.



Spostamento radiale in funzione della distanza dal fronte

Studi numerici sono stati condotti per studiare l'influenza dell'avanzamento del fronte sul comportamento della galleria. Panet e Guenot riportano i risultati di analisi numeriche effettuate con il programma agli elementi finiti ROSALIE (Laboratoire Central des Ponts et Chaussées).

Le analisi sono state effettuate considerando un mezzo elastico e un mezzo puramente coesivo con valori di coesione variabili in funzione del seguente parametro, definito numero di stabilità:

$$N_s = \frac{\sigma^0}{c_u}$$

Per il caso di comportamento elasto-plastico è stato adottato il criterio di rottura di Von Mises.

La figura 6.4 mostra l'andamento degli spostamenti, in funzione della distanza dal fronte x , per diversi valori di N_s (N_s è uguale a 1 per il caso elastico).

Per tenere conto dell'installazione differita nel tempo del rivestimento è stato introdotto, da Panet, il parametro λ_d che definisce il valore della pressione fittizia che permette di tenere in conto l'opera di sostegno operata dalla presenza del fronte al momento dell'installazione del rivestimento.

Con riferimento alla figura 6.3 si ha:

$$\sigma_f = (1 - \lambda_d) \cdot \sigma^0$$

In un mezzo elastico il valore di λ_d associato all'installazione del rivestimento al fronte è pari a:

$$\lambda_d = 0.265 = \frac{u(0)}{u^\infty}$$

In un mezzo elasto-plastico, tuttavia, questa relazione non è più valida poiché la curva caratteristica del terreno non è più lineare e il parametro λ non è più uguale a $u(x)/u^\infty$.

Inoltre, il fronte della stessa galleria si plasticizza. Per applicare con successo questo metodo progettuale, è essenziale conoscere la variazione della pressione di supporto fittizia σ_f in funzione della distanza dal fronte.

Questo è mostrato in figura 6.4(b) per diversi valori di N_s . Queste curve sono state ottenute confrontando le curve di reazione del terreno con le corrispondenti curve della figura 6.4a (convergenza in funzione della distanza dal fronte). Le curve di reazione del terreno sono state ricavate mediante modelli matematici agli elementi finiti. Dalla figura 6.4b si può notare che la pressione di supporto, in corrispondenza del fronte della galleria, diminuisce da $0.735 \sigma^0$ a $0.42 \sigma^0$, come N_s aumenta da 1 a 3.

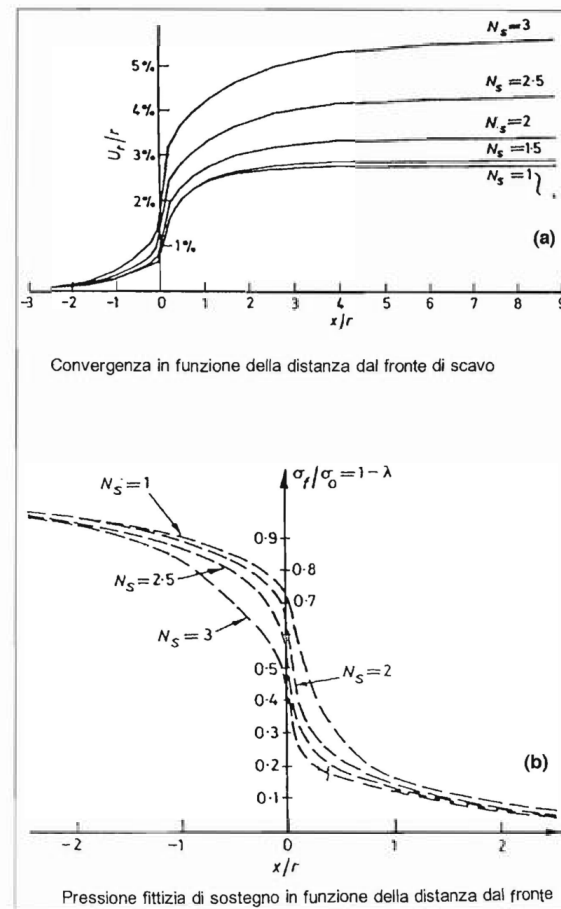


Figura 6.4. Andamento delle convergenze e della pressione fittizia di sostegno in funzione della distanza dal fronte

4.3.3. Metodo del tasso di deconfinamento critico λ_E (Panet, 1990)

Il metodo convergenza-confinamento proposto da Panet permette di analizzare l'interazione fra l'ammasso roccioso ed il sostegno in funzione dell'avanzamento del fronte di scavo.

La sua applicazione agli ammassi rocciosi a debole resistenza suppone la definizione di un mezzo continuo equivalente al quale attribuire un comportamento elastoplastico rammollente. In questi ammassi, lo scavo di una galleria situata a profondità tali da sviluppare la resistenza massima (gallerie profonde $H > 2D$), provoca elevate convergenze legate alla formazione di una zona decompressa attorno al cavo.

Sotto queste ipotesi, il criterio di Panet consente di verificare le condizioni di stabilità del cavo in funzione del valore critico del tasso di deconfinamento (λ_e) del materiale (valore cui si manifestano le prime plasticizzazioni). Tale indice, in relazione al criterio di rottura di Mohr-Coulomb, è funzione del coefficiente di spinta passiva K_p e del fattore di stabilità N secondo l'equazione:

$$\lambda_e = \frac{1}{K_p + 1} \left[K_p - 1 + \frac{2}{N} \right]$$

dove $N = \frac{2\sigma_z}{\sigma_c}$

Nel caso di una galleria priva di rivestimento, se $N < 1$, non si raggiunge mai la resistenza massima dell'ammasso roccioso. Raggiunto il limite di rottura ($N > 1$) l'autore suggerisce i seguenti valori limite del tasso di deconfinamento, ai quali corrispondono determinate condizioni di stabilità del fronte:

- se $0,6 < \lambda_e < 1$ il fronte di scavo è stabile; le pressioni raggiungono il valore massimo di resistenza dell'ammasso a tergo del fronte;
- se $0,3 < \lambda_e < 0,6$ il fronte di scavo è stabile a breve termine; al fronte di scavo le pressioni raggiungono il valore di resistenza massima prima in vicinanza del bordo poi verso il nucleo;
- se $\lambda_e < 0,3$ il fronte di scavo instabile; il fronte di scavo è in condizioni di instabilità per cui necessita di interventi preventivi di consolidamento.

Nel caso di un ammasso con comportamento elastico lineare, le tensioni radiale e circonferenziale sono legate al tasso di deconfinamento dalle seguenti espressioni:

$$\sigma_r = (1-\lambda)\sigma^0 \quad \sigma_\Theta = (1+\lambda)\sigma^0$$

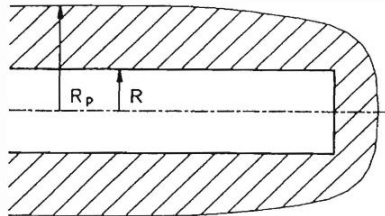
Se il criterio di rottura è espresso nella forma:

$$f(\sigma_1, \sigma_3) = 0$$

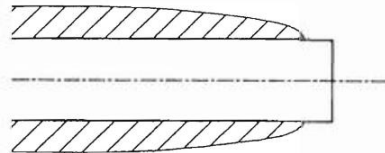
le condizioni di rottura sono ottenute, alla parete della galleria, per un valore del tasso di deconfinamento λ_e tale che (vedi figura 6.12)

$$f\left[(1+\lambda_e)\cdot\sigma^0, (1-\lambda_e)\cdot\sigma^0\right] = 0$$

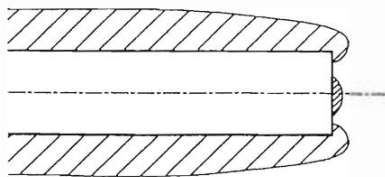
Nel caso del criterio di rottura di Tresca si ha



$N > 5$



$N < 2$



$2 < N < 5$

Figura 6.14. Modalità di plasticizzazione del cavo, all'avanzare del fronte di scavo

arretrata rispetto al fronte dovuta ad un eccesso di compressione sia radiale sia circonferenziale all'asse della galleria, e una zona di raccordo, tra le due zone, ad una distanza dal fronte tale che si ha una rotazione degli sforzi principali.

L'analisi delle condizioni di stabilità del fronte è essenziale per la scelta delle modalità di scavo e del tipo di sostegno.

Nel caso di instabilità del fronte di scavo, si deve ricorrere ad un sistema di sostegno che possa garantire la stabilità del fronte di scavo (presostegno o preconfinamento).

$$\lambda_e = \frac{C}{\sigma^0} = \frac{1}{N}$$

avendosi

$$N = \frac{2 \cdot \sigma^0}{\sigma_c}$$

Nel caso di una galleria non sostenuta, l'inizio della zona plastica si ha quando il tasso di deconfinamento diventa superiore a λ_e , e conseguentemente si sviluppa una zona plastica di raggio R_p (vedi figura 6.13).

Una volta che si sviluppa la zona plastica, è molto importante, in pratica, distinguere tre differenti situazioni (vedi figura 6.14):

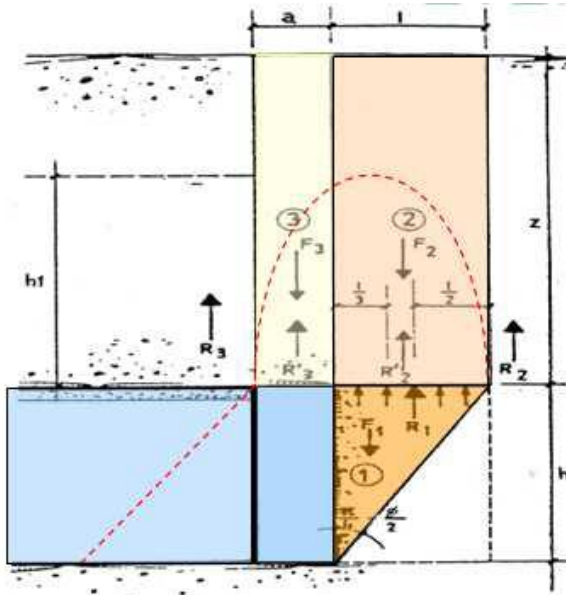
- la zona plastica è presente dietro il fronte di scavo e si può ammettere in prima approssimazione che si ha $N < 2$;
- il fronte di scavo è direttamente interessato dalla zona plastica, che si è sviluppata anche davanti al fronte. In questo caso si ha $N > 5$, la stabilità del fronte diventa critica e quindi si deve fare ricorso a tecniche di confinamento del fronte o di presostegno;
- abbiamo poi situazioni intermedie in cui $2 < N < 5$ e nelle quali si possono distinguere più zone di plasticizzazione: una zona davanti al fronte dovuta ad un eccesso di compressione radiale, una zona

METODO DI TAMEZ

La valutazione della stabilità del fronte di scavo può essere condotta mediante l'impiego di metodi analitici semplificati all'equilibrio limite. In particolare si fa riferimento alle teorie di Tamez e Cornejo che ipotizzano che esistano dei prismi di terreno in distacco secondo sezioni longitudinali, giungendo a definire un coefficiente di sicurezza FSF nei confronti della stabilità del fronte di scavo. Il metodo dell'equilibrio limite proposto da Tamez tiene conto della riduzione dello stato di confinamento triassiale del nucleo di terreno oltre il fronte per mezzo di un meccanismo di rottura del tipo effetto volta, con il quale il volume di terreno gravante sulla corona della galleria è definito da un paraboloide, approssimato mediante tre solidi prismatici, come illustrato nella figura seguente.

In questo modo si determinano le massime tensioni tangenziali che si possono sviluppare sulle facce di ogni prisma senza che avvengano scorrimenti (forze resistenti) e le forze di massa di ogni prisma (forze agenti). Il rapporto tra i momenti delle forze resistenti e delle forze agenti fornisce un coefficiente di sicurezza, denominato FSF (face security factor).

Al valore di FS definito dall'equilibrio limite può essere associato, indicativamente, un tipo di comportamento deformativo del fronte di scavo, secondo quanto descritto nella tabella esposta nel seguito.



FS	Comportamento del fronte di scavo
>2	Comportamento elastico
1.5 - 2	Comportamento <u>elasto</u> - plastico: cedimenti normalmente ammissibili
1.3 - 1.5	Comportamento <u>elasto</u> - plastico: cedimenti importanti
1 - 1.3	Incipiente rottura
<1	Rottura

FACE STABILITY ANALYSIS

Enrique Tamez Gonzáles - Diseño Geotécnico de Túneles (1997)

Stratigraphy and geotechnical properties

Overburden layers	ΔH [m]	γ_n [kNm^{-3}]	c'/Cu [kPa]	ϕ' [°]
layers ordering: from tunnel crown to ground surface				
IIIb	35.0	26.5	167	41.0

Tunnel Face layers	ΔH [m]	γ_n [kNm^{-3}]	c'/Cu [kPa]	ϕ' [°]
layers ordering: invert-crown				
IIIb	10.9	26.5	167	41.0

Excavation cross section and Failure Mechanism geometry

Total Overburden	H [m]	35.0
Surface load	q_s [kPa]	0.0
water table level above tunnel invert	H_w [m]	2.00
Tunnel full face area	A_{EXCAV} [m^2]	93.3
Tunnel face height	A [m]	10.90
Tunnel face width	D [m]	11.80

Equivalent tunnel diameter	D_{eq} [m]	10.90
Free span length	a [m]	3.0
45.90		
Failure Mechanism geometry		
Discharge zone height	Z_d [m]	20.06
Length of prisms in advance	L_p [m]	4.97

Failure Mechanism Prisms - Average geotechnical properties

Prisms 1		
Average buoyant unit weight	γ_b [kNm^{-3}]	24.7
Average saturated unit weight	γ_n [kNm^{-3}]	26.5
Average cohesion	c_u [kPa]	167.0
Average friction angle	ϕ'_E [°]	41.0
Coefficient of passive earth pressure	K_p [-]	4.81

Prisms 2-3		
Average buoyant unit weight	γ_b [kNm^{-3}]	26.5
Average saturated unit weight	γ_n [kNm^{-3}]	26.5
Average cohesion within Discharge Zone	c_u [kPa]	167.0
Average friction angle within Discharge Zone	ϕ'_p [°]	41.0
Friction Coefficient within Discharge Zone	K_f [-]	0.40

Prismatic volumes shear resistance and Safety factors

Failure Mechanism wedges - Effective stresses		
Eff. vert. stress at discharge-zone top	σ'_{vd} [kPa]	396
Eff. vertical stress at 1/3 discharge zone	σ'_{vd} [kPa]	264
Eff. vertical stress at 2/3 discharge zone	σ'_{vd} [kPa]	132
Undist. eff. vertical stress at crown	σ'_v [kPa]	928
Undist. eff. vert. stress at tunnel springline	σ'_{v0} [kPa]	1072

Pore Pressure distribution		
pore pressure at discharge-zone top	u_d [kPa]	0
pore pressure at 1/3 discharge-zone	$u_{d1/3}$ [kPa]	0
pore pressure at 2/3 discharge-zone	$u_{d2/3}$ [kPa]	0
pore pressure at tunnel springline	u_0 [kPa]	0
pore pressure at tunnel invert	u_i [kPa]	20

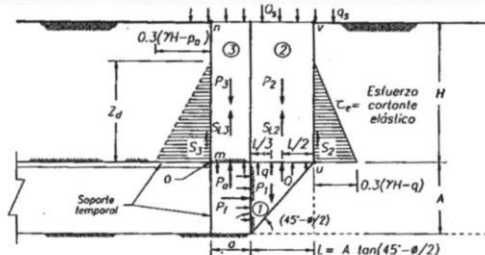
Failure Mechanism wedges - Unit strengths		
Face wedge unit strength (prism 1)	q [kPa]	855
Unit shear strength (prisms 2)	τ_{m2} [kPa]	184.3
Unit shear strength (prism 3)	τ_{m3} [kPa]	135.0

Tunnel-face global stability ($M\Sigma_u/M\Sigma_v$)	FS_g	2.33
<i>Admissible Safety Factors: 2.0 (rockmass brittle behaviour) / 1.6 (rockmass ductile behaviour)</i>		

Crown prism stress-field check (lateral boundaries)	
$k_c/0.3(\gamma H - p_a) = 0.2$	plastic deformations
Crown prism vertical-stress field (Terzaghi's arching effect) C_{v0} [kPa]	
z_1 : Vertical dist. from tunnel boundary [m] = 0.01	0.29

Crown-wedge stability (vertical sliding) <i>(Shear stresses: elastic field)</i>	FS_c	2.44
Crown wedge local stability (against plasticization):		verified

Simplified failure mechanism at tunnel face - Acting forces equilibrium



Un secondo metodo per valutare la stabilità del fronte è basato sulla definizione del rapporto di stabilità definito da Broms e Bennermark (1967) nella seguente maniera:

$$N = \frac{\sigma_s + \gamma z - \sigma_T}{c_u}$$

dove:

- γ = peso dell'unità di volume del terreno
- z = profondità dell'asse della galleria
- σ_s = sovraccarico eventualmente presente in superficie
- σ_T = eventuale pressione di sostegno applicata al fronte
- c_u = resistenza al taglio, in condizioni non drenate, alla profondità della galleria.

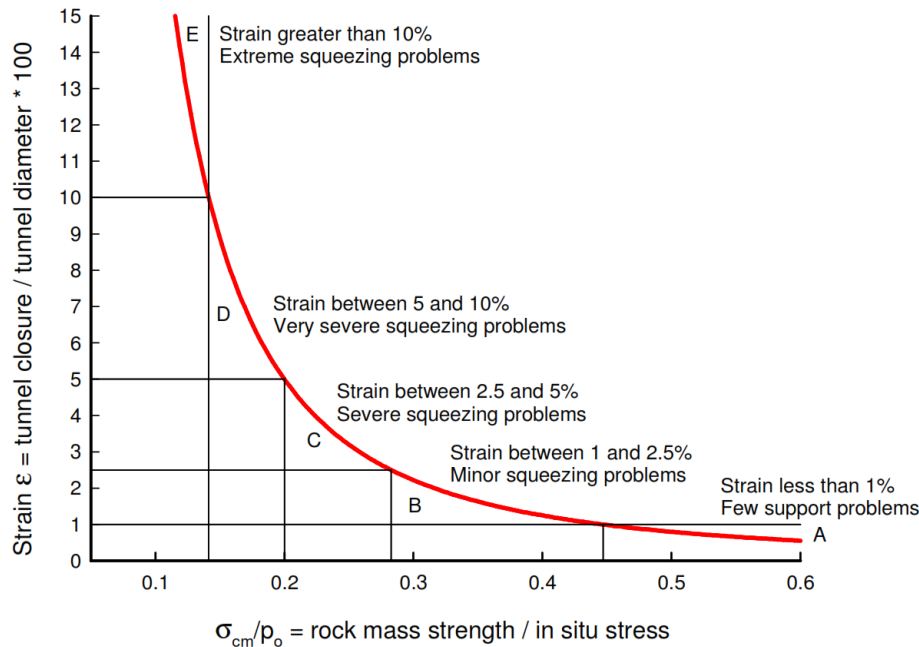
Sulla base di prove di estrusione eseguite in laboratorio e d'osservazioni in sito, Broms e Bennermark (1967) hanno concluso che il valore del rapporto di stabilità critico N_c perché si manifesti il collasso è pari a circa 6. A conclusioni simili giunse Peck (1969).

Il rapporto di stabilità definito da Broms e Bennermark può ovviamente essere visto come un coefficiente di sicurezza, ma tenendo tuttavia in conto che un valore del rapporto di stabilità più elevato corrisponde ad un coefficiente di sicurezza più basso e pertanto il margine di sicurezza non è facilmente definibile.

La seguente tabella fornisce una indicazione della relazione fra il numero di stabilità e le deformazioni attese (P.B. Attewell in Geddes, 1978).

N	Deformazioni
< 1	Trascurabili
1 – 2	Elastiche
2 – 4	Elasto-plastiche
4-6	Plastiche
> 6	Collasso

Tabella 1. Relazione fra il numero di stabilità e le deformazioni attese



	Strain ε %	Geotechnical issues	Support types
A	Less than 1	Few stability problems and very simple tunnel support design methods can be used. Tunnel support recommendations based upon rock mass classifications provide an adequate basis for design.	Very simple tunnelling conditions, with rockbolts and shotcrete typically used for support.
B	1 to 2.5	Convergence confinement methods are used to predict the formation of a 'plastic' zone in the rock mass surrounding a tunnel and of the interaction between the progressive development of this zone and different types of support.	Minor squeezing problems which are generally dealt with by rockbolts and shotcrete; sometimes with light steel sets or lattice girders are added for additional security.
C	2.5 to 5	Two-dimensional finite element analysis, incorporating support elements and excavation sequence, are normally used for this type of problem. Face stability is generally not a major problem.	Severe squeezing problems requiring rapid installation of support and careful control of construction quality. Heavy steel sets embedded in shotcrete are generally required.
D	5 to 10	The design of the tunnel is dominated by face stability issues and, while two-dimensional finite analyses are generally carried out, some estimates of the effects of forepoling and face reinforcement are required.	Very severe squeezing and face stability problems. Forepoling and face reinforcement with steel sets embedded in shotcrete are usually necessary.
E	More than 10	Severe face instability as well as squeezing of the tunnel make this an extremely difficult three-dimensional problem for which no effective design methods are currently available. Most solutions are based on experience.	Extreme squeezing problems. Forepoling and face reinforcement are usually applied and yielding support may be required in extreme cases.

Figure 7: Approximate relationship between strain and the degree of difficulty associated with tunnelling through squeezing rock. Note that this curve is for tunnels with no support.

Rock-Support interaction

As shown by equations 6 and 7 above, the extent of the plastic or failure zone and the amount of deformation in the rock mass surrounding the tunnel can be controlled by the application of an internal support pressure p_i . This support can be provided by combinations of rockbolts, steel sets and shotcrete or concrete linings. The interaction of the deforming rock mass and the resisting support can be illustrated in the plot given in Figure 8.

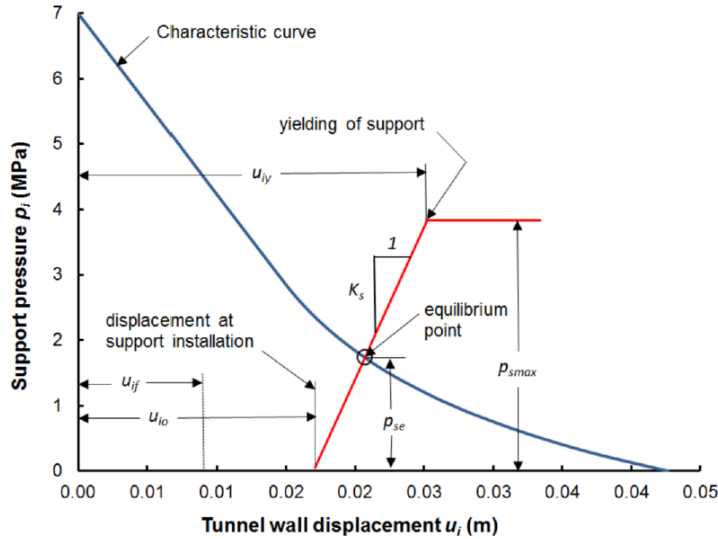


Figure 8: Rock-Support interaction plot.

Assuming that the support is installed at some distance behind the tunnel face, the displacement at this distance u_{io} is determined from Figure 7. The reaction of the installed support to on-going deformation depends upon the stiffness K_s of the support system and, as shown in Figure 8, the displacement u_{iy} of the tunnel at support yield is given by:

$$u_{iy} = u_{io} + \frac{p_{smax}}{K_s} \quad (12)$$

where p_{smax} is the capacity of the support.

If the support has sufficient capacity the rock-support interaction curve will intersect the characteristic curve of the tunnel at an equilibrium point where the deformation of the tunnel equals that of the support. The factor of safety (FS) of the support is then defined as the ratio of capacity to demand or

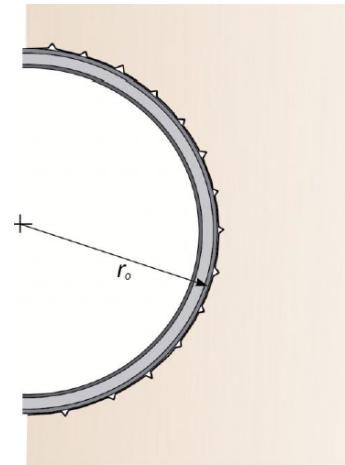
$$FS = \frac{p_{smax}}{p_{se}} \quad (13)$$

Estimation of support capacity

Hoek and Brown (1980a) and Brady and Brown (1985) published equations calculating the capacity of steel sets, shotcrete or concrete linings and rockbolts for a circular tunnel in a hydrostatic stress field.

An error in the equation for the support capacity of blocked steel sets¹ resulted in an overestimate of the support capacity of sets with very small block spacings, used to estimate the capacity of steel sets backing onto shotcrete or embedded in shotcrete. In many current tunnelling operations, particularly in TBM bored tunnels, the steel sets are placed in direct contact with the rock or with shotcrete used to backfill overbreak. Consequently, the equation for estimating the support capacity of steel sets has been simplified to that for sets in direct contact with the rock as illustrated in Figure 9.

Steel set support



σ_{ys} is the yield strength of the steel (MPa)
 E_s is the Young's modulus of the steel (MPa)
 A_s is the cross-sectional area of the section (m^2)
 s_l is the set spacing along the tunnel axis (m)
 r_o is the radius of the tunnel (m)

Figure 9 : Steel set support

The maximum support pressure p_{ssmax} of the sets is

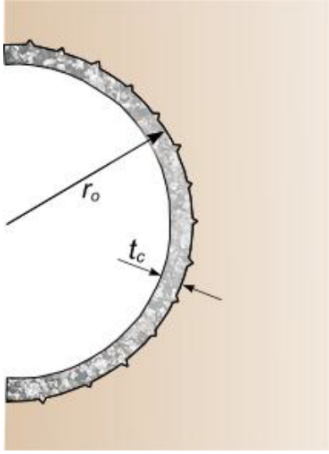
$$p_{ssmax} = \frac{A_s \sigma_{ys}}{s_l r_o} \quad (14)$$

¹ This error was pointed out by Mr Alex Lowson of Mott MacDonald who provided a corrected version of the equation. He also suggested that, in the context of this discussion, it was probably more appropriate to assume that the steel set is directly in contact with the rock surface or with a shotcrete layer used to fill overbreaks as shown in Figure 9.

The stiffness K_{ss} of the sets is

$$K_{ss} = \frac{E_s A_s}{s_l r_o^2} \quad (15)$$

Concrete or shotcrete linings



σ_{cc} is the uniaxial compressive strength of the concrete or shotcrete (MPa)
 E_c is the Young's modulus of the concrete or shotcrete (MPa)
 ν_c is the Poisson's ratio of the concrete or shotcrete
 t_c is the thickness of the lining (m)
 r_o is the radius of the tunnel (m)

Figure 10: Shotcrete support

The maximum support pressure p_{smax} is

$$p_{smax} = \frac{\sigma_{cc}}{2} \left[1 - \frac{(r_o - t_c)^2}{r_o^2} \right] \quad (16)$$

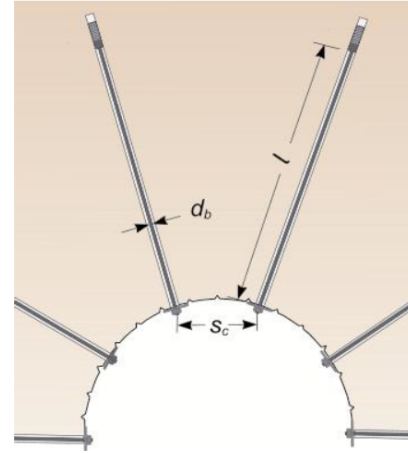
The stiffness K_{sc} is

$$K_{sc} = \frac{E_c (r_o^2 - (r_o - t_c)^2)}{2(1 - \nu^2)(r_o - t_c)r_o^2} \quad (17)$$

Rockbolts

The action of rockbolts and cables installed in the rock mass surrounding a tunnel can be complex. For example, fully grouted rockbolts act as reinforcement of the rock in much the same way as reinforcing steel acts in concrete. As a result they change the shape of the characteristic curve rather than provide internal support equivalent to that given by steel sets or shotcrete linings. On the other hand, ungrouted anchored rockbolts can be considered to resist the inward displacement of the rock mass and this is equivalent to the application of an internal support pressure in the tunnel.

For the sake of simplicity the following analysis is limited to the support provided by ungrouted mechanically or chemically anchored rockbolts or cables. More detailed numerical analyses of the interaction of rockbolts and failing rock masses are provided in other chapters in these notes.



d_b is the rockbolt or cable diameter (m)
 l is the free length of the bolt or cable (m)
 E_s is the Young's modulus of the bolt or cable (MPa)
 s_c is the circumferential bolt spacing (m)
 s_l is the longitudinal bolt spacing (m)
 T_{bf} is the ultimate bolt or cable load obtained from a pull-out test (MN)

Figure 11: Ungrouted rockbolt support

The maximum support pressure provided by a rockbolt pattern is

$$p_{sbmax} = \frac{T_{bf}}{s_l s_c} \quad (18)$$

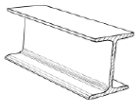

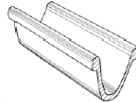
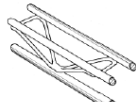
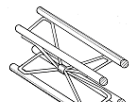


The elastic stiffness is

$$K_{sb} = \frac{E_s \pi d_b^2}{4l s_l s_c} \quad (19)$$

In applying equations 18 and 19 in a convergence-confinement analysis it is assumed that the rockbolts or cables are installed in a uniform pattern in the rock mass surrounding the tunnel. The length l of the bolts or cables should exceed the thickness of the plastic zone around the tunnel and the spacing s_c and s_l of the bolts should generally be less than half the bolt length.

Plot of maximum support pressures versus tunnel diameter

Figure 12a gives a range of typical support types used in tunnelling and the maximum support pressures for these support types are plotted in Figure 12b, for a range of tunnel radii.

Support type	Section depth - m	Flange width m	Sectional area m ²	Weight - kg/m	Curve number	Designation Metric/Imperial			
 Wide flange rib	0.307	0.305	0.0123	97	1	W310x97 / W12x65			
	0.216	0.206	0.0091	71	2	W200x71 / W8x48			
	0.162	0.154	0.00474	37.1	3	W150x37 / W6X25			
 I section rib	0.203	0.105	0.00436	34	4	S200x 34 / S8x23			
	0.152	0.084	0.00236	18.6	5	S150x18.6 / S6x12.5			
 TH section rib	0.148	0.172	0.0056	44	6	Toussaint-Heintzmann Profiles			
	0.118	0.135	0.0032	25	7				
 3 bar lattice girder	0.220	0.191	0.00197	19	8	Pantex type 130, 26 & 34mm bars			
	0.155	0.278	0.00197	18.2		Pantex type 95, 26 & 34mm bars			
 4 bar lattice girder	0.283	0.220	0.002828	27	9	Pantex type H1 220, 30 mm bars			
	0.164	0.100	0.002828	25.5		Pantex type Hi 100, 30 mm bars			
Shotcrete or concrete lining	Thickness	Curve number				Rockbolts		Diameter mm	Curve number
	1m	10							
	0.3 m	11					34	15	
	0.15 m	12					25	16	
	0.1 m	13					19	17	
	0.05 m	14					17	18	

The following assumptions were made in preparing these plots:

Yield strength of steel components $\sigma_{ys} = 245$ MPa

Uniaxial compressive strength of concrete or shotcrete $\sigma_{cc} = 35$ MPa

Steel sets are all spaced at 1 m along the tunnel axis

Rockbolts are all placed on a 1 m x 1 m grid pattern.

Note that some of the curves for steel sets are truncated to conform to the normal practice that the bend radius of a steel section should not exceed about 10 times the section depth.

The reader may find it surprising that tunnel radii of up to 20 m are included in Figure 12b. This has been done to show that the support capacity of steel sets and thin shotcrete linings fall to very low levels for large excavation radii. For large underground caverns it is more effective to use rockbolts or cables for support and, even if mesh-reinforced shotcrete is used to hold small rock pieces in place, the support capacity of this shotcrete is ignored in the overall design.

Almost every country involved in tunnelling has its own standards for steel support components and, hence, only a small selection has been included in Figure 12 in order to demonstrate the range of support pressures that can be considered. The reader is advised to consult local structural steel standards and manufacturer specifications for the properties of steel support elements available locally.

Figure 12a: Typical examples of support types used in tunnelling.

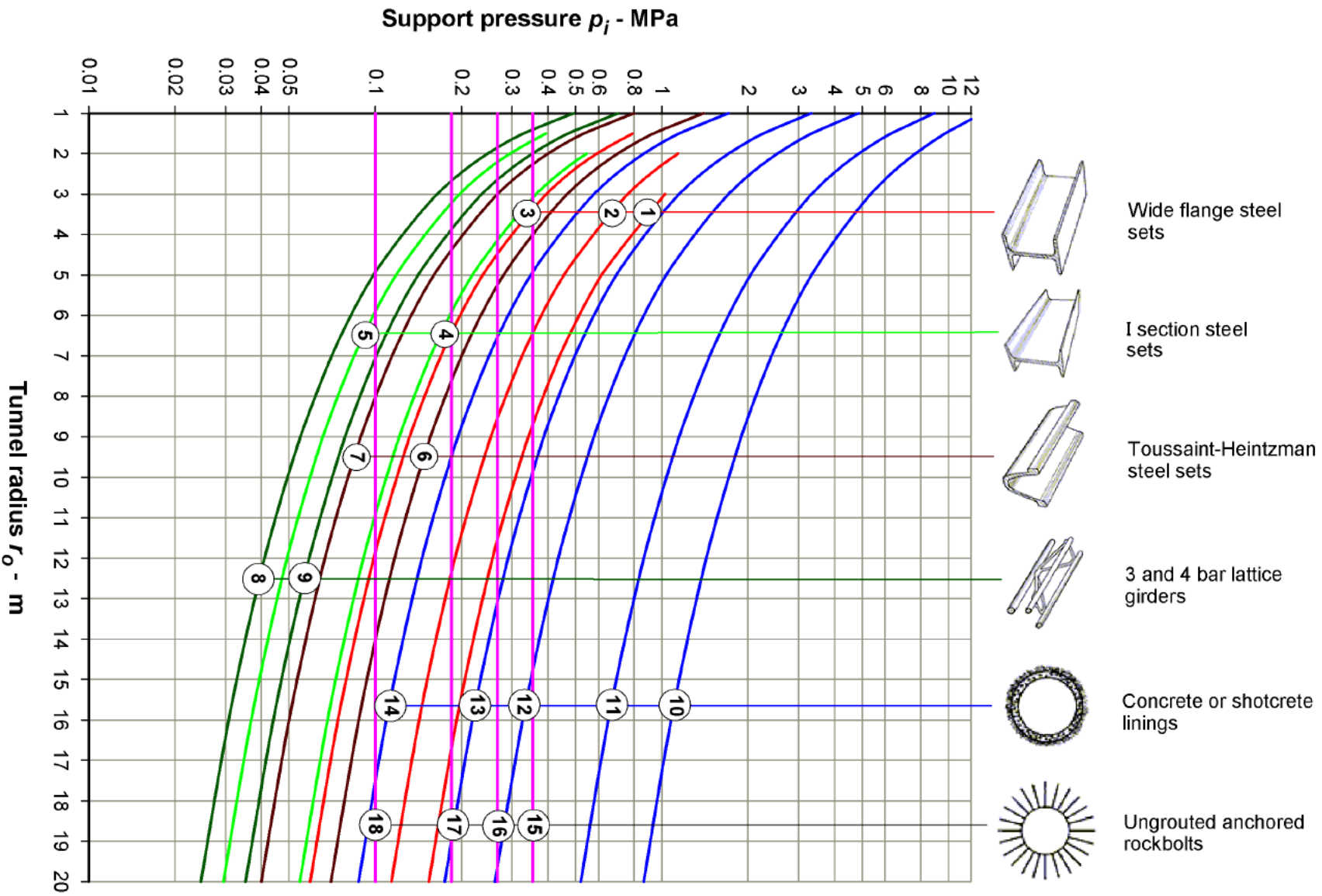


Figure 12b: Maximum support pressure versus tunnel radius for the range of support types defined in Figure 12a.

Figures 5 and 7 show that a crude estimate of the behaviour of the tunnel can be made if the ratio of rock mass strength to in situ stress is available. For the purpose of this analysis the in situ stress is estimated from the depth below surface and the unit weight of the rock. For a depth of 150 m and a unit weight of 0.027 MN/m^3 , the vertical in situ stress is approximately 4 MPa. The fault material is considered incapable of sustaining high differential stress levels and it is assumed that the horizontal and vertical stresses are equal within the fault zone.

In the case of the granodiorite, the laboratory uniaxial compressive strength is approximately 100 MPa. However, for the fault material, specimens can easily be broken by hand as shown in Figure 11. The laboratory uniaxial compressive strength of this material is estimated at approximately 10 MPa.

Based upon observations in the open pit mine slopes and utilizing the procedures described in the chapter on “Rock mass properties”, the granodiorite is estimated to have a GSI value of approximately 55. The fault zone, shown in Figure 9, has been assigned GSI = 15.

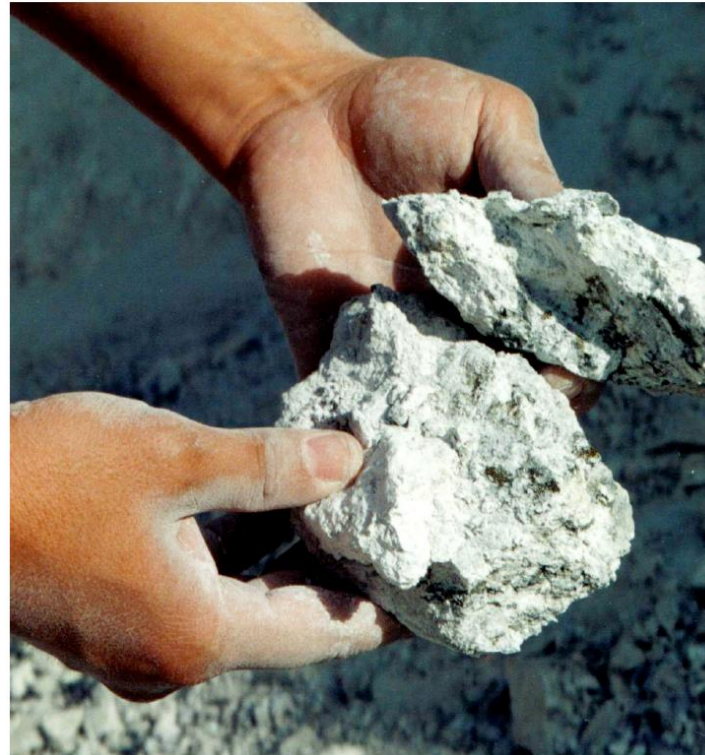


Figure 9: Heavily altered porphyry can easily be broken by hand.

The program RocLab³ implements the methodology described in the chapter on “Rock mass properties” and, in particular, the equations given in the 2002 version of the Hoek-Brown failure criterion (Hoek et al, 2002). This program has been used to calculate the global rock mass strength σ_{cm} for the granodiorite and the fault zone and the results are presented below:

Material	σ_{ci} - MPa	GSI	m_i	σ_{cm}	σ_{cm}/p_0
Granodiorite	100	55	30	33	8.25
Fault	10	15	8	0.6	0.15

Support requirements

Figures 5 and 6 show that, for the granodiorite with a ratio of rock mass strength to in situ stress of 8.25, the size of the plastic zone and the induced deformations will be negligible. This conclusion is confirmed by the appearance of an old drainage tunnel that has stood for several decades without any form of support. Based upon this evaluation, it was decided that no permanent support was required for the tunnel in the fair quality granodiorite. Spot bolts and shotcrete were installed for safety where the rock mass was more heavily jointed. The final appearance of the tunnel in granodiorite is shown in Figure 10.



Figure 10: Appearance of the drainage tunnel in fair quality granodiorite in which no permanent support was required. Spot bolts and shotcrete were installed for safety in jointed areas. The concrete lined drainage channel is shown in the centre of the tunnel floor.

In the case of the altered porphyry and fault material, the ratio of rock mass strength to in situ stress is 0.15. From Equation 9 the radius of plastic zone for a 2 m radius tunnel in this material is approximately 7.4 m without support. The tunnel wall deformation is approximately 0.18 m which translates into a tunnel strain of $(0.18/2)*100 = 9\%$.

Based on the observations by Sakurai (1983) and Chern et al (1998), the predicted strain of 9% for the mine drainage tunnel discussed earlier is clearly unacceptable and substantial support is required in order to prevent convergence and possible collapse of this section. Since this is a drainage tunnel, the final size is not a major issue and a significant amount of closure can be tolerated.

An approach that is frequently attempted in such cases is to install sufficient support behind the face of the tunnel to limit the strain to an acceptable level. Assuming a practical limit of 2% strain (from Figure 6), equation 8 and Figure 7 show that, for $\sigma_{cm}/p_o = 0.15$, an internal support pressure of approximately $p_i/p_o = 0.25$ is required to support the tunnel. For $p_o = 4$ MPa this means a support pressure $p_i = 1$ MPa.

Figure 8 shows that, for a 4 m diameter tunnel, a support in excess of 1 MPa can only be provided by a passive system of steel, sets, lattice girders, shotcrete or concrete lining or by some combination of these systems. These systems have to be installed in a fully closed ring (generally in a circular tunnel) in order to act as a load bearing structure. Rockbolts or cables, even assuming that they could be anchored in the fault material, cannot provide this level of equivalent support.

There are several problems associated with the installation of heavy passive support in this particular tunnel. These are:

1. The remainder of the drainage tunnel is horseshoe shaped as shown in Figure 10. Changing the section to circular for a relative short section of fault zone is not a very attractive proposition because of the limitations this would impose on transportation of equipment and materials through the zone.
2. The use of heavy steel sets creates practical problems in terms of bending the sets into the appropriate shape. A practical rule of thumb is that an H or I section can only be bent to a radius of about 14 times the depth of the section. Figure 11 which shows a heavy H section set being bent and there is significant buckling of the inside flange of the set.
3. The use of shotcrete or concrete lining is limited by the fact that it takes time for these materials to harden and to achieve the required strength required to provide adequate support. The use of accelerators or of thick linings can partially overcome these problems but may introduce another set of practical problems.

The practical solution adopted in the actual case upon which this example is based was to use sliding joint top hat section sets. These sets, as delivered to site, are shown in Figure 12 which illustrates how the sections fit into each other. The assembly of these sets to form a sliding joint is illustrated in Figure 14 and the installation of the sets in the tunnel is illustrated in Figure 15.

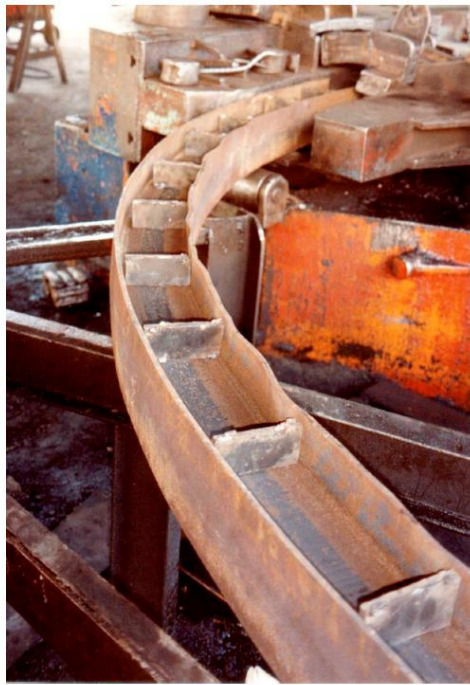


Figure 12: Buckling of an H section steel set being bent to a small radius. Temporary stiffeners have been tack welded into the section to minimise buckling but a considerable amount of work is required to straighten the flanges after these stiffeners have been removed.

Figure 13 Top hat section steel sets delivered to site ready to be transported underground.



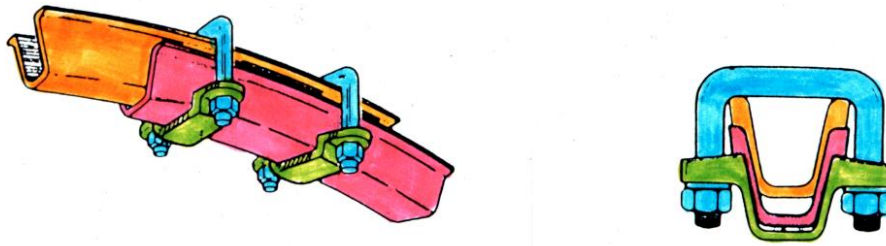


Figure 14 Assembly of a sliding joint in a top hat section steel set.



Figure 15: Installation of sliding joint top hat section steel sets immediately behind the face of a tunnel being advanced through very poor quality rock.

The sets are installed immediately behind the advancing face which, in a rock mass such as that considered here, is usually excavated by hand. The clamps holding the joints are tightened to control the frictional force in the joints which slide progressively as the face is advanced and the rock load is applied to the sets.

The use of sliding joints in steel sets allows very much lighter section sets to be used than would be the case for sets with rigid joints. These sets provide immediate protection for the workers behind the face but they permit significant deformation of the tunnel to take place as the face is advanced. In most cases, a positive stop is welded onto the sets so that, after a pre-determined amount of deformation has occurred, the joint locks and the set becomes rigid. A trial and error process has to be used to find the amount of deformation that can be permitted before the set locks. Too little deformation will result in obvious buckling of the set while too much deformation will result in loosening of the surrounding rock mass.

In the case of the tunnel illustrated in Figure 15, lagging behind the sets consists of wooden poles of about 100 mm diameter. A variety of materials can be used for lagging but wood, in the form of planks or poles, is still the most common material used in mining. In addition to the lagging, a timber mat has been propped against the face to improve the stability of the face. This is an important practical precaution since instability of the tunnel face can result in progressive ravelling ahead of the steel sets and, in some cases, collapse of the tunnel.

The way in which sliding joints work is illustrated diagrammatically in Figure 16.

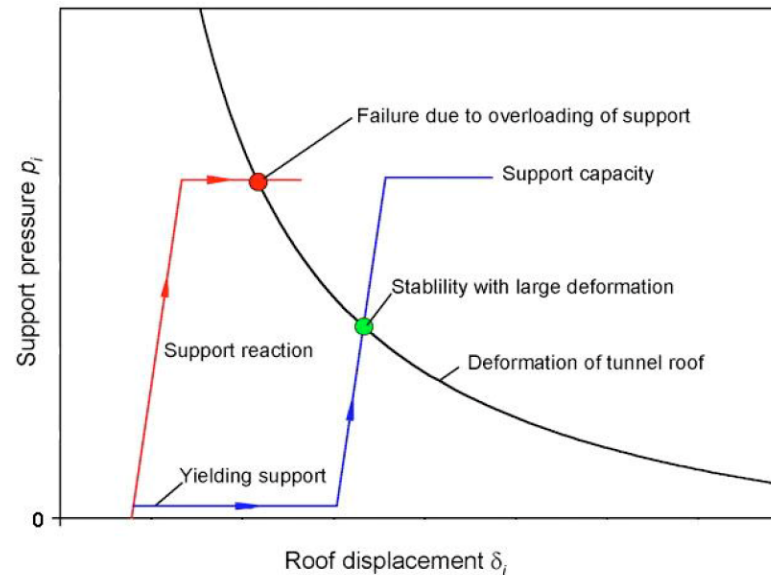


Figure 16: Delay in the activation of passive support by the use of sliding joints.

Figure 16 shows that passive support in the form of steel sets, lattice girders, shotcrete or concrete linings can fail if installed too close to the face. This is because the support pressure required to achieve stability is larger than the capacity of the support system. As the displacements in the tunnel increase as the face moves away from the section under consideration, the support pressure required to achieve equilibrium decreases as illustrated by the curve in Figure 16. Hence, delaying the activation of the support system can stabilize the tunnel at support pressures within the capacity of the support.

This can be achieved by delaying the installation of the support system but this can be very dangerous since workers at the face have to work in an unsupported tunnel. Introducing “yielding elements” into the support system can overcome this problem since the activation of the support is delayed but the support system is in place to catch runaway stability if this should occur.

Many systems have been used to introduce these yielding elements into tunnels with squeezing problems. An example is the use of sliding joints in steel sets as shown in Figure 16. Another system is to use “stress controllers” in which controlled buckling of an inner steel tube provides the yielding required and the system locks and becomes more rigid when a pre-determined deformation has occurred. This system, developed by Professor Wulf Schubert (Schubert, 1996) at the University of Graz in Austria, is illustrated in Figures 17 and 18.



Figure 17: A row of stress controllers installed in a slot in the shotcrete lining in a tunnel



Figure 18: Section through a stress controller showing the buckling inner tube. After Schubert, 1996.

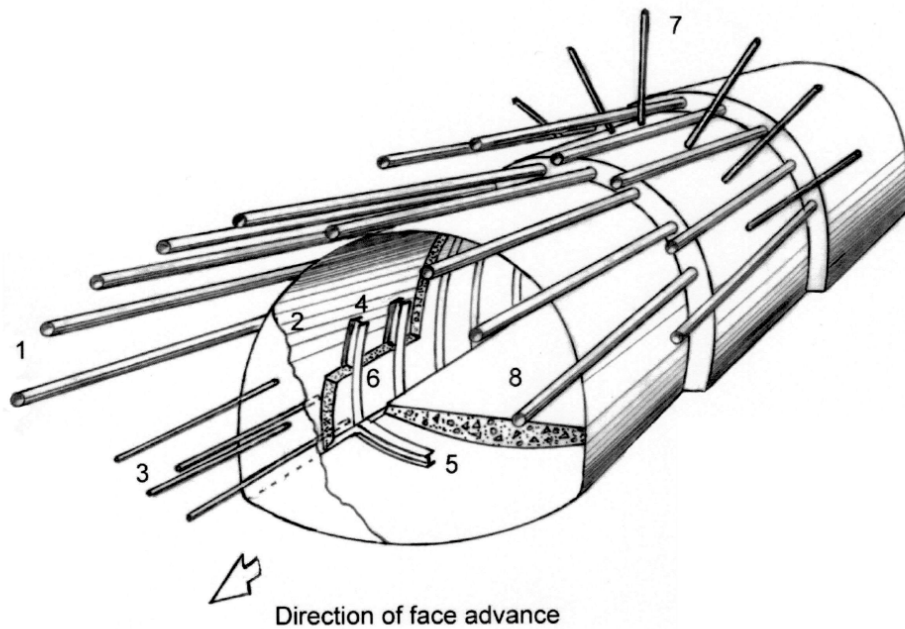
As an alternative to supporting the face, as illustrated in Figure 15, spiles or forepoles can be used to create an umbrella of reinforced rock ahead of the advancing face. Figure 19 illustrate the general principles of the technique. In the example illustrated, spiling is being used to advance a 7 m span, 3 m high tunnel top heading through a clay-rich fault zone material in a tunnel in India. The spiles, consisting of 25 mm steel bars, were driven in by means of a heavy sledgehammer.



Figure 19: Spiling in very poor quality clay-rich fault zone material.

Figure 20 shows a more elaborate system used in large span tunnels in poor quality rock masses. This system relies on grouted fiberglass dowels, which can be cut relatively easily, to stabilize the face ahead of the tunnel and grouted forepoles to provide a protective umbrella over the face. These forepoles consist of 75 to 140 mm diameter steel pipes through which grout is injected. In order for the forepoles to work effectively the rock mass should behave in a frictional manner so that arches or bridges can form between individual forepoles. The technique is not very effective in fault gouge material containing a significant proportion of clay unless the forepole spacing is very close. The forepoles are installed by means of a special drilling machine as illustrated in Figure 21.

While these forepole umbrella systems can add significantly to the cost of driving tunnels and can also result in very slow advance rates, they have been used very successfully in driving many transportation tunnels in Europe (Carrieri et al, 1991).



Direction of face advance

- 1 Forepoles – typically 75 or 114 mm diameter pipes, 12 m long installed every 8 m to create a 4 m overlap between successive forepole umbrellas.
- 2 Shotcrete – applied immediately behind the face and to the face, in cases where face stability is a problem. Typically, this initial coat is 25 to 50 mm thick.
- 3 Grouted fiberglass dowels – Installed midway between forepole umbrella installation steps to reinforce the rock immediately ahead of the face. These dowels are usually 6 to 12 m long and are spaced on a 1 m x 1 m grid.
- 4 Steel sets – installed as close to the face as possible and designed to support the forepole umbrella and the stresses acting on the tunnel.
- 5 Invert struts – installed to control floor heave and to provide a footing for the steel sets.
- 6 Shotcrete – typically steel fibre reinforced shotcrete applied as soon as possible to embed the steel sets to improve their lateral stability and also to create a structural lining.
- 7 Rockbolts as required. In very poor quality ground it may be necessary to use self-drilling rockbolts in which a disposable bit is used and is grouted into place with the bolt.
- 8 Invert lining – either shotcrete or concrete can be used, depending upon the end use of the tunnel.



Figure 21: Installation of 12 m long 75 mm diameter pipe forepoles in an 11 m span tunnel top heading in a fault zone.

Figure 20: Full face 10 m span tunnel excavation through weak rock under the protection of a forepole umbrella. The final concrete lining is not included in this figure.

Analysis of tunnel behaviour

Assume that a circular tunnel of radius r_o is subjected to hydrostatic stresses p_o and a uniform internal support pressure p_i as illustrated in Figure 3. Failure of the rock mass surrounding the tunnel occurs when the internal pressure p_i is less than a critical support pressure p_{cr} , which is defined by:

$$p_{cr} = \frac{2p_o - \sigma_{cm}}{1+k} \quad (4)$$

If the internal support pressure p_i is greater than the critical support pressure p_{cr} , no failure occurs, the behaviour of the rock mass surrounding the tunnel is elastic and the inward radial elastic displacement u_{ie} of the tunnel wall is given by:

$$u_{ie} = \frac{r_o(1+\nu)}{E_m}(p_o - p_i) \quad (5)$$

where E_m is the Young's modulus or deformation modulus and ν is the Poisson's ratio of the rock.

When the internal support pressure p_i is less than the critical support pressure p_{cr} , failure occurs and the radius r_p of the plastic zone around the tunnel is given by:

$$r_p = r_o \left[\frac{2(p_o(k-1) + \sigma_{cm})}{(1+k)((k-1)p_i + \sigma_{cm})} \right]^{\frac{1}{k-1}} \quad (6)$$

For plastic failure, the inward radial displacement u_{ip} of the walls of the tunnel is:

$$u_{ip} = \frac{r_o(1+\nu)}{E} \left[2(1-\nu)(p_o - p_{cr}) \left(\frac{r_p}{r_o} \right)^2 - (1-2\nu)(p_o - p_i) \right] \quad (7)$$

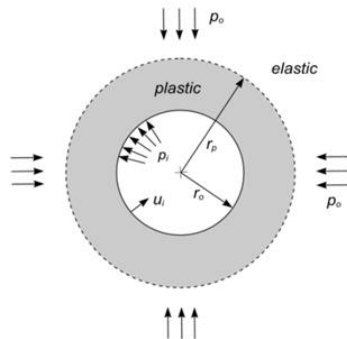
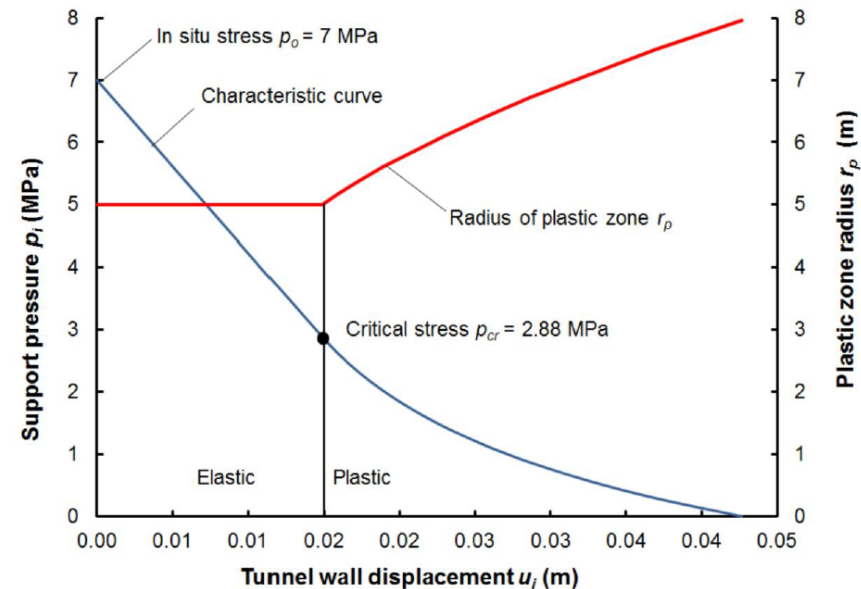


Figure 3: Plastic zone surrounding a circular tunnel.

Characteristic curve for a tunnel

Equations 4 to 7, presented above, define the relationship between internal support pressure p_i and the tunnel deformation u_i for an advancing circular tunnel in a hydrostatic stress field. A plot of u_i versus p_i is generally known as the *Characteristic Curve* for the tunnel and an example is given in Figure 4. This curve is based on the assumption that the rock at the tunnel face provides an initial support pressure equal to the in situ stress p_o . As the tunnel face advances and the face moves away from the section under consideration, the support pressure gradually decreases until it reaches zero at some distance behind the face. Also included in Figure 4 is the radius of the plastic zone r_p , calculated from equation 6.

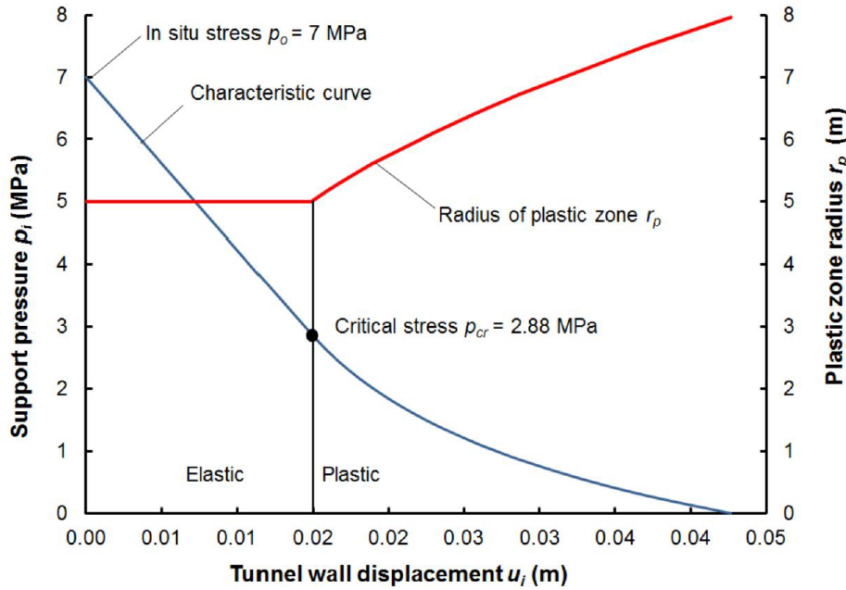


Input:	Output:
Tunnel radius $r_o = 5$ m	Rock mass UCS $\sigma_{cm} = 4.53$ MPa
Friction angle $\phi = 23^\circ$	Rock mass constant $k = 2.28$
Cohesion $c = 1.5$ MPa	Critical pressure $p_{cr} = 2.88$ MPa
Modulus $E = 1800$ MPa	Max tunnel displacement = 0.0427 m
Poisson's ratio $\nu = 0.3$	Max plastic zone radius = 7.96 m
In situ stress $p_o = 7$ MPa	Plastic zone/tunnel radius = 1.592

Figure 4: Characteristic curve for a tunnel excavated in weak rock.

Characteristic curve for a tunnel

Equations 4 to 7, presented above, define the relationship between internal support pressure p_i and the tunnel deformation u_i for an advancing circular tunnel in a hydrostatic stress field. A plot of u_i versus p_i is generally known as the *Characteristic Curve* for the tunnel and an example is given in Figure 4. This curve is based on the assumption that the rock at the tunnel face provides an initial support pressure equal to the in situ stress p_o . As the tunnel face advances and the face moves away from the section under consideration, the support pressure gradually decreases until it reaches zero at some distance behind the face. Also included in Figure 4 is the radius of the plastic zone r_p , calculated from equation 6.



Input:	Output:
Tunnel radius $r_o = 5$ m	Rock mass UCS $\sigma_{cm} = 4.53$ MPa
Friction angle $\phi = 23^\circ$	Rock mass constant $k = 2.28$
Cohesion $c = 1.5$ MPa	Critical pressure $p_{cr} = 2.88$ MPa
Modulus $E = 1800$ MPa	Max tunnel displacement = 0.0427 m
Poisson's ratio $\nu = 0.3$	Max plastic zone radius = 7.96 m
In situ stress $p_o = 7$ MPa	Plastic zone/tunnel radius = 1.592

Figure 4: Characteristic curve for a tunnel excavated in weak rock.

Longitudinal Displacement Profile

The calculation of the characteristic curve and the extent of the plastic zone are based on a two-dimensional analysis as shown in Figure 3. The Longitudinal Displacement Profile, shown in Figure 5, is required in order to establish the relative position of the tunnel face and the sections under consideration. It is necessary to carry out a three-dimensional analysis to determine this profile. The results of such a study have been published by Vlachopoulos and Diederichs (2009) and are summarized in Figure 5.

The Longitudinal Displacement Profile for a specific tunnel is calculated as follows:

The ratio of maximum plastic zone radius r_{pm} to the tunnel radius r_o , is calculated from equation 6 by setting $p_i = 0$:

$$\frac{r_{pm}}{r_o} = \left[\frac{2(p_o(k-1) + \sigma_{cm})}{(1+k)\sigma_{cm}} \right]^{\frac{1}{(k-1)}} \tag{8}$$

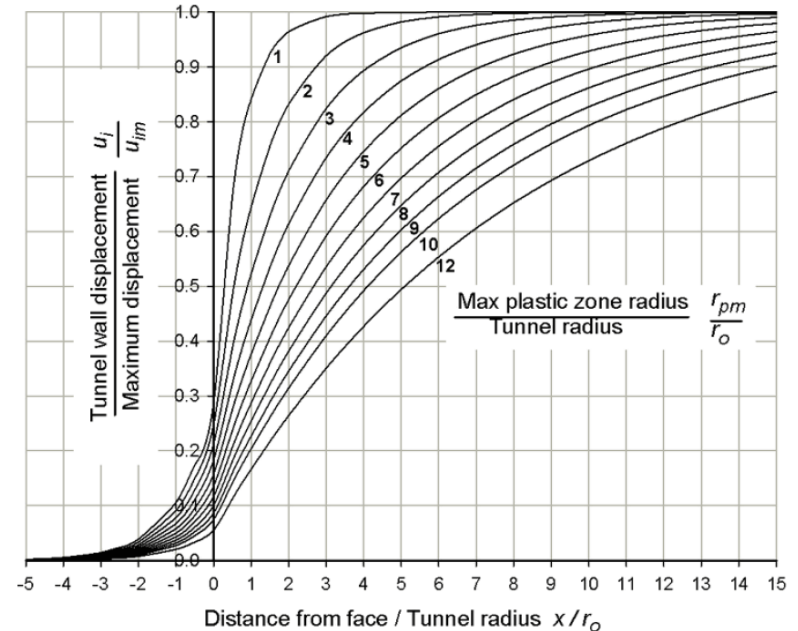


Figure 5: Longitudinal Displacement Profile (After Vlachopoulos and Diederichs, 2009).

The displacement at the tunnel face u_{if} is calculated from the following equation derived by Vlachopoulos and Diederichs:

$$u_{if} = \left(\frac{u_{im}}{3}\right) e^{-0.15(r_{pm}/r_o)} \quad (9)$$

where u_{im} is the maximum displacement which occurs at r_{pm} .

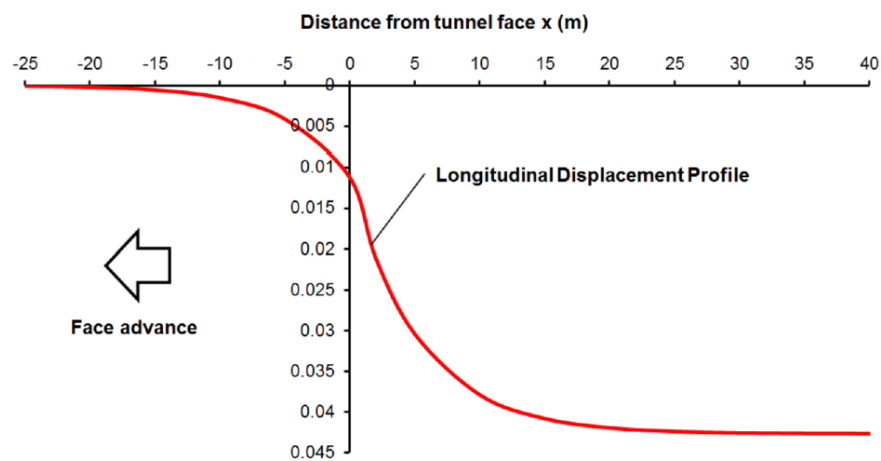
The tunnel wall displacement ahead of the face ($x < 0$) is:

$$u_i = \frac{u_{if}}{u_{im}} \cdot e^{x/r_o} \quad (10)$$

The tunnel wall displacement behind the face ($x > 0$) is:

$$u_i = 1 - \left(1 - \frac{u_{if}}{u_{im}}\right) \cdot e^{(-3x/r_o)/(2r_{pm}/r_o)} \quad (11)$$

A Longitudinal Displacement Profile for a typical tunnel is plotted in Figure 6.



Input:	Output:
Tunnel radius $r_o = 5$ m	Max plastic zone/tunnel radius $r_{pm}/r_o = 1.592$
In situ stress $p_o = 7$ MPa	Tunnel face displacement $u_{if} = 0.011197$ m
Rock mass UCS $\sigma_{cm} = 4.53$ MPa	Maximum tunnel displacement $u_{im} = 0.0427$ m
Rock mass constant $k = 2.28$	Face displacement/Max displacement $u_{if}/u_{im} = 0.2622$

Figure 6: Longitudinal Displacement Profile for tunnel considered in Figure 4.

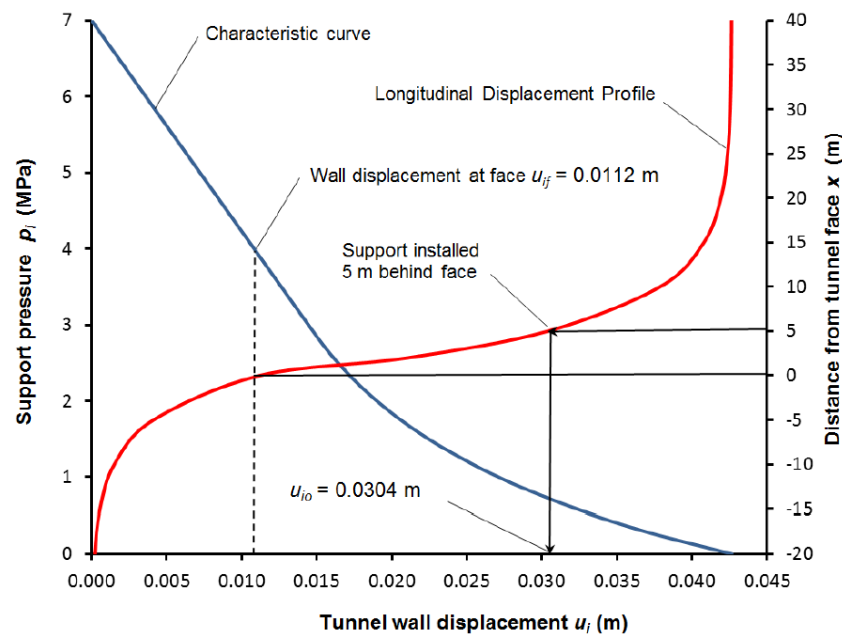


Figure 7: Combined Characteristic Curve and Longitudinal Displacement Profile plot.

Combining the Characteristic Curve from Figure 4 and the Longitudinal Displacement Profile from Figure 6, as was done by Carranza-Torres and Fairhurst (2000), gives the plot presented in Figure 7. This plot allows the tunnel wall displacement at a given distance behind the face to be determined. Hence, as shown in Figure 7, support installed 5 m behind the face will correspond to a tunnel wall displacement $u_i = 0.0304$ m and the minimum support required to stabilize the tunnel is of the order of 0.6 MPa.

Example of rock-support interaction analysis

This example is for the 5 m radius tunnel defined in Figures 4, 6 and 7 with support installed at a distance of 5 m behind the advancing face. As shown in Figure 7, a minimum support pressure of approximately 0.6 MPa is required to stabilize this tunnel. Figure 12b shows that, for a 5 m radius tunnel, this requires either heavy steel sets at 1 m spacing or a reasonably thick shotcrete lining. Because of the low stiffness of rockbolt patterns it is difficult to estimate the support performance of rockbolts except by trial and error and a pattern of 34 mm diameter ungrouted end-anchored bolts on a 1 m x 1 m grid spacing will be included in this analysis.

The calculations for the three rock-support interaction curves are given in Figure 13. Note that all three support systems are assumed to act independently and no effort has been made to analyse the support interaction of two or more combined support systems. A plot of the three support curves and their interaction with the characteristic curve for the tunnel is presented in Figure 14.

A 0.3 m thick unreinforced shotcrete lining provides effective support with factors of safety of greater than 2, as shown in Figure 13. Both rockbolts and the steel sets give a factor of safety of approximately 1.0 which is inadequate. However, the steel sets used in conjunction with a shotcrete lining are probably the most appropriate solution for this example.

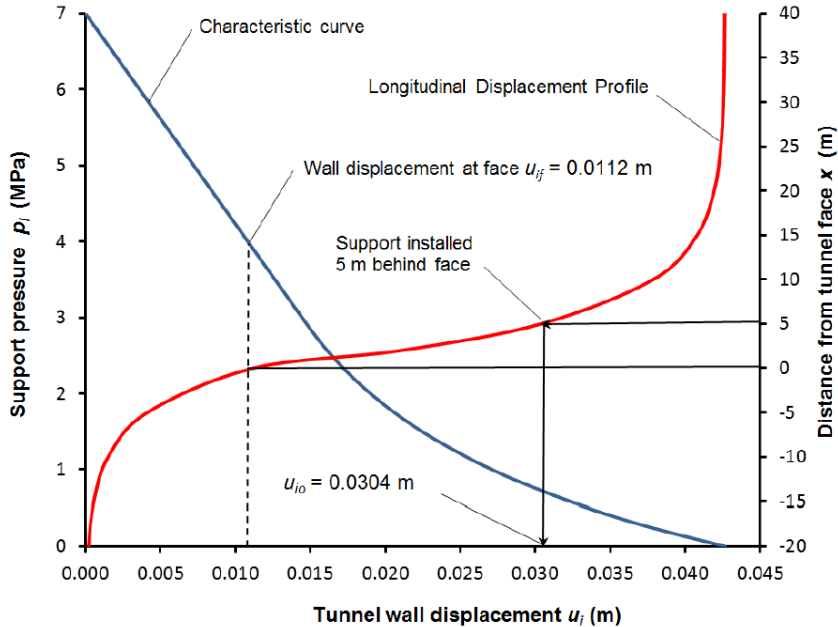


Figure 7: Combined Characteristic Curve and Longitudinal Displacement Profile plot.

Steel sets W310x97 (Metric) W12x65 (Imperial) wide flange steel set

Input:			Output	
Cross sectional area	Ass =	0.0123 m ²	Max pss =	0.6027 MPa
Steel youngs modulus	Ess =	207000 MPa	uismax =	0.00118 m
Yield strength	Sys =	245 MPa	Stiff. Kss =	509.22 MPa/m
tunnel radius	ro =	5 m	strain % =	0.02367
Set spacing along tunnel	Ss =	1 m	Yield uiy =	0.03157 m

Steel set support interaction curve:	x	0.0304	0.0316	0.06
	y	0	0.6027	0.6027

Approximate Factor of safety for steel set support = 1

Shotcrete or concrete 0.3m thick unreinforced shotcrete

Input:			Output:	
Young's modulus of concrete	Ecc =	30000 MPa	Max psc =	2.037 MPa
Poisson's ration of concete	gcc =	0.2	uicmax =	0.00526 m
Lining thickness	tcc =	0.3 m	Stiff Ksc =	387 MPa/m
tunnel radius	ro =	5 m	strain % =	0.10528
UCS of concrete or shotcrete	sconc =	35 MPa	Yield uiy =	0.03565 m

Shotcrete lining suport interaction curve:	x	0.0304	0.0357	0.06
	y	0	2.037	2.037

Approximate Factor of safety for shotcrete support = 3.4

UngROUTed rockbolts 34mm diameter ungrouted end-anchored rockbolts

Input:			Output	
Free bolt or cable length	Lrb =	3 m	Max psr =	0.354 MPa
Diameter of bolt or cable	drb =	0.034 m	uirmax =	0.00565 m
Young's modulus of bolt or cable	Erb =	207000 MPa	Stiffness =	63 MPa/m
Ultimate failure load in pull test	Tbfail =	0.354 MN	strain % =	0.11302
Tunnel radius	ro =	5 m	Yield uiy =	0.03604 m
Circumferential bolt spacing	src =	1 m		
Longitudinal bolt spacing	srl =	1 m		

Rockbolt suport interaction curve:	x	0.0304	0.03604	0.06
	y	0	0.354	0.354

Approximate Factor of safety for rockbolt support = 1.0

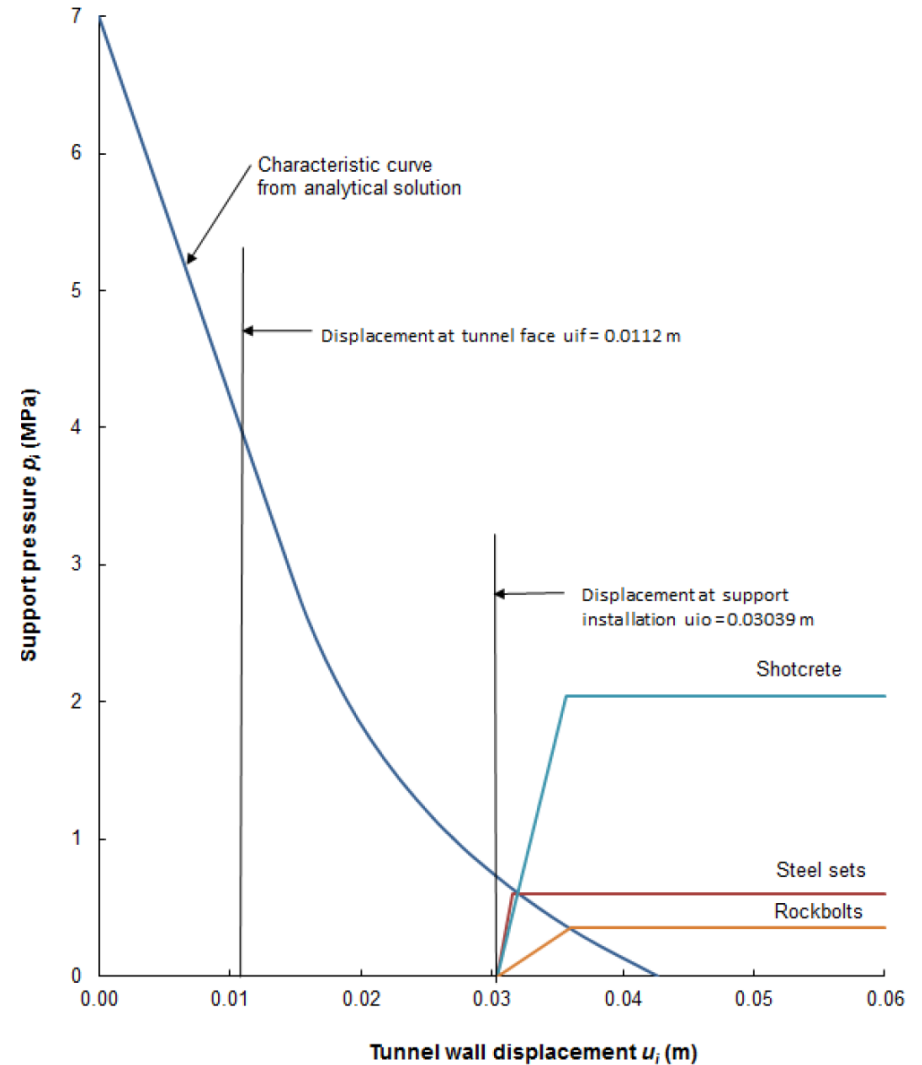


Figure 13: Rock-support interaction calculations for the example considered.

Figure 14: Rock-support interaction plot for the example considered.

Conclusions and recommendations

The rock-support interaction analysis or, as it is sometimes called, the convergence-confinement analyses discussed in these notes is useful for understanding the process of rock mass deformation around an advancing tunnel and the response of support installed inside the tunnel. The analysis demonstrates the importance of tunnel size upon the support capacity of steel sets and shotcrete linings and, in contrast, the lack of sensitivity of rockbolt support to tunnel size. The analysis presented above has been incorporated into the program RocSupport (www.rocscience.com).

The reader should understand that the estimates of the capacity of the support required to stabilize a tunnel are extremely crude as a result of the simplifying assumptions used in the analysis. Remember that the tunnel is assumed to be circular, the in situ stresses are identical in all directions, the rock mass is homogeneous and isotropic and it behaves in an elastic-perfectly plastic manner. In an actual tunnel, the profile is very seldom perfectly circular, in situ stresses are very seldom the same in all directions, the rock mass is generally not homogeneous and isotropic and the failure process is generally far more complex than the elastic-plastic model assumed. In this analysis the calculation of the capacity of the steel sets and the shotcrete lining is based upon the assumption that there are no bending moments or shear forces induced in these support elements and that the loading is characterized by pure axial thrust. The deviations from these simplifying assumptions in an actual tunnel mean that important bending moments and shear forces can be induced in the lining and these may result in premature failure of the support systems.

It is strongly recommended that this analysis should be used as a teaching tool and to give very crude first estimates of possible support requirements. For actual tunnel design use should be made of much more comprehensive analyses such as that published by Hoek et al, 2008, and Carranza-Torres and Diederichs, 2009. These analyses are incorporated into the program Phase2 Version8 (www.rocscience.com).

ABSTRACT: In the majority of modern rock tunnels the deformation and hence the stability of the tunnel is controlled by a combination of reinforcement and support systems. The reinforcement consists of rockbolts or cables which modify the properties of the rock mass in much the same way as reinforcement does in concrete. The support systems generally involve steel sets or lattice girders fully embedded in shotcrete and these provide resistance to control the convergence of the tunnel. This paper describes the methods that can be used to optimize the design of tunnels using a combination of reinforcement and support methods. Particular attention is given to tunnels in very weak rock or soil in which large deformations can occur. Two case histories are presented to illustrate the integration of geotechnical and structural design methods. The first is a 12 m span two lane highway tunnel, excavated by top heading and benching in a very weak rock mass and the second involves a 25 km long, 5.5 m diameter water supply tunnel through the Andes in Venezuela.

1 INTRODUCTION

Current practice in tunnel reinforcement and lining design tends to vary a great deal, depending upon national or owner imposed design requirements, local tradition and practice and the experience of the tunnel designer. There are no universally accepted guidelines on how to assess the safety of a tunnel or the acceptability of a design and this means that engineering judgment and experience play a very large role in the design of tunnel reinforcement and linings.

There is a general desire to define a factor of safety for tunnel design but this has proved to be an extremely difficult task and there are very few methods that are considered acceptable. One of these methods, described by Kaiser (1985), and Sauer et al (1994), involves the use of support capacity diagrams and, indeed, there are a few tunnel design companies that use this methodology. However, the available papers are generally lacking in detail and there is no mention of this method in design guidelines such as the Tunnel Lining Design Guide published by the British Tunnelling Society (2004). Consequently, the average tunnel designer is left with few options other than the use of tunnel classification systems (Barton et al, 1974, Bieniawski, 1973), gener-

al empirical guidelines and the advice of experienced tunnel consultants. The main difficulty with this approach is to decide when the design is acceptable (Hoek, 1992).

In an effort to remedy some of these problems, the authors have set out to present two relatively complex case histories in sufficient detail that tunnel designers can follow the use of support capacity diagrams as a tunnel design tool. Based on a paper by Carranza-Torres and Diederichs (2009), the derivation of the equations used to define these support capacity curves are presented in an appendix and it is relatively simple to program these equations in a spreadsheet.

The support capacity diagrams presented in this paper are based on elastic analyses and the authors recognize that this is a simplification compared to much more sophisticated non-linear models that are used in structural engineering. However, given the uncertainties associated with the loads imposed on tunnel linings, this simplification is considered to be justified. These loads depend upon the adequacy of the geological model, the properties of the rock mass surrounding the tunnel, the in situ stresses and the groundwater conditions. All of these contributing factors are open to a wide range of interpretations, particularly during the design stages in a tunnelling project. Consequently, the aim in developing the elastic support capacity diagrams presented in this paper is to provide the tunnel designer with a set of tools of comparable accuracy to the input data.

2 CASE HISTORY 1 – A SHALLOW TUNNEL AND ADJACENT OPEN CUT

This case history, assembled from a number of actual tunnel designs, involves a 12 m span highway tunnel excavated by drill and blast methods using a top heading and bench approach. Once the tunnel has been excavated and a final concrete lining has been cast in place, an open cut is excavated close to and downhill from the tunnel to accommodate a second carriageway.

The overall geometry of the slope, the tunnel and the adjacent cut is shown in Figure 1. The rock mass is a gently dipping interbedded sedimentary sequence of jointed sandstone, bedded sandstone and a series of shear zones parallel to bedding. The properties of the individual rock units, based on a nearby tunnel in a similar rock mass, are listed in Table 1 and the corresponding Mohr envelopes are plotted in Figure 2.

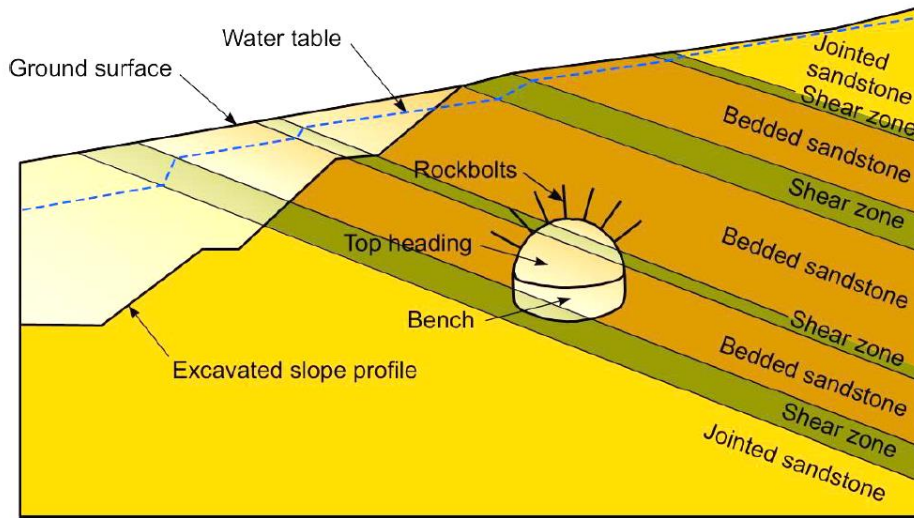


Figure 1. Geometry of the original slope showing the rock layers, the location and geometry of the tunnel and slope excavations and the original water table.

Table 1. Rock mass properties

Property	Jointed sandstone		Bedded sandstone		Shear zones	
	Peak	Residual	Peak	Residual	Peak	Residual
Cohesive strength c - MPa	2.0	1.5	1.4	1.2	0.8	0.8
Friction angle ϕ - degrees	52	50	50	47	40	40
Rock mass modulus E - MPa	9500		4000		650	
Poisson's ratio	0.25		0.25		0.3	
Permeability - m/sec	1×10^{-6}		1×10^{-6}		1×10^{-7}	

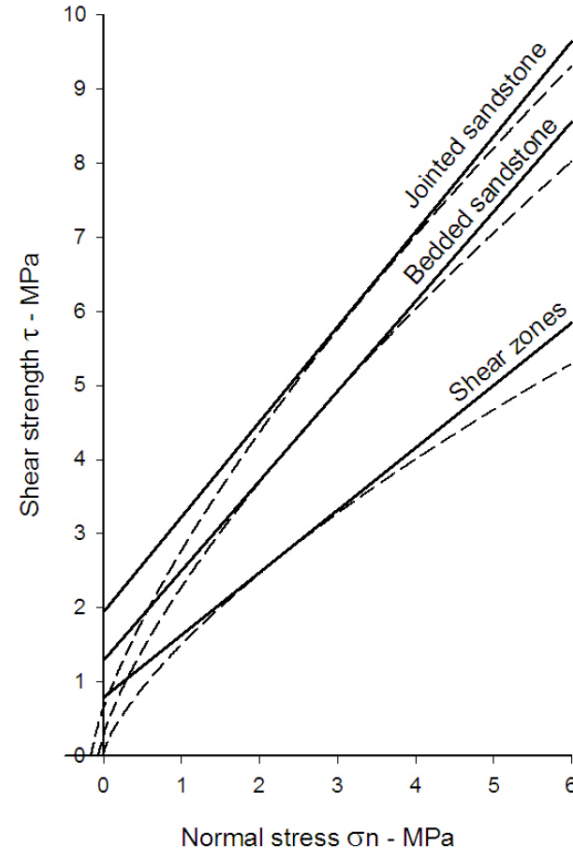


Figure 2. Mohr failure envelopes for individual rock units.

Note that the friction angles shown in Table 1 may appear to be unusually high, particularly to soil mechanics readers. This is because the tunnel is very shallow and the average confining stress in the rock mass surrounding the tunnel is only about 1 MPa. Under these conditions the Mohr failure envelopes are strongly curved, as shown by the dashed lines in Figure 2 (Hoek et al, 2002) and the Mohr Coulomb parameters are estimated from tangents to the curved envelopes.

2.1 *In situ stress conditions*

The vertical stress acting on the rock mass in which this tunnel will be excavated is given by the product of the depth below surface and the unit weight of the rock. Horizontal stress magnitudes and directions can vary greatly, depending upon the tectonic history of the area, the variation in stiffness of different rock units in the rock mass and the local topography. As a starting point for this analysis it has been assumed that the ratio of vertical to horizontal stresses parallel to the tunnel axis is 2:1 and that the ratio normal to the tunnel axis is 1.5:1.

If no in situ stress measurements are available in the vicinity of the tunnel then it is prudent for the tunnel designer to check the sensitivity of the design to variations in these ratios between 0.5:1 and 2:1. If the design proves to be sensitive to horizontal stress variations then steps should be taken to have in situ stress measurements made before the design proceeds to completion. An alternative is to leave sufficient flexibility in the contract to allow design changes during construction and to rely on the back analysis of tunnel convergence measurements to determine the in situ stresses acting on the tunnel.

2.2 *Groundwater conditions*

The excavation of the tunnel and the slope for the adjacent carriageway result in changes in the groundwater conditions in the slope. These changes have a significant impact on the effective stresses in the rock mass surrounding the tunnel. Consequently, a full analysis of these groundwater conditions is a starting point for this analysis of the tunnel stability.

Assuming a permeability of 1×10^{-7} m/sec for the shear zones and 1×10^{-6} m/sec for the jointed and bedded sandstones (see Table 1), a finite element analysis of the groundwater conditions in the slope was carried out. The resulting water tables, for different stages of tunnel and slope excavation, are shown in Figure 3. In this analysis it was assumed that the tunnel acts as a drain except for an extreme long term condition in which the tunnel drains are blocked.

In the finite element analysis of the tunnel lining that follows the pore water pressures and the resulting effective stresses, from the groundwater analysis described above, have been incorporated into the tunnel stability model.

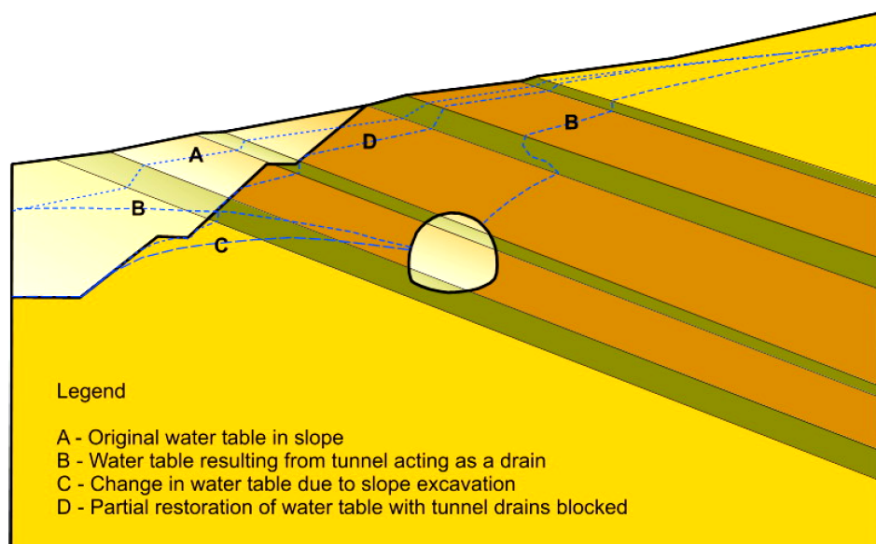


Figure 3. Water tables at different stages of tunnel and slope excavation and assuming long term blockage of the tunnel drains.

The client's requirements for the lining of the tunnel are as follows:

1. An initial lining consisting of steel sets or lattice girders embedded in shotcrete, with the addition of rockbolts if required, sufficient to stabilize the tunnel during construction and until the final lining is placed.
2. A drainage layer consisting of porous geotextile fabric, connected to drainage pipes in the final tunnel invert.
3. A waterproof membrane to prevent water entering into the space behind the final concrete lining.
4. A cast in place concrete lining and invert capable of resisting loads imposed by the surrounding rock mass for both short and long term operation of the tunnel. The factor of safety of the final reinforced concrete lining should exceed 2.0 for normal operating loads and 1.5 for unusual and long term loads.

A typical tunnel lining, designed to meet such requirements, is illustrated in Figure 4.

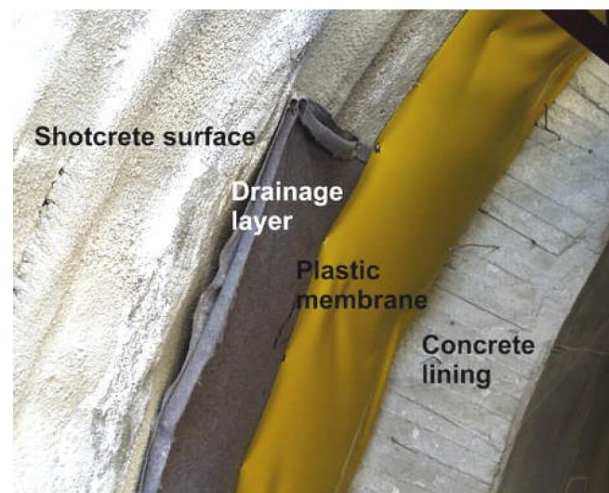


Figure 4. Construction of a complete tunnel lining consisting of an initial lining of lattice girders embedded in shotcrete, a geotextile drainage layer, a waterproof plastic membrane and a cast-in-place concrete final lining.

2.4 Top heading versus full face excavation

An important issue that has to be considered by any drill and blast tunnel designer is whether to specify excavation of the tunnel using a top heading and bench approach or a full face excavation method. Small diameter tunnels, less than say 6 m span, are invariably driven by full face methods since stabilization of the face, if required, is relatively simple. At the other end of the spectrum, large underground caverns are almost always excavated in multiple stages from a top heading or from side drifts. The 12 m span transportation tunnel considered in this example falls in the range where either top heading and bench or full face excavation can be used. Full face excavation has many advantages in terms of geometrical simplicity and, in ground of adequate strength, greater rates of tunnel excavation. Consequently, where possible it is the preferred method of tunneling.

One of the technical factors that controls the choice of which method to use is the stability of the tunnel face. When the stresses in the rock mass surrounding a tunnel exceed the strength of the rock mass a zone of failure or a “plastic” zone is formed around the tunnel. As shown in the derivation of longitudinal displacement profiles for tunnels in Appendix 1, when the radius of the plastic zone around a tunnel exceeds twice the radius of the tunnel, the zone of failure around the tunnel interacts with the failed rock ahead of the tunnel face to form a continuous bullet shaped plastic zone. This three-dimensional plastic zone becomes increasingly difficult to stabilize as the ratio of stress to available rock mass strength increases.

Stabilizing the plastic zone ahead of the tunnel face is generally achieved by means of fully grouted fiberglass dowels parallel to the tunnel axis. The reason for using fiberglass dowels is that they can be cut off as the tunnel advances and they do not damage conveyor belts in the muck disposal system. These dowels are typically placed in a grid pattern of 1 m x 1 m and their total length is approximately equal to the span of the tunnel. For 12 m long dowels an overlap of 3 to 4 m is generally used to ensure that there is continuous support of the face.

Lunardi (2000) discusses the action of face reinforcement in considerable detail and the authors have no disagreement with his statement that “... In order to prevent instability of the face, and therefore the cavity (tunnel), preconditioning measures must be adopted, appropriately balanced between the face and the cavity, of an intensity adequate to the actual stress conditions relative to the strength and deformation properties of the medium”. The preconditioning to which he refers includes the placement of fiberglass dowels, forepoles and other devices that control the deformation of the rock mass ahead of the tunnel face. Achieving an appropriate balance between the face and the tunnel cavity requires a three dimensional analysis of the bullet shaped plastic zone discussed above.

In addition to the stability of the face, consideration has also to be given to the deformations that control the stability of the tunnel itself. Depending upon the in situ stress field and the characteristics of the rock mass surrounding the tunnel, these deformations may be more important than those in the rock ahead of the face. In such cases, the control of the tunnel deformations will determine the choice between top heading and bench and full face excavation.

Practical considerations related to the size of the tunnel, availability of specialized equipment required for the installation of pre-reinforcement, local contracting experience and the preference of the owner can also play an important role in choosing between top heading and bench and full face excavation methods.

In the tunnel under consideration in this model (Figure 1), the owner considered that the risk of losing control of the face due to the presence of the weak shear zones is unacceptably high. Consequently the use of a top heading and bench approach has been specified, in spite of the fact that it may have been possible to drive this tunnel by full face excavation.

2.5 Analysis of face stability

The analysis of the stability of a top heading or a full face tunnel face requires a three dimensional analysis. In simple cases this can be done by means of an axi-symmetric application of a two-dimensional numerical analysis (see Figure A1.3 in Appendix 1). In more complex cases, such as that under consideration in this example, a full three-dimensional analysis is required.

The purpose of the three-dimensional analysis is to simulate in the most realistic possible way the mechanical process of excavation and support and reinforcement installation behind the face and, if applicable, on the face itself to investigate whether the face shows signs of instability. In these three-dimensional models, face instability normally manifests itself as caving of the face resulting in a plastic failure zone that extends ahead of the face or, if the tunnel is relatively shallow as in this example, towards the ground surface. Excessively large displacements can occur and the numerical model tends not to converge (i.e., reach an asymptotic value) as the excavation sequence progresses.

Figure 5 shows the three-dimensional numerical model used to analyze the stability of the face in this example. Note that only half of the model, as defined by a vertical plane cutting through the tunnel axis, is represented in this figure. The model considers excavation of the top heading through the interbedded sedimentary sequence introduced in Figure 1. Mechanical properties of the different rock types are those indicated in Figure 2 and Table 1. The in situ

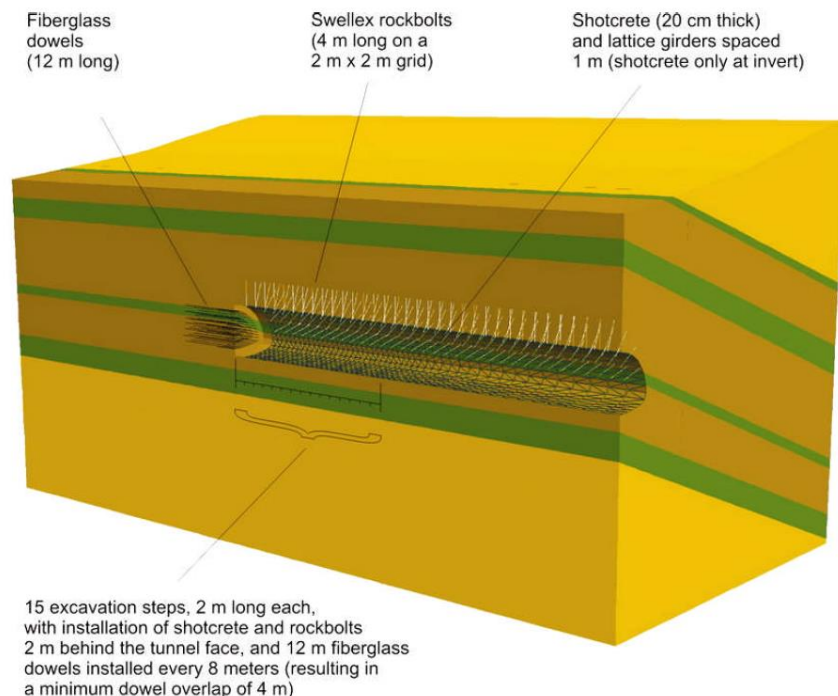


Figure 5. View of the three-dimensional numerical model used to analyze stability of the tunnel face.

stress conditions prior to excavation assumed for the model are those discussed in Section 2.1, while the groundwater conditions correspond to the worst case scenario, that of the original water table (configuration A) in Figure 3.

As indicated in Figure 5, the three-dimensional model simulates the mechanical process of advancing the top heading in increments of 2 meters, corresponding to the design blast round length of 2 m, and installing shotcrete and rockbolts at a distance of 2 meters behind the face, corresponding to the design length of installation of support and reinforcement behind the face. The geometrical and mechanical characteristics of the support and reinforcement used are the same considered in the two-dimensional numerical analyses to be discussed in later sections. In addition, the model simulates the process of installation of a set of 60 fiberglass dowels in a circumferential pattern at the face, with an approximate spacing of 1 meter between dowel heads. In this case, the dowels are installed at intervals of 8 meters on the face, leading to a minimum overlap length of 4 meters between two sets of dowels. The geometrical and mechanical properties of fiberglass dowels are normally provided by the manufacturer; this example considers dowels of 18 mm diameter, with a Young's modulus of 40,000 MPa and a tensile strength of 1000 MPa.

A total of 15 excavation stages have been considered in this example leading to a total length of sequential advance of 30 meters. For the last stage (indicated in Figure 5) the stability conditions at the face have been inspected. Figure 6 represents contours of resulting magnitude of displacements at this stage. Displacements at the face are below one millimeter. The resulting plastic failure zone is also of limited extent of less than 50 centimeters and does not show any tendency to develop into a caving zone towards the ground surface. Comparison of equivalent results from a model without fiberglass dowels installed at the face reveals that these dowels do indeed make a mechanical contribution to the stability of the tunnel face. Both the extent of plastic zone and resulting displacements at the face, when no fiberglass dowels are considered, are at least twice the values shown in Figure 6.

It is doubtful whether fiberglass dowel reinforcement is actually required in this example and it is probable that the top heading could be advanced safely without reinforcement or with a simpler restraint in the form of a face buttress (Hoek, 2001). However, the calculations presented in Figures 5 and 6 demonstrate the procedure that can be used to analyze the need for face reinforcement and the stabilization that can be achieved by the installation of such reinforcement.

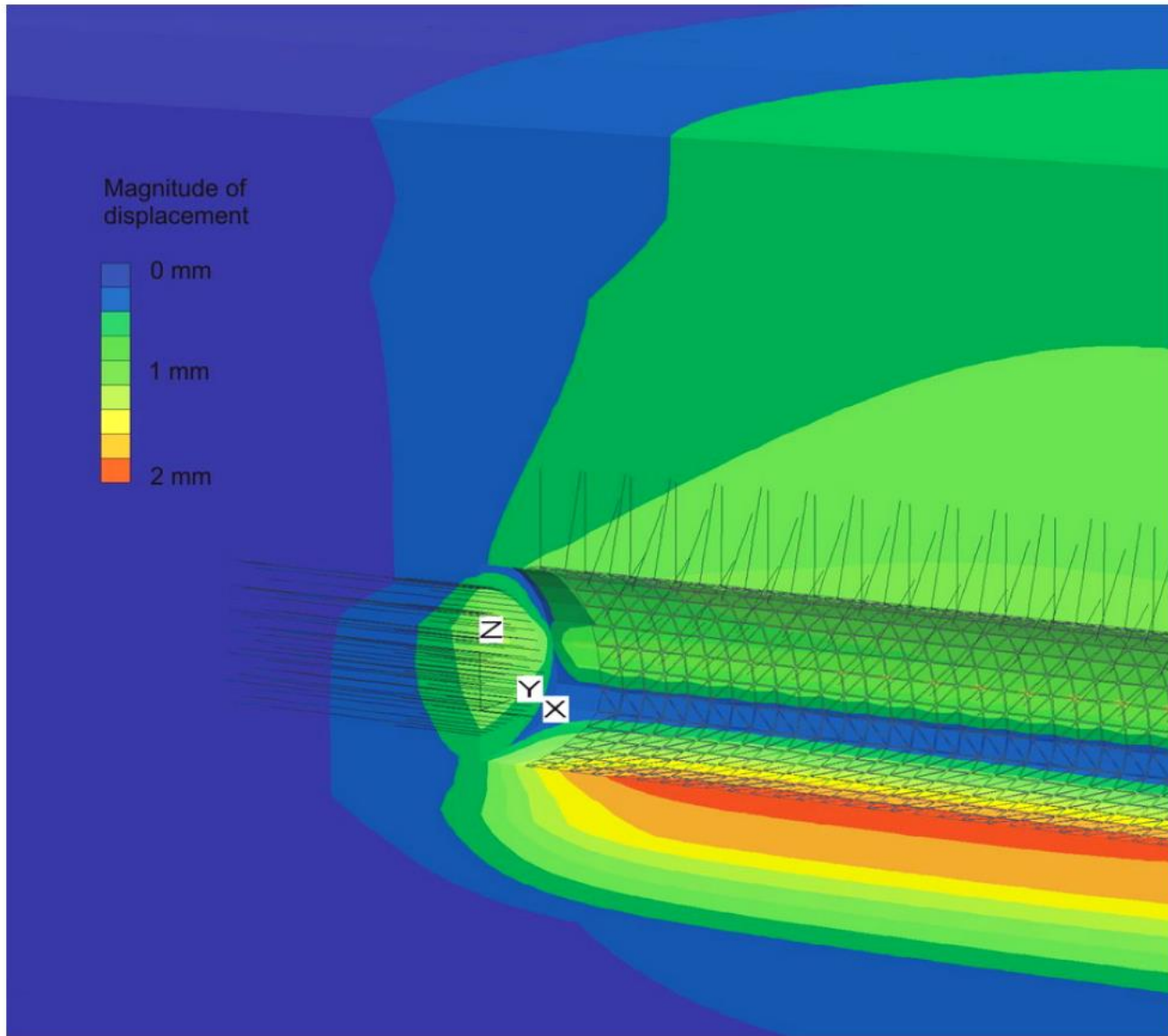


Figure 6. Representation of contours of magnitude of displacements for the last stage of excavation in the three-dimensional model of Figure 5.

2.6 Characteristic curve and longitudinal deformation profile

The next step in the design procedure is to determine the point at which the support in the tunnel is installed and activated. In a 12 m span tunnel this would normally be at a distance of between 2 and 4 m behind the face and a distance of 2 m has been chosen for this analysis.

In using a two dimensional analysis of the rock-support interaction it is necessary to simulate the three-dimensional tunnel advance by means of some deformation control process. This means that the deformation that takes place at a distance of 2 m behind the face must be known and controlled to allow the support to be installed and activated. This can be done by calculating the characteristic curve for the rock mass surrounding the tunnel by progressively reducing either an internal support pressure or by progressively decreasing the deformation modulus of an inclusion in the tunnel. In complex situations, such as that under consideration here, the modulus reduction method is preferred since it automatically accommodates variations in the surrounding stress field due to a non-circular tunnel shape and progressive failure in the rock mass as the tunnel deforms.

Figure 7 shows the characteristic curve for this tunnel and the stepwise reduction of the modulus of the inclusion in the tunnel. The analysis required to generate the characteristic curve also shows the extent of failure around the tunnel and this is important in calculating the longitudinal deformation profile in the next stage of the analysis.

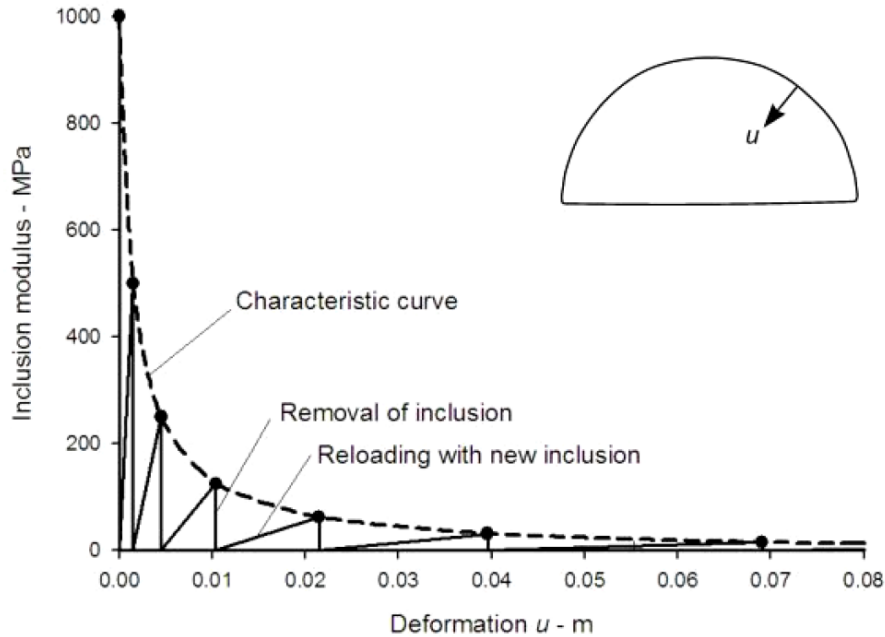


Figure 7. Characteristic curve for the unsupported, undrained tunnel excavated by a full face method. Note that any monitoring point can be chosen on the tunnel boundary since, although the magnitude of the deformations will vary, the shape of the excavation curve will remain constant.

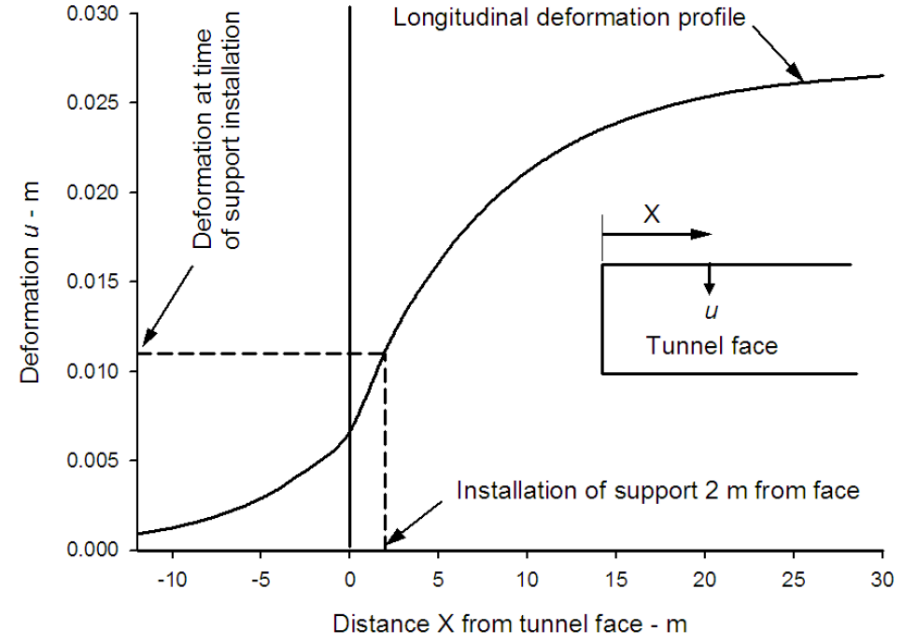


Figure 8. Longitudinal deformation profile for a 12 m span tunnel where the radius of the plastic zone is less than twice the radius of the tunnel.

Figure 8 gives a plot for the longitudinal deformation profile for the tunnel in this example. As shown in Appendix 1, this profile depends upon the ratio of the radius of the plastic zone to the radius of the tunnel and, for this example, this ratio is approximately 2:1. Figure A1.5 in Appendix 1 shows that the tunnel closure at the face is approximately one quarter of the final closure at many meters behind the face. The deformation profiles are calculated from equations A1.6 and A1.7.

From Figure 8 it can be seen that installation and activation of the support at a distance of 2 m behind the advancing face corresponds to a deformation of 0.011 m. Using this value in Figure 7, the modulus of the inclusion required to limit the tunnel deformation to this value is approximately 100 MPa. Hence, in constructing the two dimensional model to simulate the three-dimensional effects of the advancing face, an inclusion with a modulus of 100 MPa has been used for the first stage of the calculation. Excavation of this inclusion activates the installed support system and allows it to react to the additional deformation that occurs as the tunnel advances.

2.7 Analysis of top heading with a flat floor

For large span tunnels the top heading shape preferred by contractors is illustrated in Figure 9. This consists of an arched roof and a flat floor. The flat floor is simple to excavate and it provides an excellent road base for construction traffic. In good rock at low to moderate stress levels, this top heading shape is acceptable. The suitability of this top heading profile for this example is investigated below.



Figure 9. A simple top heading shape in good quality interbedded sandstones and siltstones. The tunnel arch is supported by means of rockbolts and a layer of shotcrete and no face support is required. The flat floor requires no special treatment other than good drainage of surface water accumulations.

Figure 10 gives a cross section through a typical support system used for the initial support of a large span tunnel. This consists of 3 bar lattice girders embedded in a 20 cm thick shotcrete layer. The lattice girders are spaced at 1 m intervals along the tunnel and rockbolts are installed between every second girder at a spacing of 2 m. In this case the rockbolts are 4 m long standard Swellex bolts on a 2 m x 2 m grid spacing.

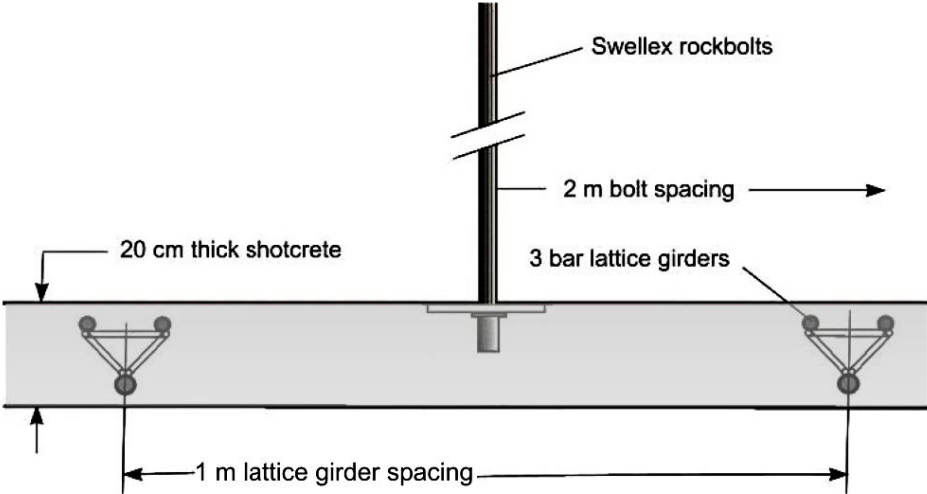


Figure 10. Reinforcement and support for the top heading arch consisting of standard Swellex rockbolts on a 2 m x 2 m grid and 3 bar lattice girders spaced at 1 m centers and embedded in a 20 cm thick shotcrete lining (Not to scale).

An important issue that has to be considered in the design of this support system is the time-dependent properties of the shotcrete layer. As described above, the support system is installed 2 m behind the face and activated immediately. The rockbolts and lattice girders respond to the deformation of the rock mass surrounding the tunnel as soon as the tunnel advances but the shotcrete is only 1 day old at this stage and it has not yet developed its full capacity. While it does not carry its full share of the load, because its stiffness is low, this load may be sufficient to induce failure in the shotcrete.

Choosing the shotcrete properties is not quite as simple as one would think. Many tunnel designers turn to structural codes such as the American Concrete Code (ACI 318 - Building Code and Commentary) and follow the recommendations set out in these documents. However, in their Guidelines for Tunnel Lining Design the Technical Committee on Tunnel Lining Design of the Underground Technology Research Council states the following:

“Structural codes should be used with caution. Most codes have been written for above ground structures on the basis of assumptions that do not consider ground-lining interaction. Accordingly, the blind application of structural design codes is likely to produce limits on the capacity of linings that are not warranted in the light of the substantial contributions from the ground and the important influence of construction method on both the capacity and cost of linings.

Specific load factors are not recommended in these guidelines. The loading conditions should be evaluated by a careful, systematic review of the geologic and construction influences. It is important that the evaluation of ground loads and structural details be coordinated to select a factor of safety.”

In the support capacity calculations given in this paper the authors have adopted a policy of using the ultimate uniaxial compressive and tensile strengths of shotcrete and concrete and calculating a range of factors of safety. This eliminates the complication of hidden or unknown load factors or safety factors and, by including a family of factor of safety plots in the support capacity diagrams, the user is presented with a clear picture of performance of the lining being designed.

Melbye and Garshol (2000) give shotcrete mix designs and uniaxial strength results, many from in situ cores, for 35 tunneling projects around the world. These results are plotted in Figure 11 and it can be seen that the 28 day strength varies from 25 to 86 MPa. This variation depends upon the mix design, whether the wet or dry shotcrete method was used, whether the shotcrete was applied manually or by robot and upon local factors such as haulage distance between the batch plant and the face. It is the responsibility of the tunnel designer to discuss all of these issues with the shotcrete supplier in order to determine the optimum shotcrete product for a particular site.

For the model under consideration the sequence of loading and the corresponding shotcrete properties are defined in Figure 12 and Table 2 in which the age dependent properties have been assembled from a number of tunnel case histories. In constructing the numerical model used to analyze this case these properties have been incorporated into the shotcrete lining at the stages of excavation shown.

In the case of the top heading with an unsupported and unreinforced flat floor, as illustrated in Figure 13, the heave of the floor induces bending in the lower parts of the lining arch. These bending moments can overload the 3 day old shotcrete and they can also permit deformations sufficient to allow failure propagation in the adjacent rock mass. This failure may have a detrimental influence on the loading of the lower legs of the arch when the bench is excavated.

In order to study the response of the support system to the excavation sequence and consequent tunnel deformations, a set of support capacity diagrams have been plotted in Figure 14. Note that the rockbolts are not part of the support system since they act as reinforcement and alter the properties of the rock mass surrounding the tunnel. Nevertheless these bolts play an important role in stabilizing the tunnel arch and in supporting the shotcrete shell.

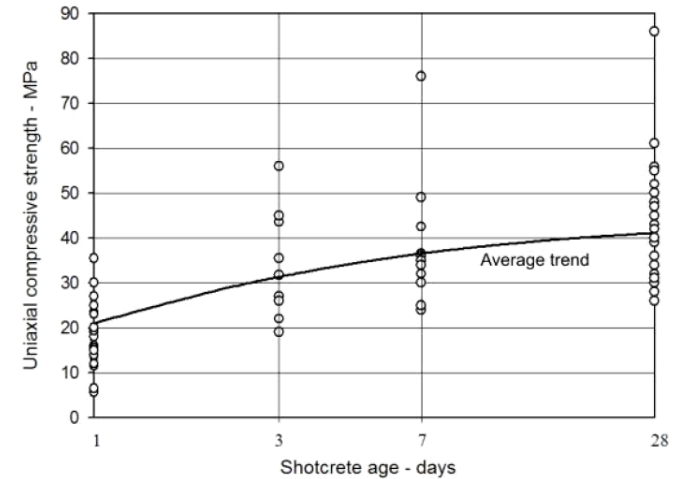


Figure 11. Uniaxial compressive strength development with time for shotcrete linings in tunnels around the world. After Melbye and Garshol (2000).

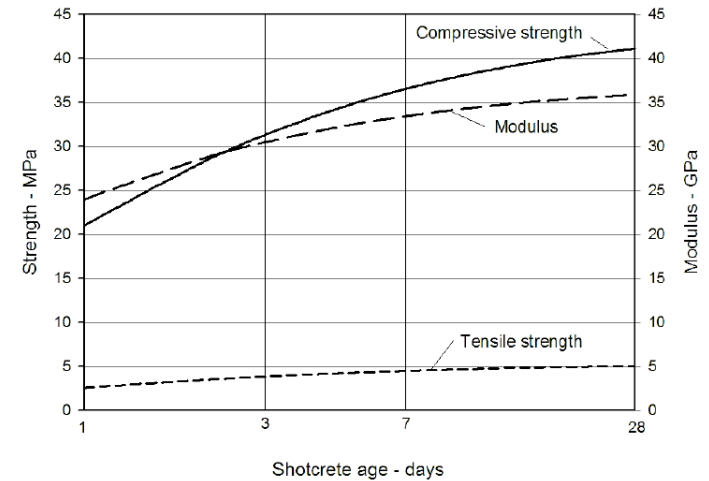


Figure 12. Assumed time dependent properties for shotcrete.

Table2. Excavation sequence and shotcrete properties

	Compressive strength σ_{csh}	Tensile strength σ_{tsh}	Deformation modulus E_{sh}
Day 1 – installation and activation of support	21.0 MPa	- 2.6 MPa	24,000 MPa
Day 3 –top heading convergence at about 10 m behind the face	31.0 MPa	- 4.0 MPa	30,000 MPa
Day 28+ - excavation of bench which may be as much as 1 year after top heading excavation	41.4 MPa	- 5.0 MPa	36,000 MPa

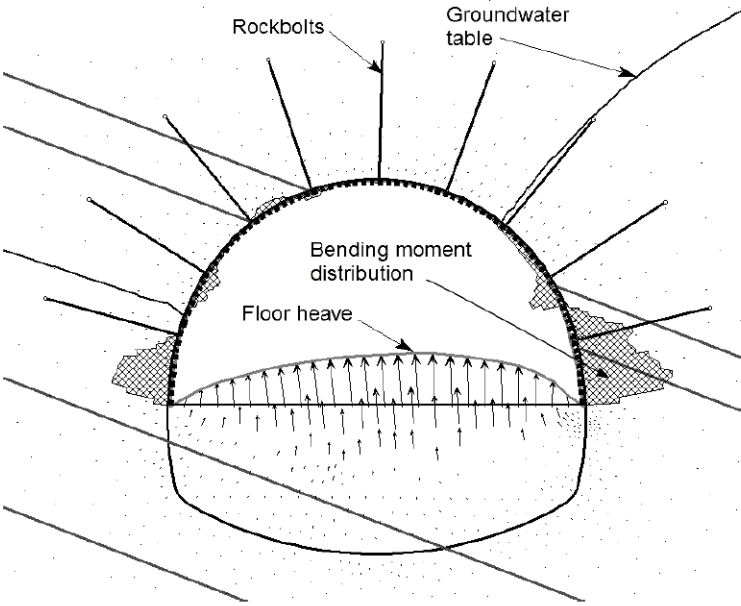


Figure 13. Bending moment distribution in the lining of the top heading with a flat unsupported floor on day 3 after installation of the support.

The derivation of the equations required to calculate these figures is given in Appendix 2. The calculation process results in a set of moment versus axial thrust and moment versus shear force diagrams for the lattice girders and the shotcrete. In the case of the shotcrete, the diagrams are calculated for 1 day, 3 day and 28 day strengths as defined in Table 2. From the numerical analysis, the axial forces, bending moments and shear forces in the installed top heading arch support are distributed onto the lattice girders and the shotcrete shell by means of equations A2.24 to A2.29 in Appendix 2. The resulting values, for the 1 day and 3 day loading conditions, are plotted as points in Figure 14.

Because of the shallow depth of the tunnel the axial loads carried by the support system are very low. Similarly, bending moments and shear forces in the lattice girders are small. However, the bending moments in the shotcrete lining are sufficient to exceed the capacity of the shotcrete at ages of 1 day and 3 days, as shown in the moment versus axial thrust diagram for the shotcrete, assuming a factor of safety of 1. This analysis illustrates that, for the in situ stresses, rock mass properties, excavation sequence and lining properties chosen, a top heading with a flat unreinforced and unsupported floor is not an appropriate choice.

The excessive bending moments in the lower portions of the top heading arch can be addressed in a number of ways including the installation of stressed anchors to limit the bending of the upper arch legs, increasing the thickness of the shotcrete shell, placing additional reinforcement in the lower arch legs or placing a temporary invert to limit the floor heave and the “pinching” of the arch. In this example, the placement of a temporary shotcrete invert will be investigated.

Examining Figure 14 may suggest to the reader that, since the loads carried by the lattice girders are so small, the shotcrete could be dispensed with and the lattice girders used on their own to carry the loads. This would be a serious mistake since these capacity plots are only valid when the lattice girders and the shotcrete act as a composite structure. The shotcrete, even when very young, provides lateral confinement for the lattice girders and this is essential to prevent buckling failure of these slender structures in the wide span tunnel.

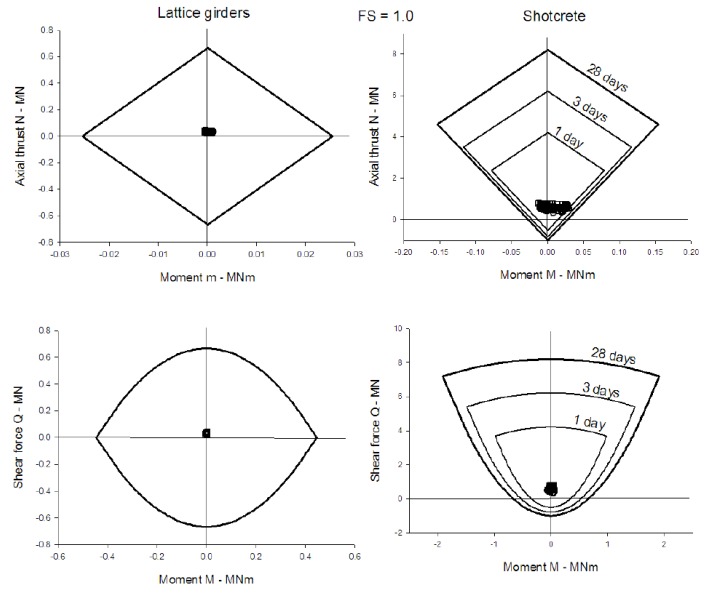


Figure 14. Support capacity diagrams for a 20 cm shotcrete lining, reinforced with 3 bar lattice girders, placed in a top heading excavation with a flat floor (see Figure 9).

2.8 Analysis of top heading with a curved shotcrete invert

A temporary shotcrete invert, such as that illustrated in Figure 15, is generally constructed from unreinforced shotcrete, typically 20 cm thick, so that it can be broken easily during benching. Backfill is placed over this invert in order to form a road surface for construction traffic.

It is important that a smooth connection is provided between this invert and the top heading arch legs in order to prevent the formation of stress concentration points. The shear capacity of the connection between the arch legs and the shotcrete invert can be deficient if the shotcrete is placed at different times. This problem can be overcome by adding reinforcement, such as that illustrated in Figure 16, to ensure that the loads in the arch are transferred into the invert. This reinforcement should be designed so that it can either be cut off or bent downward and incorporated into the lower arch legs when the temporary shotcrete invert is excavated.

A numerical analysis of top heading lining with a curved shotcrete invert covered by backfill results in the bending moment shown in Figure 17 and the corresponding support capacity plots given in Figure 18. In this case the analysis has been extended to include the removal of the bench and the placement and activation of the lower arch legs and the tunnel bottom invert. Since the structure of the arch legs is identical to the top heading arch it is permissible to plot the points for these two components on the same support capacity diagrams.

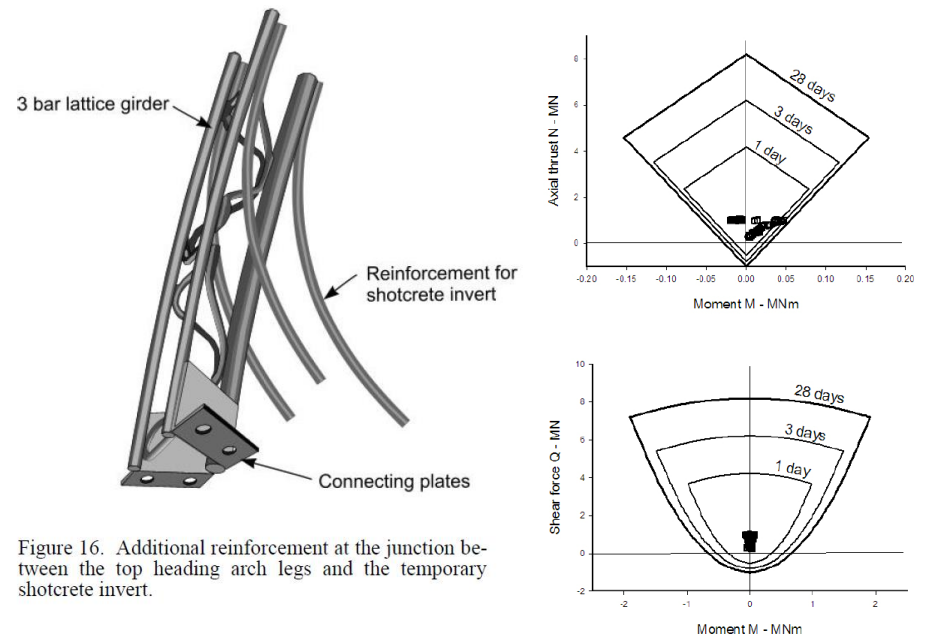


Figure 16. Additional reinforcement at the junction between the top heading arch legs and the temporary shotcrete invert.

Figure 18. Support capacity plots for the 20 cm thick unreinforced shotcrete invert in Figure 17.



Figure 15. Top heading and bench excavation in a weak rock tunnel where a temporary shotcrete invert was used to control floor heave.

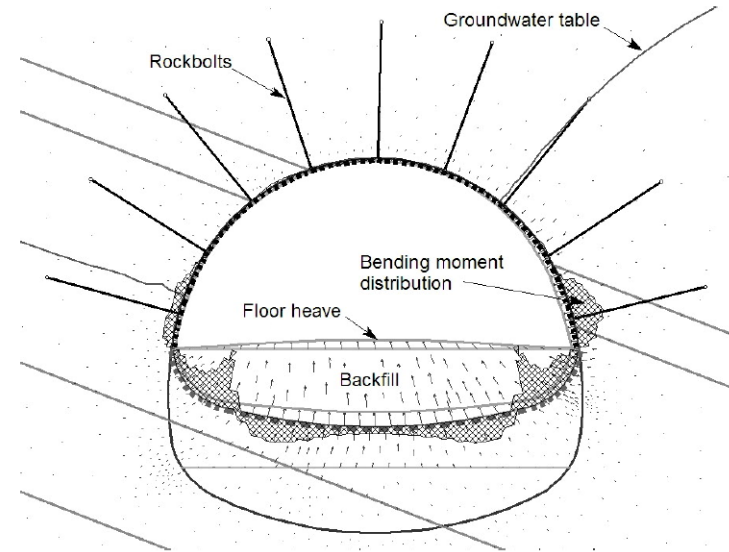


Figure 17. Bending moment distribution in a top heading lining with a curved shotcrete invert covered by backfill (see Figure 15).

Figure 17 shows that the results of this analysis of the top heading arch are similar to those for the top heading with the flat floor, shown in Figure 13, except that the bending moments in the arch are reduced by the placement of the shotcrete invert. The support capacity plots for the unreinforced invert, given in Figure 18, show that the bending moments induced in the invert are just sufficient to induce tensile cracking in the 1 day and 3 day old shotcrete. While this would be a problem elsewhere it is considered to be acceptable here since the shotcrete invert is constrained by the overlying backfill and some minor cracking will be of little consequence. However, if the designer is uneasy about this cracking or if the client is reluctant to accept any indication of failure, the invert can be made thicker or it can be reinforced with polypropylene fibers to increase its capacity.

The support capacity plots for the shotcrete arch and lower legs for the case of the curved shotcrete invert are shown in Figure 19. The Moment-Axial thrust points for the shotcrete all fall well within the capacity curves for the corresponding age of shotcrete. This confirms that the use of the shotcrete invert has reduced the bending moments that resulted in problems in the top heading excavated with a flat floor (Figure 14).

A check on the invert on the bottom of the tunnel shows no overstressing and, hence, the complete lining is stable and the design can proceed to the installation of the final lining. Note that, if there is a large time delay (say for more than 1 year) between the excavation of the tunnel and the installation of the final lining, it may be necessary to recalculate the lining forces for a reduced rock mass strength to allow for time-dependent deterioration.

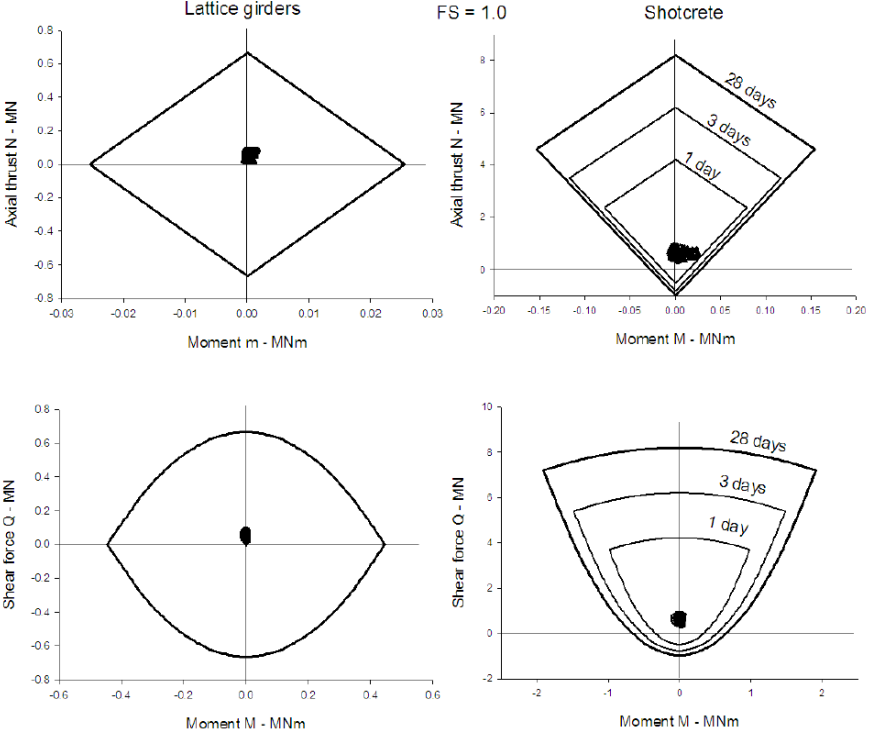


Figure 19. Support capacity diagrams for a 20 cm shotcrete lining, reinforced with 3 bar lattice girders, placed in a top heading excavation with a curved shotcrete invert (see Figure 15).

The next step after the excavation and stabilization of the full tunnel profile is the installation of a final lining. The typical geometry of this lining was shown in Figure 4 and it is given in detail in Figure 20. In this example it is assumed that the final lining itself consists of 30 cm thick cast-in-place concrete reinforced by means of 20 mm diameter steel reinforcing rods spaced at 18 cm x 22 cm apart.

For simplicity the properties of the cast in place concrete final lining are assumed to be the same as those of the initial shotcrete lining, as defined in Table 2. Because the final lining is installed in a stable tunnel it carries no initial load except for its self-weight. Hence, only the 28 day properties are relevant in the following calculations. Loads are imposed on the final lining as a result of stress changes, changes in the groundwater conditions, changes in the characteristics of the initial support system or deterioration of the rock mass surrounding the tunnel. All of these changes are assumed to occur in this example and the consequences will be examined in the analysis that follows.

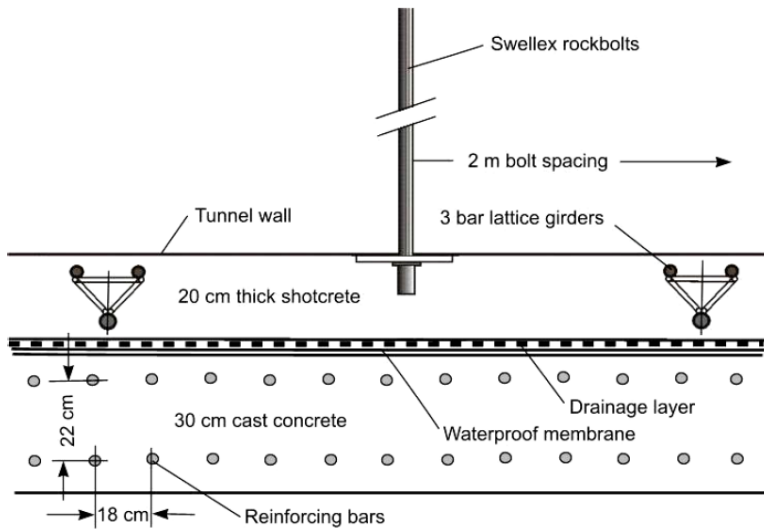


Figure 20. Geometry of composite final lining consisting of a 20 cm thick initial shotcrete lining, a drainage layer, a waterproof membrane and a 30 cm thick cast concrete lining (Not to scale).

After the installation of the final lining the open cut for the adjacent highway carriageway is excavated as defined in Figure 1. This results not only in changes in the stress field surrounding the tunnel but also changes in the groundwater conditions as defined by curve C in Figure 3. In designing the final lining these changes have to be accommodated and a factor of safety in excess of 2.0 has to be provided by the lining for these “normal” loading conditions.

The long term loading conditions, for which a factor of safety of 1.5 has been specified for this example, include corrosion of all the rockbolts, blockage of the tunnel drains and deterioration of the rock mass surrounding the tunnel. Other extraordinary long term-loading conditions may apply in specific cases and these should also be included. Basically, the aim of the designer should be to ensure that the tunnel will remain stable and operational under all possible conditions that could occur during its service life.

The participation of the initial shotcrete lining has been a matter of contention for many years. Until relatively recently tunnel designers in some countries were required to ignore the contribu-

tion of all initial reinforcement and shotcrete linings in calculating the support capacity of the final lining. However, this very conservative approach has changed and the International Tunneling Association’s Guidelines for the Design of Tunnels (1988) gives the following recommendation: “An initial lining of shotcrete may be considered to participate in providing stability to the tunnel only when the long-term durability of the shotcrete is preserved. Requirements for achieving long-term durability include the absence of aggressive water, the limitation of concrete additives for accelerating the setting (liquid accelerators), and avoiding shotcrete shadows behind steel reinforcement”.

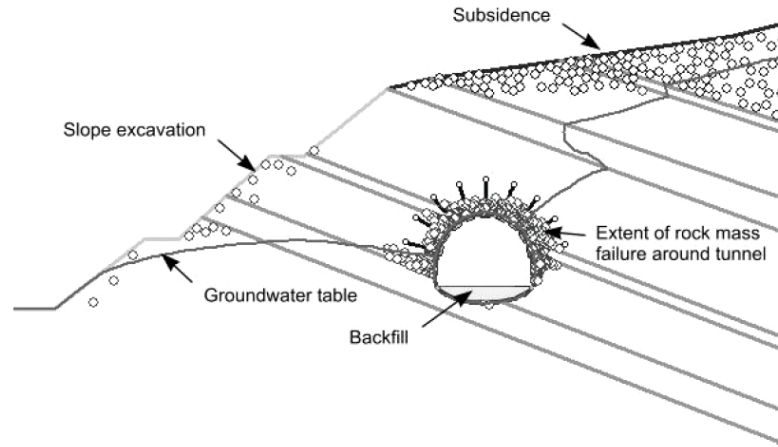


Figure 21. Changes in stress and groundwater conditions as a result of excavation of the open cut for an adjacent carriageway can result in propagation of failure zones in the rock mass.

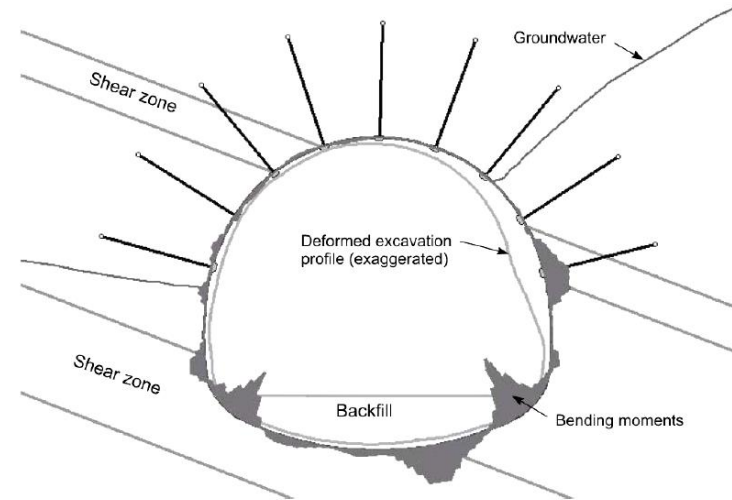


Figure 22. Distribution of bending moments and deformations of the final tunnel profile after installation of the final lining and excavation of the adjacent cut.

The extent of rock mass failure surrounding the tunnel, after installation of the final lining and excavation of the adjacent open cut is shown in Figure 21. Note that some rock mass failure of the surface occurs as a result of surface subsidence and stress relief due to the open cut excavation. While this is not significant in the design of the tunnel lining it does highlight the need for the designer to check on surface subsidence and slope stability issues. In shallow tunnel such as this one, caving to surface can be a critical issue and it has to be checked very carefully during the sequential excavation of the tunnel.

The bending moments and the deformations induced in the final lining are shown in Figure 22. Note that the presence of the two shear zones has a significant influence of these distributions, particularly on the right hand side of the tunnel arch. As shown in the support capacity plots in Figure 23, these bending moments are the most significant forces to be considered in the lining design since all other forces are very low.

Detailed plots of the moment-thrust relationships for the final lining for three model stages are given in Figure 24. These show that the lining carries practically no load at the time of installation. The forces in the lining change slightly when the adjacent open cut is excavated and they change by a significant amount when the long term loads are applied. These loads are induced by a reduction of the residual strength of the failed rock surrounding the tunnel, an elimination of all rockbolts and changes in the groundwater conditions as a result of blockage of the drains. The factor of safety for the lining for these long term loads is approximately 2.0.

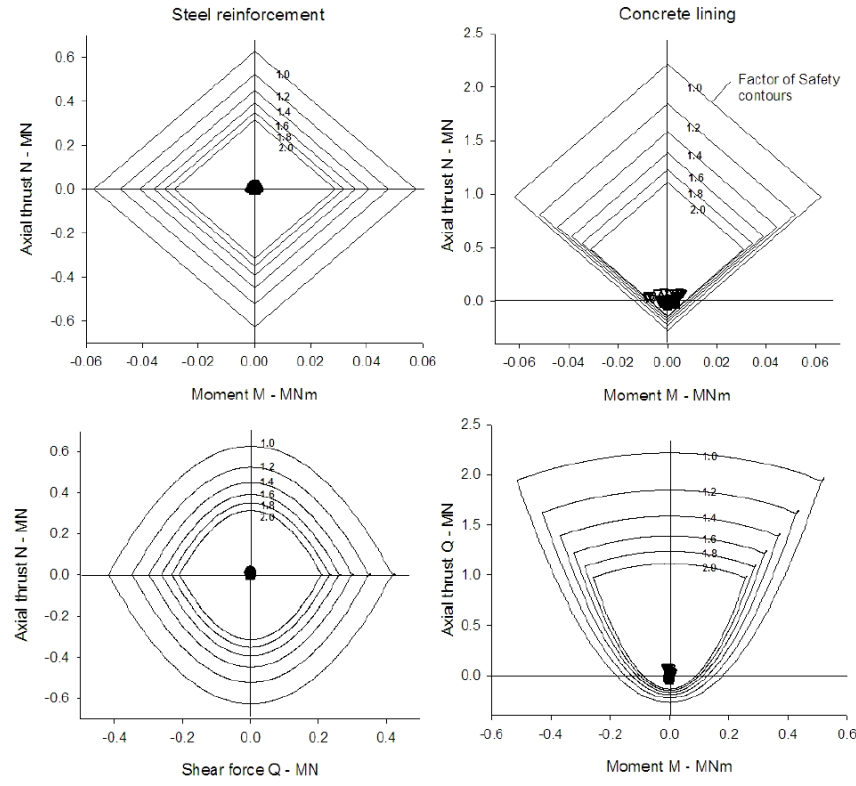


Figure 23. Support capacity plots for the final concrete lining.

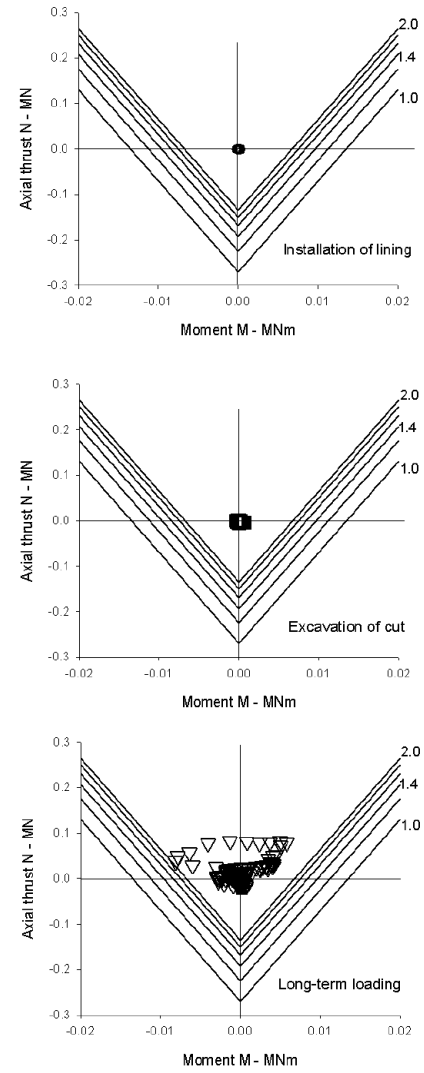


Figure 24. Detail of moment versus axial thrust development in the final concrete lining from the installation of the lining, the excavation of the open cut and long-term loading conditions.

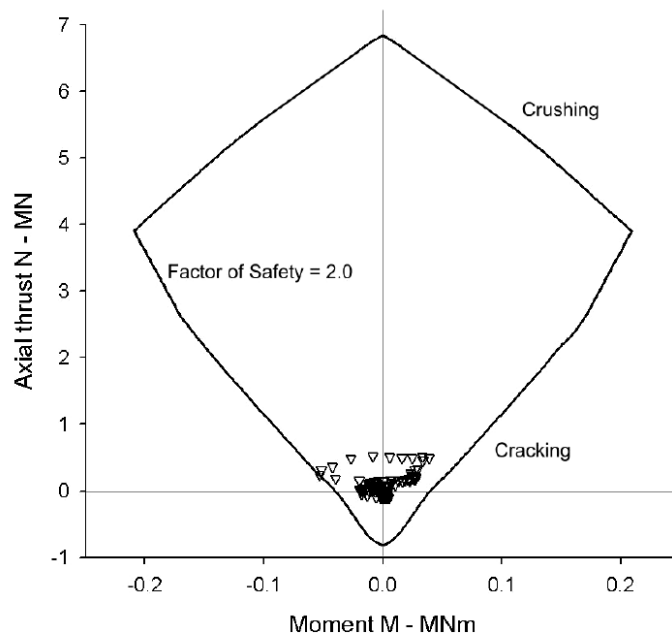


Figure 25. Minimum Moment-Thrust capacity for the reinforced concrete final lining calculated by the structural program Response 2000 (Bentz, 2000) for a factor of safety of 2.0.

Figure 25 gives a minimum moment-thrust capacity diagram for the reinforced final lining for a factor of safety of 2.0, generated using the structural program Response 2000 (Bentz, 2000). This is a sectional analysis program that will calculate the strength and ductility of a reinforced concrete cross-section subjected to shear, moment, and axial load. All three loads are considered simultaneously to find the full load-deformation response using the modified compression field theory (Vecchio and Collins, 1986).

The total moment-thrust points for the final lining under long-term loading conditions are also plotted in Figure 25. The relationship of these points to the capacity curve, defined by cracking of the concrete, is similar to that illustrated in Figure 24 for the concrete component of the lining. This comparison serves as a confirmation that, at least for the low load considered in this example, the elastic support capacity plots derived in Appendix 2 are an appropriate tool to use for reinforced concrete lining design.

The separation of the forces in the concrete (or shotcrete) and the steel reinforcement, as has been done in Figures 19 and 23, gives information on the contribution made by each of these components and on the combination of forces that control the design process. In this example the bending moments in the concrete are by far the most important forces and, when combined with the relative low tensile strength of concrete, they determine the performance of the lining.

3 CASE HISTORY 2 – A DEEP TUNNEL IN WEAK GROUND

This case history is based on the Yacambú-Quibor tunnel currently under construction in the Northern Andes in Venezuela. Aspects of this project are described by Guevara (2004). Design and construction details are simplified for the purposes of this example. This analysis involves new construction within the central portion of a 25 km tunnel, 5.2 m in diameter, in highly variable metamorphic rock at depths of up to 1200 m below surface (Figure 26).

The tunnel is designed for water transport, under moderate velocity and head, from a rainforest region in the south to an agricultural centre to the north. The tunnel will include the facilities to drain and inspect the tunnel with vehicle access after construction and during service life.

The design problem discussed here relates to a typical tunnel profile in highly deformed graphitic phyllite (Figure 27). The deformation in the rock mass is the result of the tectonic processes inherent in the Andes Mountains and is also the result of the proximity of the tunnel to a large regional fault related to the intersection of three major crustal plates. The fault passes through the tunnel as seen in Figure 26. A second fault has been identified on surface but it is not known whether this will be intersected at tunnel depth. This analysis is related to the section of tunnel identified in this figure where the average depth of overburden is approximately 1150 m. The in situ stresses at depth are assumed to be approximately equal (30 MPa) in all directions as a result of the low shear resistance due to the fact that the tectonic history of the rock mass has reduced its properties to their residual values.

Tests on intact core samples of this rock gave uniaxial compressive strength values of 15 MPa to 110 MPa (Salcedo, 1983). The high variability in results is due to the orientation of the phyllitic foliation with respect to the loading direction. As seen in Figure 27, the rock mass in the tunnel is tightly folded and no particular orientation of fabric presents itself over a significant portion of the tunnel profile. On the scale of the tunnel, therefore, isotropic rock mass strength can be assumed. Back analyses of monitored sections of the excavated tunnel confirm that the average uniaxial compressive strength of the intact graphitic phyllite is approximately 50 MPa and this value has been assumed for this analysis.

The rock mass was assessed using the Geological Strength Index (GSI) system (Marinos and Hoek, 2001) and rock mass strength parameters, according to Hoek et al. (2002), are shown in Figure 28. A GSI value of 25 is assigned to the rock mass over this section of the tunnel. As the rock mass is already in a deformed (residual) state, it is assumed to act plastically in response to stress change and deformation. The long term strength of the rock mass is assumed to correspond to moderate disturbance according to the GSI system with a Disturbance factor $D = 0.2$. The deformation modulus of the rock mass is estimated to be 1650 MPa, based on the methodology of Hoek and Diederichs (2006).

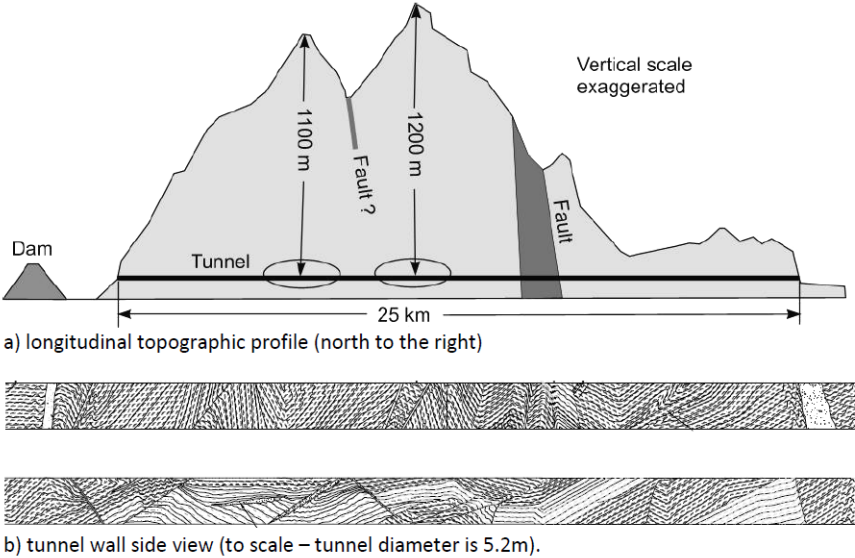


Figure 26. a) Longitudinal topographical profile along tunnel alignment. Major regional faults are shown. Ellipses indicate zones of interest for this case study. b) Two typical tunnel wall maps showing high variability in geological structure and fabric alignment.

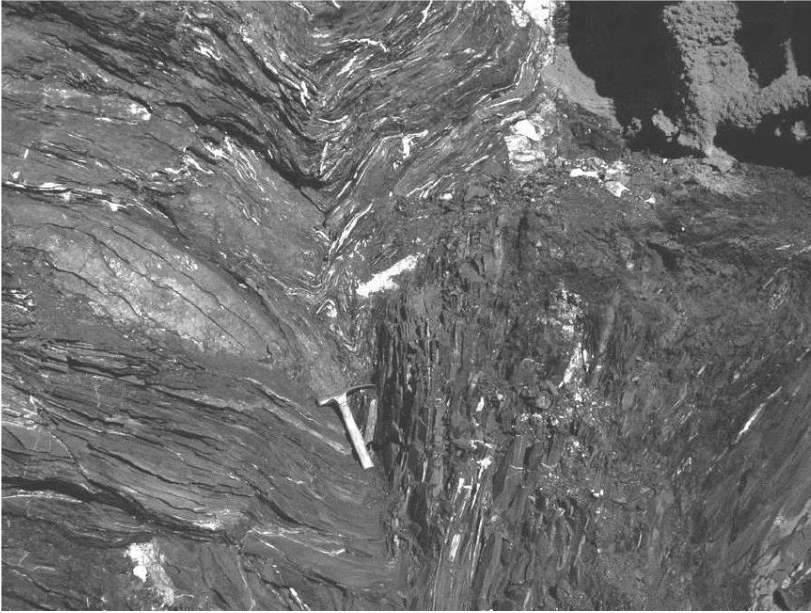


Figure 27. Graphitic phyllite in the tunnel face. Note the tight secondary folding and high variability of fabric orientation – rock hammer in center is 45cm long.

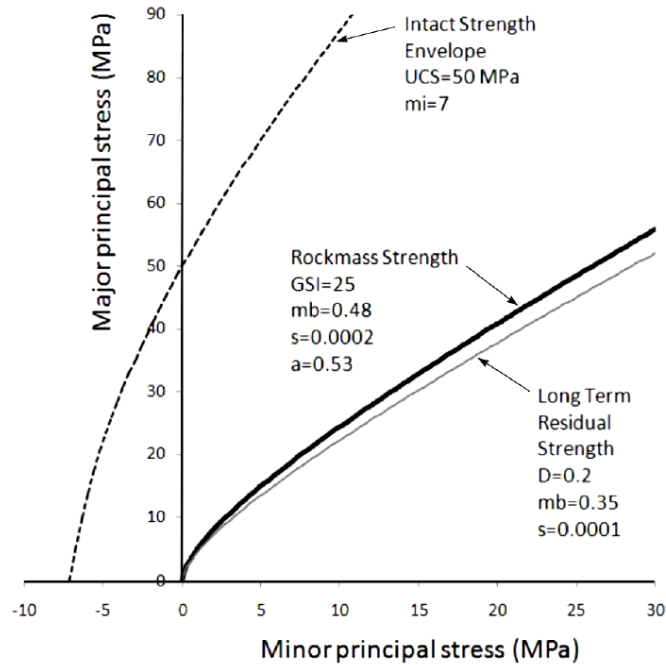


Figure 28: Rock mass strength parameters for Case 2 analysis. In situ stress = 28MPa.

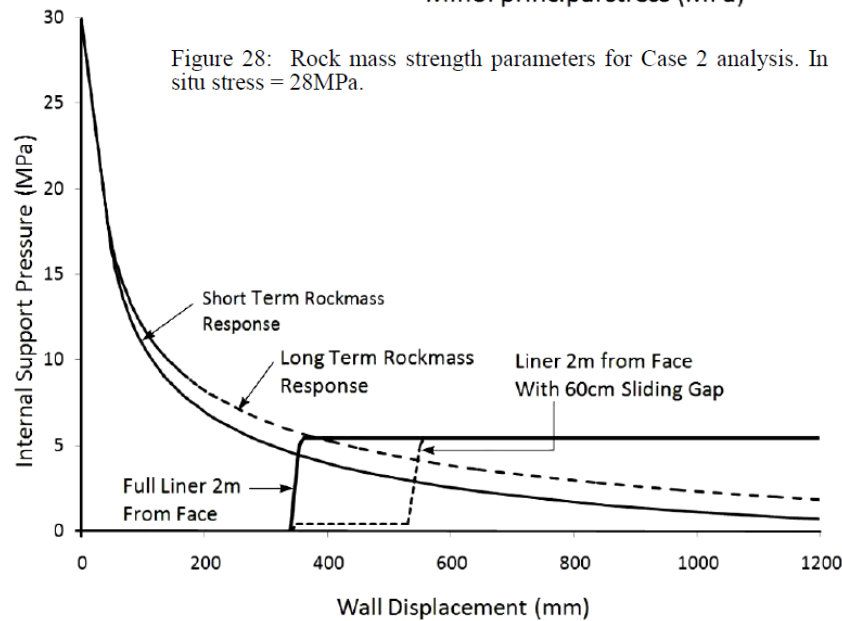


Figure 29. Convergence confinement analysis (according to method of Carranza-Torres and Fairhurst, 2000) for short and long term ground response (unsupported). Liner load development for 60 cm shotcrete section with W6 x 20 steel section. Dashed support load curve represents delayed loading due to sliding joint.

Tunnelling in these conditions is extremely difficult (Hoek and Marinos, 2000). Preliminary analysis of an unsupported tunnel in this rock mass at this depth indicates closure in excess of 50%. The key to liner design is to sequence the installation of support to avoid overload while still maintaining a safe working environment at and near the face.

Numerous challenges have been encountered over the long history of this construction project (a complete history of which is beyond the scope of this paper) and, due to the high cost of an additional concrete lining, it has been decided that the support system installed during construction will act as the final lining. In addition to resisting cracking and spalling this liner must control displacements to preserve the minimum tunnel size required for vehicular access during operation.

After several iterations in liner design over the years, each with its own lessons, the current design was adopted. A circular profile with steel arches (W6 X 20) at 1 m intervals, embedded in 60 cm of shotcrete applied in two passes of 20 cm and 40 cm thickness, is specified. There is a requirement to install support early to provide a safe working space at the face. Activation of the full lining, however, has to be delayed to prevent an unacceptable build-up of internal loads due to the high closure rates near the tunnel face. Premature installation of the final lining could result in buckling of the primary support system, associated expansion of the plastic zone and increase in final closure.

Specifications for the support were based, in part, on analytical convergence-confinement calculations (Carranza-Torres and Fairhurst, 2000). In this analysis, illustrated in Figure 29, the liner is treated as a single 60 cm thick concrete shell enclosing one W6 x 20 steel set per metre. The relationship between wall displacement and location along the tunnel (the linear displacement profile) is estimated based on the methodology described in Appendix 1 for a normalized plastic zone radius P_r of 6.5. Installation of the full liner near the face results in a low short term factor of safety and an unacceptable long term factor of safety of approximately 1.0. This long-term factor of safety is increased to approximately 1.4 with the installation of sliding joints. This prediction for the supported tunnel is conservative as it ignores the overall displacement reduction due to rock-support interaction.

Sliding joints, shown in Figure 30, allow controlled convergence (closure) of the steel sets without excessive loading of the steel. These joints provide resistance against moments but allow slip at low axial loads until the gap is closed. At this time the liner builds up load as a closed circle. The sliding joint is fabricated on site using two heavy steel plates constraining the set flanges through the tensioning of bolts as shown in the inset in Figure 30. The opposing steel sections are clamped by this device with a controlled gap (in this case 25 to 30 cm). This technique has proved to be very effective at Yacambú-Quibor. Alternative yielding support systems have also been widely used in squeezing ground conditions in Europe (Schubert, 1996).



Figure 30. Circular steel arches (W6 X 20) with two sliding joints (detail in inset).

The original design called for the complete steel set to be erected near the face and a 20 cm layer of shotcrete sprayed over the sets with 1 m gaps left over the sliding joints as shown in Figure 31. The two sliding joints are installed just below the spring line for a total circumferential closure of 60 cm (2 x 30 cm). Once the gap is closed by tunnel deformation, the gap is filled with shotcrete and an additional 40 cm of shotcrete, reinforced by means of circumferential rebar, is applied to the inside of the liner. The effect of the sliding gap is illustrated by the dashed support response line in Figure 29. This simple convergence-confinement analysis does not consider moments and neglects the interaction between support layers. In addition the stabilizing effect of the liner and the resultant reduction in rock mass displacement are not considered. Nevertheless, this analysis correctly indicates the need for delayed loading of the liner.

Due to difficulties with face instability, the contractor found it necessary to implement the support system in two stages with a short 1.5 m bench (from floor to springline) maintained to buttress the face. The upper semicircular section of the steel set is installed at the face to provide a primary safety system. The arch sections rest on the bench and are covered in shotcrete. The bench is then excavated approximately 1.5 m from the face and the circular arch, including the pair of sliding joints, is completed. The first 20 cm shotcrete layer is completed at this stage (Figure 32a).

A reinforcement cage is assembled adjacent to the initial shotcrete lining as seen in Figure 31. Once joint closure is achieved (within 5 to 15m of the face) the gap is closed with shotcrete to complete the final 40 cm thick final lining. The final lining section is illustrated in Figure 32b.



Figure 31. Initial Liner composed of circular steel arch and 20 cm of shotcrete. Inset shows detail of sliding joint with shotcrete gap. Note rebar in place to reinforce final shotcrete layer.

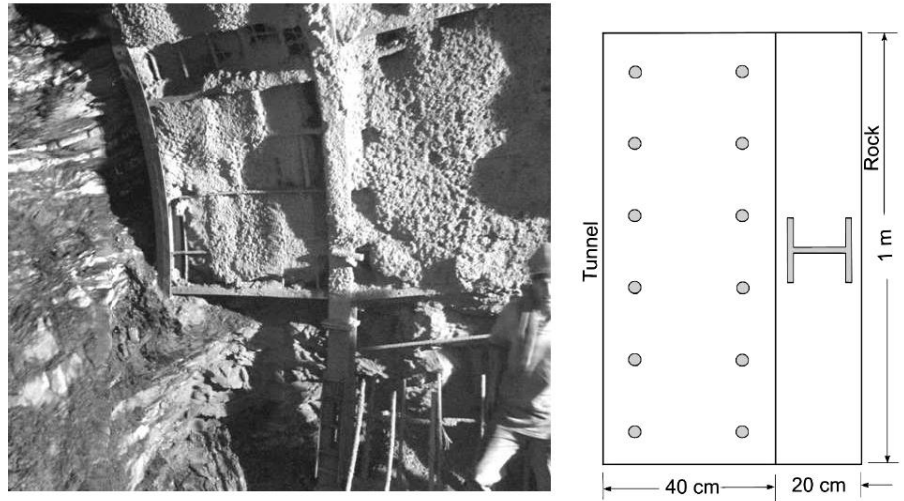


Figure 32. a) Configuration of mid-height bench (partially disintegrated in this photograph) and upper steel arch installed ahead of lower section and sliding joint. b) Final 60 cm section with outer shotcrete and steel set composite section and inner reinforced shotcrete section. The tunnel is to the left and rock mass is to the right of the section.

The following analysis represents a more rigorous consideration of the interactions between the liner components and the construction sequence. The first step in the design process is to determine the normalized maximum unsupported failure radius via a simple plane strain analysis of the unsupported tunnel. In this case, the ratio of maximum plastic radius to tunnel radius is 6.5.

Next, the longitudinal deformation profile can be calculated using the methodology given in Appendix 1. Alternatively, since the stresses are isotropic and the tunnel is circular, an axisymmetric model (Figure 33b) can be used for this purpose. A longitudinal deformation profile for the unsupported tunnel is shown as a dashed line (“Disp. vs Distance”) in Figure 33a. An estimate of the displacement profile for the supported tunnel (with liner and sliding joints) is presented in Figure 33a as a dotted line for comparison.

A 2D finite element plane strain analysis is then applied to the full face construction sequence (unsupported). The technique of progressive face replacement described in the previous section (Figure 7) is used here. The resulting points on the ground reaction curve (“Disp. vs Support Pressure” curve in Figure 33a) can be assigned locations along the tunnel (filled diamonds in Figure 33a) using the (dashed) longitudinal deformation profile.

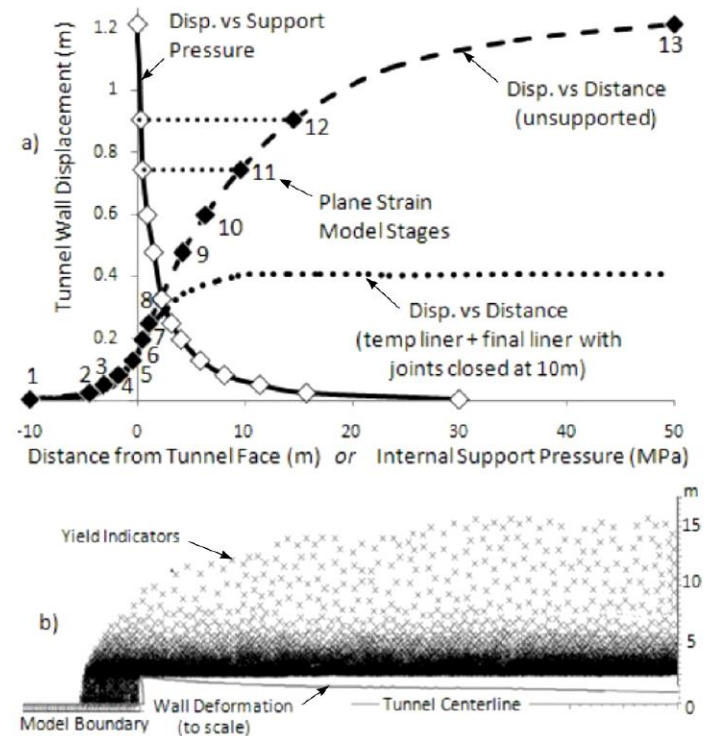


Figure 33 a) Ground reaction curve “Disp. vs Support Pressure” and corresponding longitudinal displacement profile “Disp vs Distance (un-supported)” for a axisymmetric model. Normalized plastic radius = 6.5. Longitudinal displacement profile function fitted based on Appendix 1. Point symbols and number ID’s represent corresponding stages in plane strain model (related symbols are linked between two curves as shown for stage 11 and 12 by dotted lines). Supported longitudinal deformation profile (dashed line without symbols) shown for comparison. b) Axisymmetric model used for calibration showing yield indicators (x’s) and wall displacement along tunnel (Vlachopoulos & Diederichs 2009b).

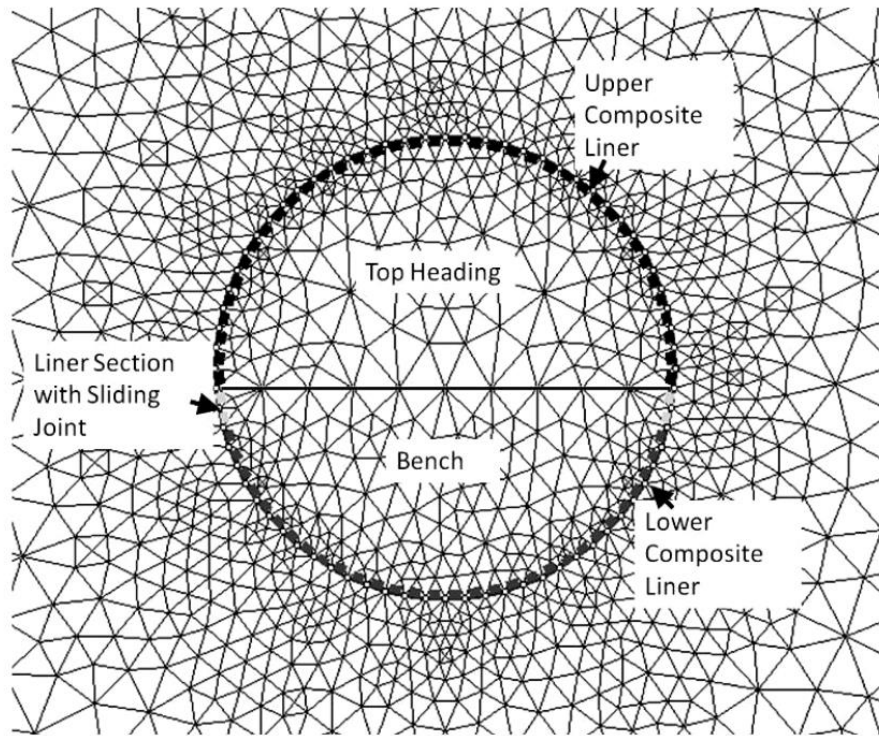


Figure 34. Finite element mesh, geometry of excavation stages and liner segments for 2D plane strain analysis of sequenced excavation and support.

The same correlation of model stage to tunnel location can be used for the benched tunnel model with offset stages of bench excavation and with appropriate installation of support (remember that the model support is installed at the beginning of the stage while the displacements are reported at the end of the stage). The benched tunnel model is illustrated in Figure 34.

It is anticipated that the steel sets and the initial 20 cm shotcrete layer will undergo some limited yielding after the sliding joints close. The upper half of the arch, installed in the bench, may also yield prior to this due to the moments induced by a reduction in the arch radius. This partial arch and the complete arch, with sliding joints, are modeled as separate but joined layers with appropriate material and section properties. They are assumed to act plastically with yield in the steel and a 33% reduction in residual uniaxial compressive strength of the shotcrete after yield.

Following the geometry in Figure 34, the bench excavation sequence lags behind the top heading by 2 stages. The upper composite liner is installed immediately behind the face (start of stage 7 in Figure 33). The lower composite liner and the sliding joints are installed approximately 1 m behind the bench (beginning of stage 9), and the filler sections of 20 cm shotcrete are installed and assumed to set by the beginning of stage 10. In this analysis the sliding joint gap closes automatically two stages later (within stage 11) between 6 and 10 m from the face.

The final lining is applied behind the gap closure, beginning of stage 12 (10 m from the face) for this analysis. This final lining is applied as an elastic composite according to the methodology in Appendix 2. For the purposes of this analysis, a symmetrical reinforcement array of 6 x 25 mm rebar per metre, 75 mm from each surface is used. The moment of inertia, section depth and total area are calculated for the rebar arrangement. The procedure is then similar as that described in Appendix 2 for steel sets. The relevant properties are given in Table 3.

The aging of shotcrete is neglected here as the excavation rate is very slow (approximately 1 m per day). The shotcrete used at the site was of very high quality and 7 day strength and stiffness values are used.

The short- and long-term liner loads are shown in Figure 35 for the full face excavation and for the top heading and bench option. The compromise required to provide a bench for face support results in a less uniform loading of the two halves of the arch and the build-up of moments in the sliding joint area. This effect is exaggerated dramatically if the final lining is installed before the sliding gap has closed.

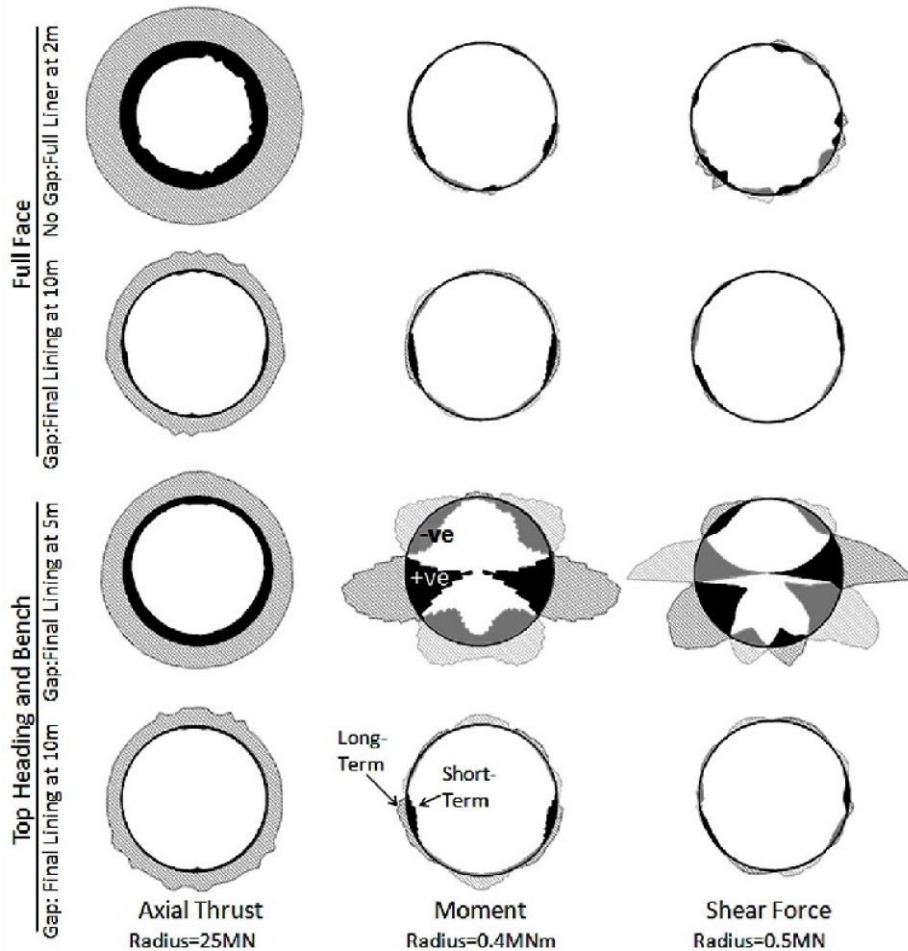


Figure 35. Relative magnitudes and distribution of total axial load, moment and shear load in the final 40 cm thick reinforced layer. Values plotted inside tunnel as solid represent short term loading conditions. Hatched values outside of tunnel represent long term conditions. Dark shading indicates positive values for moment and shear, light shading indicates negative values. This inner final liner layer is modeled elastically. This plot does not include residual loadings in the plastic outer lining layer (steel sets embedded in 20 cm shotcrete).

To analyze the loadings within the steel and concrete components of the final inside lining layer, the equations in Appendix 2 are used to partition the loads and moments and to generate elastic capacity envelopes for comparison as shown for the full face options in Figure 36.

Table 3. Liner properties for reinforced 40 cm inner liner (for use with Appendix 2).

Tunnel Radius	2.52	m	Width of Section	1	m
Rebar Properties			Shotcrete Properties		
Number of Pairs per Section	6		Height of Section	0.4	m
Height of Rebar Section	0.25	m	Young's Modulus	30000	MPa
Area of Section	0.005985	m ²	Poisson's Ratio	0.2	
Moment of Inertia	9.40E-05	m ⁴	Compressive Strength	40	MPa
Young's Modulus	200000	MPa	Tensile Strength	-4	MPa
Poisson's Ratio	0.3				
Compressive Strength	400	MPa			
Tensile Strength	-400	MPa	Number of sets n	1	

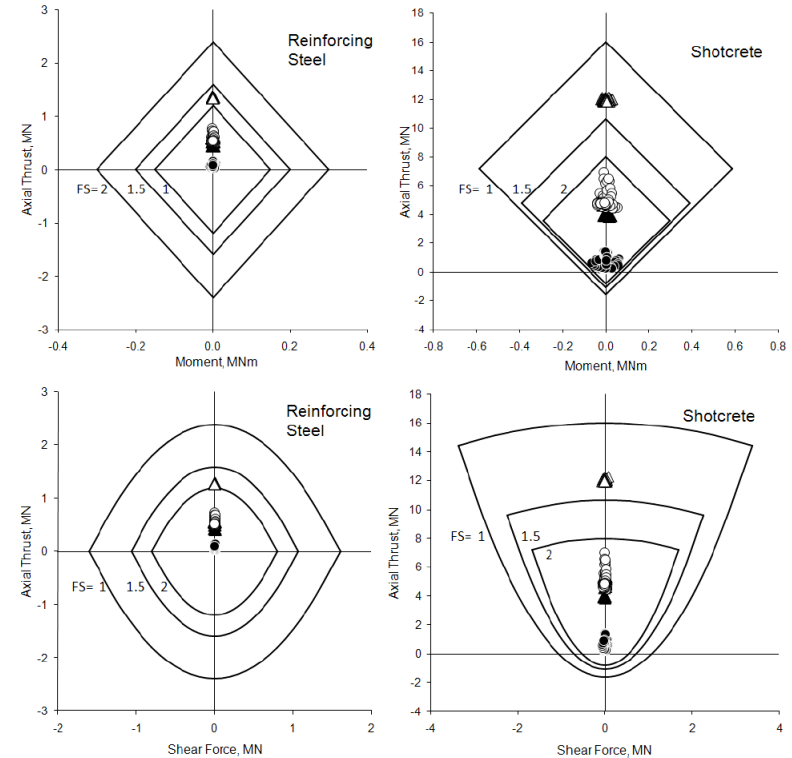


Figure 36. Partitioned liner loads compared to component capacity envelopes for full face tunnel option. Circles represent a full 60 cm lining, as per Figure 32b, installed in one step 2 m from the face. Triangles represent the option involving W 6x 20 sets installed at the face with a sliding gap in combination with 20 cm of shotcrete, followed at 10 m distance by a filled gap and 40 cm of reinforce shotcrete. These plots are for the inner 40 cm of reinforced shotcrete only. Filled symbols represent short term loading while open symbols are for long term loading.

The most obvious result from Figure 36 is the large axial thrust predicted in the full lining installed near the face with no sliding joints. This confirms the conclusion from Figure 29 and points to the definite requirement to allow deformation prior to full lining installation. For the full face excavation, the liner with a sliding joint and with the final reinforced layer applied at 10 m from the face performs well, giving a factor of safety for long term loading greater than 2 for all loading combinations. The limiting state is the short term moment in the shotcrete component. In this case the gap closed automatically in response to loading, between 5 and 10 m from the face, well before final lining installation.

As discussed, logistical and safety issues related to deformation and deterioration of the face mandated the adoption of a top heading and short bench sequence. This required the lining to be installed as an immediate top and slightly delayed bottom section. The partitioned capacity plots for top heading and bench excavation are shown in Figure 37.

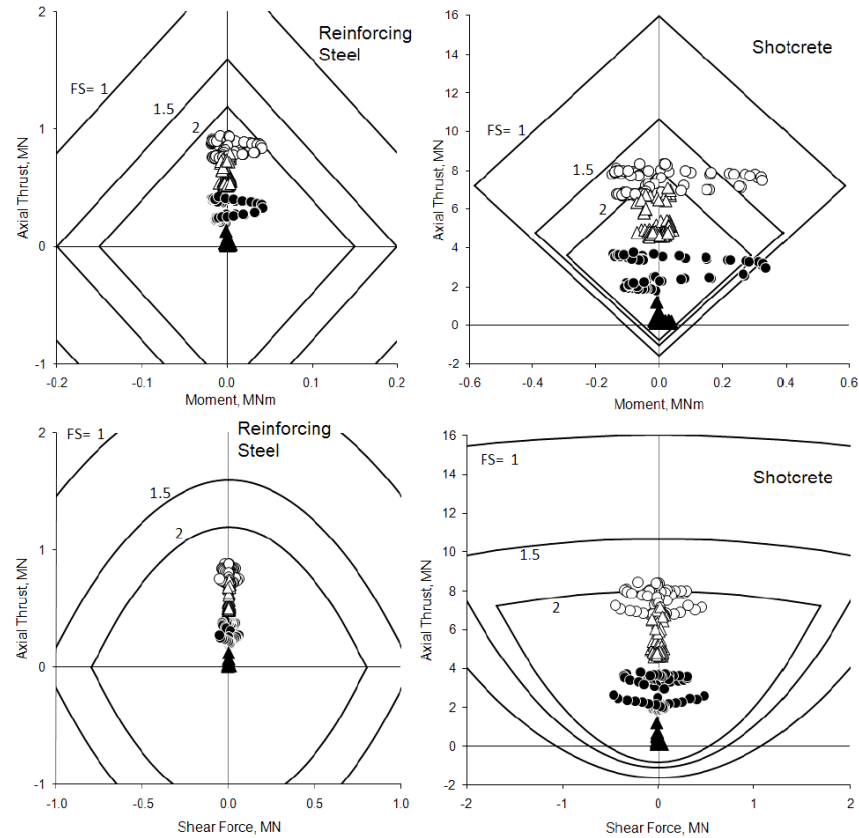


Figure 37. Partitioned liner loads compared to component capacity envelopes for top heading and bench options. In these analyses, the sliding joint (gap) closes automatically under load between 5 and 10 m. Circles represent completion of the final lining at 5 m from the face (before gap closure). Triangles represent the completion of the final lining at 10 m from the face (after gap closure). These plots are for the inner 40 cm of reinforced shotcrete only. Filled symbols represent short term loading while open symbols represent long term loading.

For the top heading and bench option, the predicted performance is adequate in short and long term loading provided that the gap (sliding joint) is filled and the final lining completed after the joint has fully closed or the deformations have stabilized. The penalty for delaying liner completion will be unacceptable degradation and yielding of the initial 20 cm lining and the steel sets resulting in service and safety problems. While this initial composite layer is expected to yield to some degree, excessive yielding should be avoided. In addition, a long delay in the installation of the final liner could lead to loss of wall control.

The ideal condition is to fill the gap with shotcrete immediately upon joint closure to complete the lining. In this example, the joint or gap closes between 6 m and 10 m from the face. The triangles in Figure 37 represent completion of the final liner at 10 m. The limiting state in this case is the short term moment in the shotcrete ($FS > 2$). The open circles in Figure 37 represent the case of premature completion of the final lining at 5 m from the face.

This design requires careful construction monitoring and management. If the gap is filled with shotcrete and the final lining completed before the joints are allowed to close or before deformations have stabilized, the penalty is increased axial, shear and moment loading throughout the liner. In the case shown here, cracking will be induced due to high moments for short term loading and the factor of safety for all loading combinations drops for long term loading.

Even with excellent construction management, however, it is possible that liner completion could take place too soon for some individual segments or rounds within the tunnel. From a hazard mitigation perspective it is important to understand the consequences of this possibility. The factors of safety illustrated in Figures 36 and 37 refer to initial cracking of the liner. Figure 38 illustrates an alternative analysis of the results in which the non-partitioned liner loadings and capacity envelopes are calculated in a non-linear fashion, using the program Response 2000 (Bentz, 2000) that allows plastic (cracked) moments.

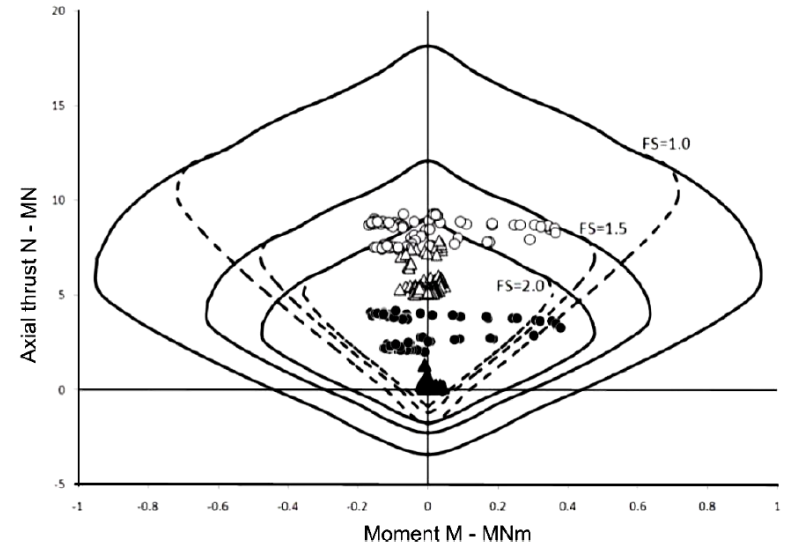


Figure 38. Total (non-partitioned) thrusts and moments from modeled inner liner of 40 cm reinforced shotcrete. Dashed envelopes represent limits for initial cracking of shotcrete. Solid envelopes represent capacity limits accounting for the development of additional moment capacity in the cracked liner as well as accounting for the tensile strength of the reinforcement (Vecchio and Collins, 1986). Triangles represent installation of the final lining at 10 m; circles represent completion at 5 m. Filled symbols indicate short term loading; open symbols indicate long term loading. Sliding joint closes automatically between 5 and 10 m from the face.

Figure 38 shows that the critical loading, in the case of premature completion of the liner, is the short term moment. This is indicated by the calculated values falling outside the capacity envelopes for cracking. These envelopes are equivalent to the elastic envelopes for the partitioned liner, presented in the previous figures. This case still falls within the solid capacity envelopes representing the ultimate load capacity of the liner with tension cracks fully developed and internal loading redistributed. This indicates that the prematurely installed final lining will not collapse catastrophically in compression or bending. Instead, cracks would become visible during the construction phase of the tunnel and repairs can be made.

The ultimate result is a reduced long term factor of safety for all loading conditions, again reinforcing the need for good construction management to ensure the correct installation sequence for potentially variable rock mass conditions and deformation rates.

The appearance of the tunnel, constructed as described in this example, is shown in Figure 39.



Figure 39. Completed section of tunnel with a 60 cm thick reinforced shotcrete lining, placed in two layers as described above.

4 CONCLUSIONS

A methodology for the design of tunnel linings has been presented. While this approach has been used by specialist tunnel designers for many years, it has never been described comprehensively in a single document that allows the reader to follow all the derivations and the step by step calculations. To make this process as easy as possible to follow, the authors have included two case history based examples, one for a very shallow tunnel and the other for a very deep tunnel. These examples have been chosen to highlight the complex loading conditions that can occur under different geological and topographic conditions and how these complexities can be incorporated into a rational lining design.

The support capacity diagrams are based on elastic analysis of the support elements and this implies that no tensile cracking or compressive crushing of the shotcrete or concrete elements is acceptable. These simplified calculations allow the user to optimize the design of the lining components relatively quickly and efficiently. It has been demonstrated that, where tensile cracking becomes an important consideration, more sophisticated non-linear structural design approaches, which allow for crack development, can be used.

In a typical tunnel design in which support consists of steel sets embedded in shotcrete, the designer needs to know the contribution of each of these support elements and to be able to adjust the number and dimensions of each to accommodate the loads imposed on the lining. In current tunnel design, these loads are obtained from numerical analyses in which “beam elements” are attached to the tunnel boundary and the axial thrust, bending moments and shear forces induced in these elements are computed directly.

Note that these beam elements constitute “tunnel support” and they interact with the surrounding rock mass to limit the convergence of the tunnel. On the other hand, rockbolts act as “tunnel reinforcement” in that they change the mechanical properties of the rock mass surrounding the tunnel. Hence, it is possible to carry out a numerical analysis of a tunnel reinforced by means of rockbolts and supported by means of a composite lining. The loads imposed on the lining will be reduced by the reinforcement and the composite lining will respond to these reduced loads. The analysis that follows is valid whether rockbolts are present or not, provided that the numerical analysis correctly models the load transfer from the rock mass onto the lining.

Figure A2.1 represents the problem to be analyzed involving a section of composite liner of width b comprising n steel sets and n units of shotcrete —note that if n units of each material exist along the width b , this is equivalent to saying that the units are spaced at $s = b/n$. The composite section in Figure 1 can be regarded as an equivalent section of width b and thickness t_{eq} . The steel sets are assumed to be symmetrically placed in the shotcrete lining so that the neutral axes of both the steel sets and the shotcrete lining are coincident. For the purposes of this analysis it is assumed that the complete shell behaves elastically. This is a reasonable assumption since the tunnel designer generally attempts to design the lining so that it will not fail.

The following analysis is excerpted from Carranza-Torres and Diederichs (2009).

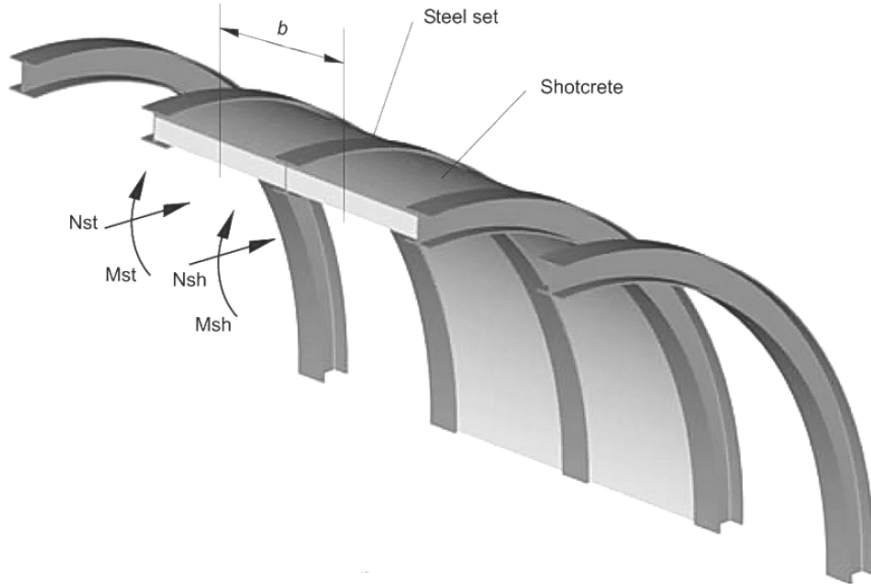


Figure A2.1: A section of width b in a composite lining consisting of steel sets, spaced at a distance s , embedded in shotcrete. Moments M_{st} and axial thrusts N_{st} are induced in the steel sets and moments M_{sh} and thrusts N_{sh} are induced in the shotcrete shell.

In order to calculate the moments and axial thrusts induced in the steel sets and the shotcrete shell and to compare these with the capacity of the steel sets and shotcrete, the following steps are required:

1. An “equivalent” rectangular section with a width of b , a thickness t_{eq} and a modulus of E_{eq} , is determined.
2. The capacity of the steel sets and the shotcrete lining are determined.
3. A numerical model of the tunnel is constructed and beam elements representing the equivalent rectangular section are applied to the tunnel perimeter.
4. The bending moments and axial thrusts are redistributed back onto the steel sets and shotcrete lining.

9.1 Calculation of equivalent section

The properties of the equivalent rectangular section are calculated as follows. For plane strain conditions the compressibility coefficient D_{st} and flexibility coefficient K_{st} for the steel sets are:

$$D_{st} = \frac{E_{st} A_{st}}{1 - \nu_{st}^2} \quad (A2.1)$$

$$K_{st} = \frac{E_{st} I_{st}}{1 - \nu_{st}^2} \quad (A2.2)$$

where E_{st} is the Young’s modulus of the steel
 A_{st} is the cross-sectional area of each steel set
 I_{st} is the moment of inertia of each steel set and
 ν_{st} is the Poisson’s ratio of the steel

For the shotcrete shell, the compressibility and flexibility coefficients are:

$$D_{sh} = \frac{E_{sh} A_{sh}}{1 - \nu_{sh}^2} \quad (A2.3)$$

$$K_{sh} = \frac{E_{sh} I_{sh}}{1 - \nu_{sh}^2} \quad (A2.4)$$

where E_{sh} is the Young’s modulus of the shotcrete
 A_{sh} is the cross-sectional area of each unit of shotcrete = $s \cdot t_{sh}$
 I_{sh} is the moment of inertia of each unit of shotcrete = $(s \cdot t_{sh}^3) / 12$
 ν_{sh} is the Poisson’s ratio of the shotcrete

The equivalent compressibility and flexibility coefficients for the composite lining are:

$$D_{eq} = n(D_{st} + D_{sh}) \quad (A2.5)$$

$$K_{eq} = n(K_{st} + K_{sh}) \quad (A2.6)$$

The equivalent section has a width of b , an equivalent section thickness t_{eq} and the equivalent modulus E_{eq} . The equivalent compressibility and flexibility coefficients can be written as:

$$D_{eq} = b \cdot t_{eq} E_{eq} \quad (A2.7)$$

$$K_{eq} = E_{eq} \frac{bt_{eq}^3}{12} \quad (A2.8)$$

Solving for the variables t_{eq} and E_{eq}

$$t_{eq} = \sqrt{\frac{12K_{eq}}{D_{eq}}} \quad (A2.9)$$

$$E_{eq} = \frac{D_{eq}}{bt_{eq}} \quad (A2.10)$$

9.2 Calculation of support capacity

In order to check whether the induced stresses in the steel sets and shotcrete lining are within permissible limits, it is useful to plot the moments, shear forces and thrusts on support capacity diagrams. The support capacity curves are calculated as follows:

9.2.1 Moment-thrust capacity

The maximum permissible compressive and tensile stresses induced in the lining are given by:

$$\frac{\sigma_{\max}}{FS} = \frac{N}{A} + \frac{Mt}{2I} \quad (A2.11)$$

$$\frac{\sigma_{\min}}{FS} = \frac{N}{A} - \frac{Mt}{2I} \quad (A2.12)$$

where FS is the factor of safety.

The maximum and minimum permissible thrust capacity is obtained by substituting $M = 0$ in equations A2.11 and A2.12, giving:

$$N_{\max} = \frac{A\sigma_{\max}}{FS} \quad (A2.13)$$

$$N_{\min} = \frac{A\sigma_{\min}}{FS} \quad (A2.14)$$

The maximum bending moment is obtained when tensile and compressive failures occur simultaneously which, by eliminating N from equations A2.11 and A2.12, gives:

$$M_{\max} = \pm \left(\frac{\sigma_{\max} - \sigma_{\min}}{FS} \right) \frac{I}{t} \quad (A2.15)$$

The corresponding normal force N_{cr} at which these maximum moments occur is given by:

$$N_{cr} = \frac{A(\sigma_{\max} + \sigma_{\min})}{2FS} \quad (A2.16)$$

9.2.2 Shear force-thrust capacity

In terms of shear force and axial thrust relationships:

$$\sigma_{\max} = \frac{N}{A} \quad (A2.17)$$

$$\tau_{\max} = \frac{3Q}{2A} \quad (A2.18)$$

$$\sigma_{1,3} = \frac{\sigma_{\max}}{2} \pm \sqrt{\left(\frac{\sigma_{\max}}{2} \right)^2 + \tau_{\max}^2} \quad (A2.19)$$

$$FS = \frac{\sigma_c}{\sigma_1} = \frac{\sigma_t}{\sigma_3} \quad (A2.20)$$

$$\text{For failure in compression: } N = \frac{\sigma_c A}{FS} - \frac{9Q^2 FS}{4\sigma_c A} \quad (A2.21)$$

$$\text{For failure in tension: } N = \frac{\sigma_t A}{FS} - \frac{9Q^2 FS}{4\sigma_t A} \quad (A2.22)$$

The critical value of the shear force Q_{cr} associated with a particular factor of safety FS for both failure in compression and tension at the same time is:

$$Q_{cr} = \pm \frac{A}{FS} \sqrt{-\frac{4\sigma_c \sigma_t}{9}} \quad (A2.23)$$

Note that σ_t is negative.

9.3 Redistribution of thrust and moment onto steel sets and shotcrete

The bending moments, shear forces and axial thrusts are calculated by means of a numerical analysis and for the equivalent composite lining of width b and thickness t_{eq} . In order to consider the behavior of the steel sets and the shotcrete separately, it is necessary to redistribute these thrusts and moments back onto the individual support elements.

Since many of the linings are attached to curved surfaces and, in some cases, these linings are relatively thick compared to their radius R , it is necessary to consider the redistribution in terms of a thick curved beam solution. This solution is the most general since it automatically degenerates to a thin beam solution as the radius of curvature increases to infinity.

The equations for the redistribution of the moment M , axial thrust N and shear forces Q induced in any one of the beam elements representing the equivalent shell are:

$$\text{Steel set moments: } M_{st} = \frac{MK_{st}}{n(K_{st} + K_{sh})} \quad (A2.24)$$

$$\text{Shotcrete moments: } M_{sh} = \frac{MK_{sh}}{n(K_{st} + K_{sh})} \quad (A2.25)$$

$$\text{Steel set thrusts: } N_{st} = \frac{N D_{st}}{n(D_{st} + D_{sh})} + \frac{M(D_{sh} K_{st} - D_{st} K_{sh})}{nR(D_{st} + D_{sh})(K_{st} + K_{sh})} \quad (A2.26)$$

$$\text{Shotcrete thrusts: } N_{st} = \frac{N \cdot D_{sh}}{n(D_{st} + D_{sh})} - \frac{M(D_{sh}K_{st} - D_{st}K_{sh})}{nR(D_{st} + D_{sh})(K_{st} + K_{sh})} \quad (\text{A2.27})$$

$$\text{Steel set shear forces: } Q_{st} = \frac{QK_{st}}{n(K_{st} + K_{sh})} \quad (\text{A2.28})$$

$$\text{Shotcrete shear forces: } Q_{sh} = \frac{QK_{sh}}{n(K_{st} + K_{sh})} \quad (\text{A2.29})$$

The following forces induced in the lining described above are redistributed into the steel and shotcrete components as defined by Equations A2.24 to A2.29. The lining was installed in a circular tunnel with a radius of 5 m in a rock mass with properties defined by:

Modulus E = 4000 MPa
 Peak cohesion = 2 MPa, Residual cohesion = 1 MPa
 Peak friction angle = 40°, Residual friction angle = 35°

The rock mass is subjected to a horizontal stress normal to the tunnel axis of 4 MPa and a vertical stress of 2 MPa. The horizontal stress parallel to the tunnel axis is 2 MPa.

The results of these calculations are plotted in Figure A2.2.

9.4 Support capacity plots

The capacity plots described above can be calculated by means of a simple spreadsheet. The following input parameters have been assumed for this analysis:

<i>Steel sets</i>		<i>Shotcrete lining</i>	
Tunnel radius	R = 2 m	Shotcrete thickness	t _{sh} = 0.2 m
Steel set spacing	s = 0.6 m	Modulus of shotcrete	E _{sh} = 30,000 MPa
Steel set height	t _{st} = 0.162 m	Poisson's ratio	v _{sh} = 0.15
Area of steel set	A _{st} = 4.75 x 10 ⁻³ m ²	Compressive strength	σ _{csh} = 40 MPa
Moment of Inertia	I _{st} = 2.23 x 10 ⁻⁵ m ⁴	Tensile strength	σ _{tsh} = -2.5 MPa
Modulus of steel	E _{st} = 200,000 MPa	Area of shotcrete	A _{sh} = s · t _{sh} ² = 0.12 m ²
Poisson's ratio	v _{st} = 0.25	Moment of Inertia	I _{sh} = s · t _{sh} ³ / 12 = 0.0004 m ⁴
Compressive strength	σ _{cst} = 500 MPa		
Tensile strength	σ _{tst} = -500 MPa		

Calculation of Support capacity diagrams for a Factor of Safety = 1.0

<i>Steel sets</i>	M	N	<i>Shotcrete lining</i>	M	N
Maximum Thrust	0.00	2.38	Maximum Thrust	0.00	4.80
Maximum moment	0.14	0.00	Maximum moment	0.09	2.10
Minimum thrust	0.00	-2.38	Minimum thrust	0.00	-0.60
Minimum moment	-0.14	0.00	Minimum moment	-0.09	2.10
Complete fig	0.00	2.38	Complete fig	0.00	4.80

Shear force - axial thrust plot

<i>Steel sets</i>	Q	N	N	<i>Shotcrete lining</i>	Q	N	N
Maximum shear force	1.58			Maximum shear force	1.13		
Minimum shear force	-1.58			Minimum shear force	-1.13		
	1.58	0.00	0.00		1.13	4.20	4.20
	1.19	1.04	-1.04		0.85	4.46	2.10
	0.79	1.78	-1.78		0.57	4.65	0.60
	0.40	2.23	-2.23		0.28	4.76	-0.30
	0.00	2.38	-2.38		0.00	4.80	-0.60
	-0.40	2.23	-2.23		-0.28	4.76	-0.30
	-0.79	1.78	-1.78		-0.57	4.65	0.60
	-1.19	1.04	-1.04		-0.85	4.46	2.10
	-1.58	0.00	0.00		-1.13	4.20	4.20

Redistribution of forces into steel and shotcrete lining components (Equations A2.24 to A2.29)

Total M	Total Q	Steel N	Steel M	Steel Q	Shot N	Shot M	Shot Q
0.00692	0.00242	0.40880	0.00121	0.00042	1.39360	0.00294	0.00103
0.00591	0.00049	0.43527	0.00103	0.00009	1.48383	0.00251	0.00021
0.00451	0.00371	0.49292	0.00079	0.00065	1.68034	0.00192	0.00158
0.00266	0.00206	0.57431	0.00047	0.00036	1.95781	0.00113	0.00088
-0.00057	-0.00719	0.67026	-0.00010	-0.00126	2.28492	-0.00024	-0.00305
-0.00283	-0.00224	0.77803	-0.00050	-0.00039	2.65229	-0.00120	-0.00095
-0.00518	0.00738	0.86640	-0.00091	0.00129	2.95356	-0.00220	0.00313
-0.00632	-0.00213	0.91111	-0.00111	-0.00037	3.10595	-0.00269	-0.00091
-0.00680	0.00133	0.91191	-0.00119	0.00023	3.10869	-0.00289	0.00057
-0.00519	-0.00831	0.86533	-0.00091	-0.00146	2.94989	-0.00221	-0.00353
-0.00315	-0.00787	0.79319	-0.00055	-0.00138	2.70397	-0.00134	-0.00334
-0.00121	-0.00529	0.70242	-0.00021	-0.00093	2.39454	-0.00051	-0.00225
0.00239	-0.00134	0.59056	0.00042	-0.00023	2.01320	0.00101	-0.00057
0.00456	-0.00336	0.49313	0.00080	-0.00059	1.68109	0.00194	-0.00143
0.00617	0.00073	0.43500	0.00108	0.00013	1.48290	0.00262	0.00031
0.00626	-0.00133	0.40879	0.00110	-0.00023	1.39355	0.00266	-0.00057
0.00631	-0.00002	0.42241	0.00111	0.00000	1.43999	0.00268	-0.00001
0.00500	0.00211	0.48075	0.00088	0.00037	1.63887	0.00213	0.00090
0.00241	0.00237	0.57426	0.00042	0.00042	1.95762	0.00102	0.00101
-0.00028	0.00829	0.68655	-0.00005	0.00145	2.34045	-0.00012	0.00352
-0.00324	0.00972	0.79386	-0.00057	0.00170	2.70624	-0.00138	0.00413
-0.00627	0.00100	0.87449	-0.00110	0.00017	2.98111	-0.00266	0.00042
-0.00740	-0.00508	0.91454	-0.00130	-0.00089	3.11764	-0.00314	-0.00216
-0.00738	0.00174	0.90659	-0.00129	0.00030	3.09055	-0.00313	0.00074
-0.00461	0.00103	0.85673	-0.00081	0.00018	2.92057	-0.00196	0.00044
-0.00295	-0.00449	0.76633	-0.00052	-0.00079	2.61239	-0.00126	-0.00191
0.00012	-0.01188	0.65380	0.00002	-0.00208	2.22878	0.00005	-0.00505
0.00357	-0.00367	0.54585	0.00063	-0.00064	1.86081	0.00152	-0.00156
0.00526	-0.00100	0.46110	0.00092	-0.00018	1.57188	0.00224	-0.00043
0.00680	-0.00190	0.41097	0.00119	-0.00033	1.40097	0.00289	-0.00081

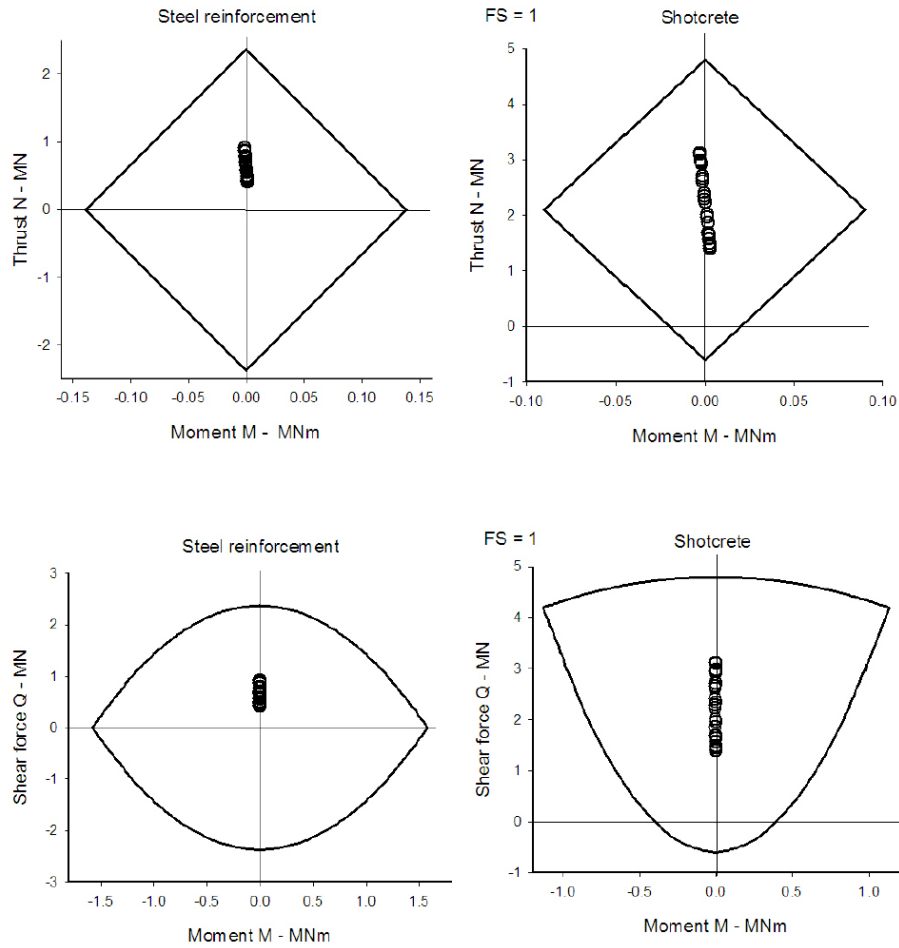


Figure A2.2. Support capacity diagrams and induced lining forces for the example described above.